Modification of simulation model for a compact adsorption cooling system

西久保, 友紀
九州大学大学院総合理工学府環境エネルギー工学専攻

令　和　元　年　度

修　　士　　論　　文

Modification of simulation model for a compact adsorption cooling system

九州大学大学院総合理工学府

環境エネルギー工学専攻

熱エネルギー変換システム工学研究室

西　久　保　友　紀

指導教員　宮崎　隆彦

Kyaw Thu

提出年月日　令和２年２月３日

Modification simulation model for a compact adsorption cooling system

ABSTRACT

This study has two main aims. One is to investigate the performance results of a compact adsorption cooling system using activated carbon as the adsorbent with ethanol as refrigerant. The other is to establish the detailed simulation model by modifying the present lumped parameter model which has been used to predict the performance of the adsorption systems. In order to achieve these targets, extensive experiments and simulation works have been carried out on the compact adsorption cooling system. The results of these studies are furnished in six chapters.

A broad literature review on the development of adsorption cooling systems utilizing activated carbon as the adsorbent and alcohol as the refrigerant are introduced. Most of the studies that have been published mainly focused on the isotherms and kinetics of the activated carbon-ethanol pair where the effects of the heat exchanger construction on the thermal energy and mass removal during in working are not considered.

From above perspective, the performance of the compact adsorption cooling system which consists of one adsorbent bed which is packed with activated carbon and another heat exchanger working as evaporator or condenser depending on the operation mode are presented. The heat exchanger employed were specially designed to advance the amount of activated carbon packing density, however to decrease the mass of heat

exchanger and volume at the same time as compared to fin tube heat exchanger. The performance of the adsorption cooling system were investigated experimentally by varying the regeneration temperature ranging from 60℃ to 80℃ and evaporation temperature ranging from 5℃ to 25℃. The results presented that the maximum peak value of the cooling effect reaches about 900W with the COP of 0.59 under the evaporation temperature of 25℃ with the desorption temperature of 80℃, the adsorption and condensation temperature of 30℃.

Influence of kinetics parameters are presented by applying two types of kinetics parameters to the lumped parameter model. Validation of kinetics parameters is also conducted in comparison to the experimental data. It was revealed that the isothermal assumption kinetics parameter didn't predict the experimental results in terms of outlet temperature obviously while the non-isothermal kinetics estimated significantly better than isothermal one.

The detailed lumped parameter model was established to overcome the failure in prediction of changes in adsorption uptake during pre-cooling and pre-heating process. The energy balance of vapor refrigerant inside adsorber is considered in the modified model. It was found that the there is a pressure change which causes changes in adsorption uptake during thermal compression process. The influence of vacant volume inside adsorber against the adsorbent bed volume was also investigated to understand the importance of adsorber design. The modification model could be useful to design the adsorber properly and extended to other simulation studies such as for adsorption heat pump and adsorption thermal storage systems.

KEY WORDS: Adsorption, Chiller, Activated carbon, Ethanol, Experiment, Simulation, Renewable energy

List of Tables

List of Figures

Nomenclature

Symbols

A	area [m^2]
A^*	adsorption potential [kJ/kg]
c	specific heat capacity [J/(kg·K)]
COP	coefficient of performance [-]
D_S	surface diffusivity [m^2/s]
D_{SO}	pre-exponential constant [m^2/s]
E	adsorption characteristic parameter [kJ/kg]
Ea	activation energy [kJ/kg]
K_m	overall mass transfer coefficient [1/s]
L	latent heat of vaporization [J/kg]
m	mass flow rate [kg/s]
M	mass [kg]
n	exponent parameter of D-A equation [-]
NTU	number of heat transfer unit [-]
P	pressure [kPa]
P_{sat}	saturation pressure
R	gas constant [J/(mol·K)]
Rp	particle radius [m]
SCP	specific cooling power [W/kg]
t	time [s]
T	temperature [K]
U	Overall heat transfer coefficient [W/(m^2·K)]
w	instantaneous uptake [kg/kg]
W	equilibrium uptake [kg/kg]
W_0	maximum uptake [kg/kg]
ΔW	Adsorption capacity [kg/kg]

Subscripts

a	adsorber
ad	adsorption
b	adsorber/desorber bed

c	condenser
ca	cooling fluid (adsorber)
ch	chilled fluid
eff	effective
eth	ethanol
eva	evaporator
de	desorption
f	fin
h	hot fluid
hex	heat exchanger
l	liquid
met	metallic part
i	inlet
o	outlet
v	vapor
sh	sensible heat
S	adsorbent
w	heat transfer medium
x	evaporator or condenser

Superscripts

bed	sorption heat exchanger

Greek symbols

α	heat capacity ratio
β	volumetric thermal expansion coefficient [1/K]
η	Fin efficiency
λ	Thermal conductivity [W/(m·K)]

Chapter 1: Introduction

In this chapter, after a brief introduction concerning the background of adsorption, basic information such as adsorption phenomena, working pair, the motivation and the organization of this thesis will be given.

Since the industrial revolution at the end of the 18th century, mankind has developed its industry using fossil fuel as the main energy source. In particular, the energy consumption of mankind has increased significantly since the energy revolution in the 1960s shifted from coal to oil. As a result, civilization and standard of living have been improved by the development of science and technology, but environmental problems such as air pollution, global warming and ozone depletion have become serious. In addition, the rapid increase in energy consumption due to the recent remarkable economic development in emerging countries has tightened the fossil fuel depletion problem. In Japan, the energy policy centered on nuclear energy has been promoted with the oil shock of the 1970s. However, the risk of nuclear energy was re-recognized by the Fukushima Daiichi nuclear power plant accident in March 2011, and a fundamental review of the future energy policy has been made. In order to deal with the above-mentioned environmental problems and energy resource depletion problems, the momentum for the introduction of renewable energy is increasing recently. In the field of refrigeration and air conditioning, adsorption cooling systems are expected as a technology for utilizing renewable energy. Recent studies on adsorption cooling have mainly focused on developing more environmental friendly systems which have high energy efficiency and be able to use various kinds of energy resource such as waste heat from industrial factory and solar energy. Downsizes of adsorption system are the size which is huge by comparison with conventional cooling systems and low performance in terms of the coefficient of performance (COP) and cooling capacity. However, invention of the compact scale adsorption cooling application has been a new interest to various air-conditioning manufactures lately [1]. This progress has allowed adsorption system to get involved in the markets for home applications and commercial applications.

1.1 Theory of adsorption

Adsorption phenomena are a surface process, which is an accumulation of liquid or gas on surface of liquid or solid. The adsorption process is depicted in Fig. 1-1. Adsorption can be determined by the strength of the interaction between an adsorbents and a refrigerant. Moreover, adsorption phenomena are generally classified as chemisorption and physisorption based on the forces and interactions of refrigerant and adsorbent.

Physisorption involves a process in which fluid molecules are anchored to the walls of a solid material. The adsorbed molecules don't go through a chemical reaction, however, they easily drop energy when being fixed which means the process dealing with adsorption is the phase change from a fluid to adsorbate and it is known as exothermic process. Furthermore, this process should be reversible. Physisorption will be happened whenever gasses that can be adsorbed is put into the contact with the adsorbent surface. The interfacial layer of adsorbent can be categorized into two regions, which are the surface layer of the adsorbent and the adsorption spot in which enhancement of the adsorptive can appear. The adsorbable gas (refrigerant) is often called adsorbate. In physisorption, the adsorption event can be aroused by intermolecular forces which associate with the van der Waals forces that are considered to be equivalent to the molecular forces of cohesion.

Chemisorption is a bonding phenomenon between surface particles of a material and a substance such as gas or liquid that contacts it. The heat released from chemically adsorption will be reached about 50 to 100 kcal/mol. The physical adsorption will occur ahead of chemisorption due to the fact that the valid distance of the van der Waals force is larger than the one for the chemical reaction. Therefore, the physical adsorption will happen firstly when the refrigerant molecules get closer to the adsorbent, and will transfer into the chemical adsorption as the distance shorten.

With regards to the adsorption cooling system, majority of adsorbate molecules are classified as polar molecular gasses that can be adsorbed by means of van der Waals constrain, such as hydrocarbons, methanol and ethanol. These refrigerants are attracted by silica gel, zeolite, and activated carbon.

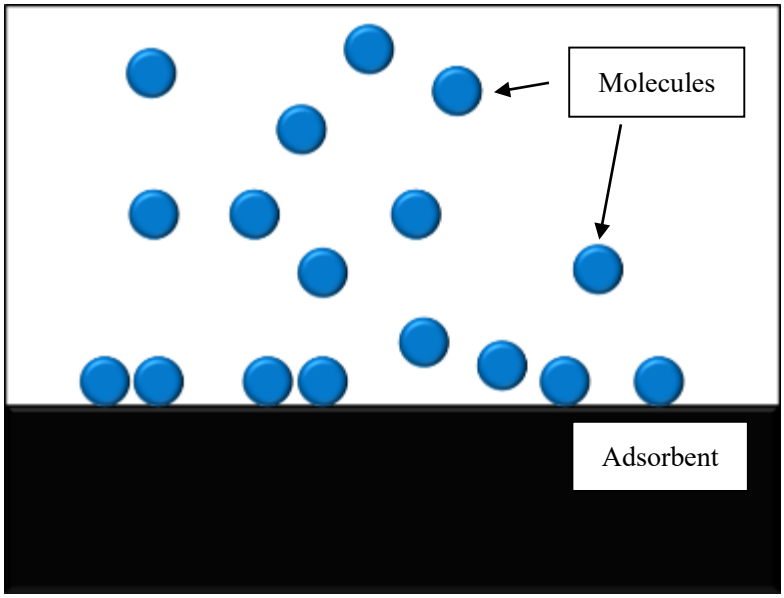

Fig. 1-1 Adsorption/desorption process

1.2 Basic adsorption cooling system

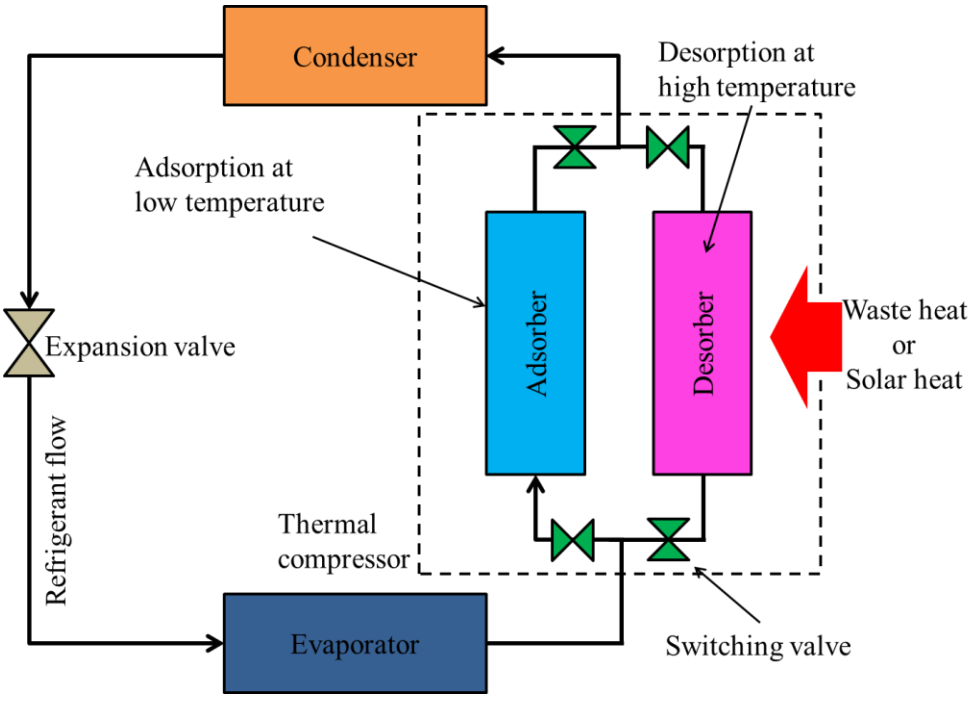

Fig. 1-2 Basic adsorption system

Fundamental adsorption cooling system has four main components which are two adsorbent beds, a condenser, an evaporator and an expansion valve. Adsorber is packed with an adsorbent material such as silica gel, zeolite, activated carbon etc. To heat up or cool down the bed, heat transfer medium is employed. It works by moving the refrigerant cyclically between sorption bed, condenser and evaporator.

Schematic diagram of fundamental adsorption system is shown in Fig. 1-2. The refrigerant desorbs from adsorbent when it is heated and adsorbs when it is cooled down. Adsorbed refrigerant at desorber will be transferred to the condenser and will be condensed. The condensed refrigerant is then transfer to the evaporator via expansion valve. The refrigerant evaporates in the evaporator, taking up the heat from chilled heat transfer medium and finally adsorbed in cooled adsorbent. The adsorption heat is removed by the cool water.

1.3 Selection of adsorbent and refrigerant pair

The choice of working pair is one of the crucial factor to gain the desirable performance. The adsorption characteristics of working pairs greatly relies on the reactivity of the surface, the surface area, the temperature and pressure of adsorbent. System performance is strongly dependent on choice of working pair. The choice criterion of adsorbent and adsorbate relies on a numbers of important requirements [2][3][4][5].

1.3.1 Selection of adsorbent

What are the crucial considerations influencing the choice of a desirable adsorbent?

- Large uptake of refrigerant
- Non-toxic and non-corrosive
- High packing density
- High thermal conductivity
- High heat of transformation of adsorption
- Reversibility and durability for numerous cyclic operation
- Availability
- low cost

The basic sorts of adsorbents widely used for adsorption system are summarized in Table 1-1. It can be categorized into mineral adsorbents such as silica gel and zeolite,

carbon adsorbents such as activated carbon fibers and powders and other adsorbents.

Table 1-1 Basic types of adsorbents [6]

Mineral adsorbents	Carbon adsorbents	Other adsorbents
Silica gel	Activated carbon powders	Synthetic polymers
Clay minerals	Activated carbon fibers	Composite adsorbents
Oxides of metals	Molecular carbon sives	Complex
Hydroxides of metals	Mesocarbon microbeads	mineral-carbons,
Pillared clays	Fullerenes	X-elutrilithe; X=Zn, Ca
Activated alumina	Heterofullerenes	Expanded graphite
Porous clay hetero-strictures (PCHs)	Carbonaceous nanomaterial	Mixed sorbents
Zeolite	Surface treated activated Carbon	MOF (metal organic framework)

1.3.2 Choice of refrigerant

What are the requires considerations influencing the choice of a desirable refrigerant?

- Low global warming potential
- Low ozone depletion potential
- Non-toxic, non-corrosive and non-flammable
- High refrigerant latent heat
- Small molecular size in order to trap on the adsorbent
- The refrigerant must not shape a solid phase with adsorbent pair
- The refrigerant should be much more evaporative than the adsorbent
- Compatibility with adsorbent in terms of bond (polar or non-polar)
- Moderate working pressure in order to prevent the system from getting bigger
- Thermally durability with the adsorbent

The refrigerant generally employed for adsorption systems are listed in Table 1-2. The physical properties, safety and environmental data for each refrigerant also can be seen. There are a bunch of refrigerant that could be utilized in the adsorption system even though they don't perfectly meet the requirements mentioned above. However, many of these refrigerants listed in Table 1-2 have been studied in this field to find out the best working pair in order to achieve as many requirements as possible.

Table 1-2 Summary physical, safety and environmental data for some refrigerants (ASHRAE Standard 34 designation)

Compositional group	Refrigerant	Chemical formula	NBP (°C)	Pc (MPa)	Safety group	ODP	GWP
CFCs	R-11	CCl_3F	23.7	4.41	A1	1	4600
	R-12	CCl_2F_2	-29.8	4.14	A1	0.82	10600
	R113	CCl_2FCClF_2	47.6	3.39	A1	0.9	6000
	R114	$CClF_2CClF_2$	3.6	3.26	A1	0.85	9800
	R115	$CClF_2CF_3$	-38.9	3.12	A1	0.4	7200
HCFCs	R-22	$CHClF_2$	-40.8	4.99	A1	0.34	1700
	R-123	$CHCl_2CF_3$	27.8	3.66	B1	0.012	120
	R-124	$CHClFCF_3$	-12	3.62	A1	0.026	620
	R-141b	CH_3CCl_2F	32	4.25		0.086	700
	R-142b	CH_3CClF_2	-9	4.12	A2	0.043	2400
HFCs	R-23	CHF_3	-82.1	4.84	A1	0.034	1700
	R-32	CH_2F_2	-51.7	5.8	A2	0	550
	R-125	CHF_2CF_3	-48.1	3.63	A1	0	3400
	R-134a	CH_2FCF_3	-26.1	4.06	A1	0	1300
	R-143a	CH_3CF_3	-47.2	3.78	A2	0	4300
	R-152a	CH_3CHF_2	-24	4.52	A2	0	120
	R-227ea	CF_3CHFCF_3	-15.6	2.98		0	3500
	R-236fa	$CF_3CH_2CF_3$	-1.4	3.2	A1	0	9400
	R-245fa	$CHF_2CH_2CF_3$	15.1	4.43	B1r	0	950
Natural refrigerant	R-290	$CH_3CH_2CH_3$	-42.2	4.25	A3	0	20
	R-600	CH_3-CH_2-CH_2-CH_3-butane	-0.5	3.8	A3	0	~20
	R-600a	$CH(CH_3)_2$-CH_3	-11.7	3.64	A3	0	~20
	R-717	NH_3-ammonia	-33.3	11.34	B2	0	<1
	R-718	H_2O-water	100	22.06	A1	0	<1
	R-729	Air	-194	3.77		0	0
	R-744	CO2-dioxide	-78.4	7.38	A1	0	1

1.4 Adsorption/Refrigerant pairs for adsorption cooling applications

As mentioned previous section, choice of working pair is strongly important in the adsorption refrigeration system. It is said that it doesn't exist the working pairs that completely satisfy the requirements mentioned in the previous adsorbent and refrigerant selection. However, there are several of typically used working pairs which almost satisfy the requirements. In this section, working pairs generally used in the adsorption system such as zeolite-water pair, silica gel-water pair and activated carbon-ammonia pair will be discussed. As for activated carbon-alcohol pair, it will be introduced more deeply in chapter2 since activated carbon-ethanol pair is main working pair and used for my research.

1.4.1 Zeolite/Water pair

Zeolite is a sort of silicate crystal consisted of alkali or alkali soil. Roughly 40 kinds of natural zeolites exist, and the primary sorts utilized in the adsorption application are chabazite, sodium-chabazite, cowlesite and faujasite. Nearly 150 kinds of zeolite can be artificially incorporate whose molecular sieves own micro pores with uniform size, and extensive shape can be gained by various technique.

A zeolite/water system for refrigeration and solar air-conditioning has been investigated over the past decade [7]. Wang, Xia and Wu (2006) [8] studied design and performance prediction of an adsorption cooling system utilizing zeolite-water pair. The system provides 8-12℃ chilled water for the fan coil powered by 350-400 ℃ exhaust gas which was supplied as regeneration source. They reached the refrigeration power of 5kW, COP of 0.25 and SCP of 200 W/kg with the cycle time of 1320s. Vasta et al (2012) [9] proposed a mobile adsorption cooling system utilizing zeolite-water pair. They employed two adsorption bed and reached the COP of roughly 0.4 whilst the SCP was approximately 600 W/kg. Zhang (2000) [10] introduced an adsorption cooling system using zeolite-water pair that is driven by waste heat obtained from a diesel engine. Developed system could reach the SCP and COP of 2.57 W/kg and 0.38 respectively. Li et al (2014) [11] studied the performance of a zeolite FAM Z01/water pair adsorption chiller. It is reported that they obtained the optimum COP at low regeneration temperature of about 65℃.

1.4.2 Silica gel/Water pair

The silica gel is a sort of formless combined silica which is rigid. The specific surface area and the pore diameters of silica gel are about 100-1000 m^2/g and 2-3 nm and 0.7 nm. (D. C. Wang *et al.*, 2010). The study of adsorption system using silica gel-water pair has been carried out mainly in Japan from in the 1980s because of its suitability for low grade thermal energy source. Sakoda et al. (1984) [12] presented a transient simulation model using silica gel/water pair for solar powered adsorption chiller. Suzuki (1986) [13] also investigated solar driven adsorption system with a COP of 0.2 using solar collector. Saha et al. (1995) [14] analyzed the effects of operating conditions on the cooling capacity and COP of an adsorption system employing silica gel/water pair. They found that hot water temperature of 50℃ is only viable when cooling water temperature of less than 25℃. Chua et al. (2001) [15] studied a lumped model and distributed model of an adsorption cooling system using silica gel/water pair. They concluded that prediction has a good agreement with experimental results. Chen et al. (2010) [16] established a small scale silica gel-water pair adsorption refrigeration system that doesn't possess the vacuum valves. They achieved the COP of 0.49 and the cooling power of 9.60kW by using regeneration temperature of 82℃.

1.4.3 Activated carbon/Ammonia pair

Activated carbon is known for its possessing huge surface area per unit volume. Activated carbon is a material which is produced from carbonaceous source materials, such as coconuts, peat, wood, coal and lignite. The goodness of ammonia as refrigerant is its high latent heat of about 1365 kJ/kg at 30℃, however, it has the drawbacks of toxicity and corrosive. It is reported that the requirement of adsorption heat for carbon-ammonia pair is about 2000-2700 kJ/kg [17]. Tamainot-Telto (2009) [18] reported adsorption chiller applications employing carbon-ammonia pairs. The simulation was executed for 26 sorts of activated carbon-ammonia pairs with three cycles and with a regeneration temperature of 100℃. They found the cooling effect was nearly 66 MJ/m^3 with the COP of 0.45 and 151 MJ/m^3 with the COP of 0.61 for ice-making and refrigeration respectively. Metcalf and Tamainot-Telto (2012) [19] proposed the optimal cycle selection in carbon/ammonia pair adsorption cycles. It is reported that they reached the cooling power of 200 W/kg and the COP of 0.4.

1.5 Objective and scopes of the present thesis

There are two main objectives of this work. One is to investigate the performance of a compact adsorption cooling system employing activated carbon/ethanol pair. This system may contribute to in the development of downsize of the heat exchanger with requirements for the cooling system. The other objective is to improve the lumped parameter model witch has been used for simulation works. By modifying the model, the more detail simulation can be obtained and new approach allows us the optimizing the size of the system. The scopes of the thesis are:

(1) To investigate the effect of heat source temperature as well as chilled fluid temperature on the performance of a compact adsorption cooling system applying activated carbon-ethanol pair.
(2) To investigate the influence of kinetics parameters when it is used in the simulation by comparing experimental results.
(3) To validate the lump parameter model for the ACP-ethanol pair between simulation and experiments
(4) To establish improved simulation model which gives more detailed dynamic behavior information of adsorption cooling system

1.6 Thesis outline

This thesis includes seven chapters which describe the study of the compact adsorption cooling system employing activated carbon-ethanol pair from both experiments and simulation perspective. The ACP-ethanol working pair was selected as it has a high adsorption capacity of activated carbons against alcohol. Variety of experiments and simulation works have been performed to find out the effect of operational conditions and heat exchanger design on the performance and new simulation model was successfully established to predict more precisely and in more detail. Following are the brief explanation of the contents for each chapter.

Chapter 1 provides a scientific background about the adsorption phenomenon and the operational theory of the adsorption cooling system. A literature review on adsorbent/adsorbate pairs and systems were also presented. The research objective and scope has also been introduced in this chapter.

Chapter 2 deals with the overall review on the past efforts of the adsorption system using activated carbon as the adsorbent material and ethanol as refrigerant. According to preliminary works, numerous methods and procedures can be employed to improve the activated carbon properties. Literature reviews on the application of the lump parameter model to predict the performance of the system are also presented. To enhance the system performance, several studies have been investigated so far. Unfortunately, based on the previous research, the performance still does not meet the minimum target requirements. In addition, the adsorption system has some disadvantages of bulkiness and cost. Since one of our targets is to install the adsorption cooling system into vehicle to utilize the waste heat as regeneration energy, the operating conditions and configurations of the system should be optimized to make it to be commercialized.

Chapter 3 describes the experimental methods, apparatus, equipment and procedures which are used and applied in this research to find out the performance of one bed of adsorption cooling system. The adsorption heat exchanger used is packed with activated carbon (MaxsorbIII) whose amount is 115g combining with some binder which helps support the activated carbon between fins of the heat exchanger as well as increase the thermal conductivity a little bit. The performance of a compact adsorption cooling system has been experimentally studied by employing various heat source temperatures ranging from 60℃ to 80℃. The influences of flow rate of heat transfer medium are also investigated and discussed in this section.

In chapter 4, the mathematical modeling for overall thermal conductance is presented. Generally, the overall thermal conductance used in the simulation is not calculated mathematically. Here, the model of UA value for a flat fin-tube adsorbent bed is developed to estimate it and assessed in comparison to that of taken by experimental results. It was found that the estimation model could predict well the overall thermal conduction for the operating conditions used in this study.

Chapter 5 presents investigating the influence of kinetics parameters when they are used in the simulation. There are two types of kinetics parameters for activated carbon/ethanol pair that has been investigated. One of which considers non-isothermal condition while the other one assume it as an isothermal condition. Here, a lumped parameter model is used as simulation model to predict the performance of the adsorption system. By predicting the transient behavior of the adsorption cooling system, its influence is revealed. Validation of two kinetics parameters is also discussed

by comparing it with experimental data. It was found that the non-isothermal kinetics parameters were desirable as compared with the one calculated by assuming the isothermal condition.

Chapter 6 introduce the detailed simulation model which takes into account the pressure change of refrigerant inside adsorber during pre-cooling and pre-heating (pressurization and depressurization) which have been neglected in the common lumped parameter model. The effect of modified mathematical model was discussed by comparing each model and experimental results. Since the experimental results during pre-cooling and pre-heating are not measured due to the limitation of facilitation, it is difficult to validate the modified model, however, it is found that there is a pressure change which causes changes in adsorption uptake during thermal compression process. The model validation will be carried out in comparison to experiment where the system consists of the two adsorbent beds, the evaporator, the condenser and expansion valve in the future work.

Overall conclusion of this study is given in Chapter 7. As a general conclusion, the present study has found that the compact adsorption cooling system using activated carbon-ethanol pair is a promising technology as it can reach the COP of nearly 0.6. From the simulation aspect, improved lumped parameter model has predicted the dynamic behavior of the adsorption system more in detail.

Chapter 2: Overview of adsorption cooling system based on activated carbon – alcohol pairs

In this chapter, the overall review of adsorption cooling system especially using activated carbon as adsorbent and alcohol as refrigerant will be conducted. As mentioned before, adsorption refrigeration and heat pump are one of environmentally benign technologies due to utilizing non-harmful substances and it can be powered by low thermal energy source such as waste heat from industry and solar thermal energy. In the present status, silica gel-water pair and zeolite-water pair have been employed in the commercialized adsorption refrigeration system for small scale applications while many researches on activated carbon have been carried out to find out the promising candidate for commercialize applications [20]. Several of refrigerants have been applied with activated carbon so far, such as CO2 [21], ammonia [22], HFCs [23], methanol [24], ethanol [25]. It is reported that the performance simulation of the activated carbon-ethanol pair was found to be promising because the specific cooling power of the activated carbon-ethanol pair was greater than that of silica gel-water pair [26]. According to their study, the activated carbon-ethanol pair require a higher regeneration temperature source in order to achieve the maximum COP against the regeneration temperature compared to that of silica gel-water pair.

2.1 Alcohol as refrigerant

It can be said that working pairs of adsorbent-refrigerant are very important factor as it determines the configuration of the system and the system performance. According to Wang et al. (2009) [27], the refrigerant should possess the quality of large latent heat per volume, saturation vapor pressure, good thermal stability and a good affinity with the adsorbent.

Generally, refrigerants are categorized into absolute pressure refrigerants and vacuum refrigerants. Alcohol refrigerants such as ethanol and methanol which have been used as refrigerant in the adsorption system are performed in vacuumed pressure and these refrigerants are generally employed as refrigerant in association with the activated carbon power or activated carbon fiber. It is reported that ethanol is found to be suitable refrigerant for activated carbon where various of refrigerant are available as working pair with activated carbon [28]. Methanol has been widely investigated in adsorption

system of which properties are similar to the one of ethanol while it is not a non-toxic refrigerant which ethanol is. Physical properties of the alcohol refrigerant are listed in Table 2-1.

Table 2-1 Physical properties of alcohol refrigerants

Alcohol refrigerant	Chemical formula	Molar mass [g/mol]	Density [kg/m^3]	Boiling point [°C]	Latent heat of vaporization [kJ/kg]
Ethanol	C_2H_5OH	46	789	79	789
Methanol	CH_3OH	36	791	65	791

2.2 Activated carbon as adsorbent

Activated carbon has been widely utilized for decades, has become extensively adaptable adsorbent because of its flexibility to be modified and highly developed internal surface area and porosity. The activated carbon will be distinctive if the original carbonaceous material or the manufacturing technique is different. Activated carbon that has high surface area is widely used in various fields, such as fuel gas storage [29], wastewater treatment [30], catalysis [31]. The adsorption capacity is one of the crucial properties which is defined by the pore size distribution and influenced by the surface functionality. Therefore, it is extremely important to comprehend the extensive factors that has an effect on the adsorption capacity of activated carbon. Many studies have been done on the modification of specific physical chemical attributes to improve their compatibility toward metal, organic/inorganic species present in aqueous solutions. Ordinarily, the adsorption capability enhances with specific surface area because of the availableness of adsorption positions, whereas the pore diameter and micropore distribution are correlated to the synthesis of the activated carbon, the degree of activation, the type of raw material and the frequency of regeneration [32].

2.3 Isotherm works of adsorbent-refrigerant

The isotherm study is the first step to determine the potential of the adsorbent-refrigerant pair in the commercialized applications. The adsorption itself refers to the amount of refrigerant on the adsorbent as a function of gas phase pressure at a constant temperature by means of an isotherm. Majority of the gas and/or vapor

adsorption isotherms are classified with the help of IUPAC classification scheme which has six types of isotherm for solid/gas equilibrium. Isotherm curve classifications can be seen in Fig. 2-1. Isotherms of ① are commonly true for microporous adsorbents for subcritical and supercritical conditions. Isotherms of type② can be found in adsorbents possessing an extensive range of pore size with either mono or multi-molecular adsorption layers. Type③ is not regular and they include capillary condensation besides the multi-molecular adsorption layer. Type④ deals with the shaping of both surface layers on the adsorbents possessing the larger pore design against the diameter of refrigerant molecule. Isotherms of ⑤ can be detected on the adsorbents that possess strong force obtained by intermolecular attraction. The final type⑥ indicates that the adsorption could have one or more steps.

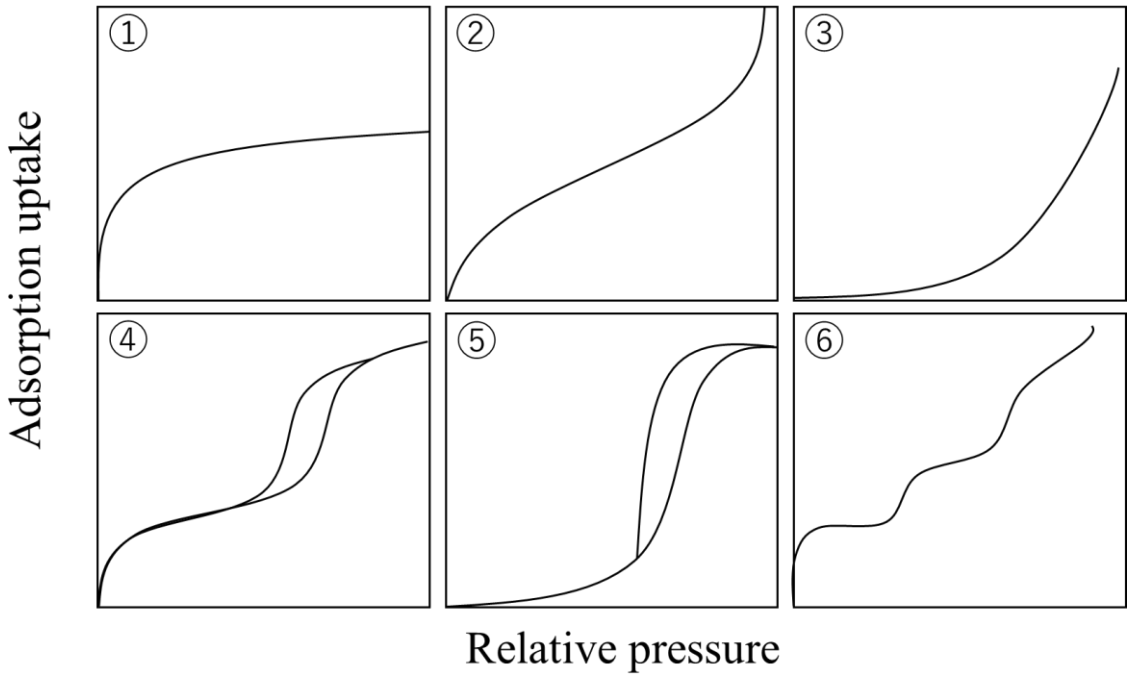

Fig. 2-1 The IUPAC classification of adsorption isotherm for solid/gas euqilibrium

Adsorption equilibrium uptake of ethanol onto an adsorbent, namely MaxsorbIII, has been investigated experimentally [33]. The experimental work found that MaxsorbIII is able adsorb up until 1.2 kg of ethanol per kilogram of adsorbent and it was shown that MaxsorbIII-ethanol pair adsorption cycle can perform a specific cooling effect around 420 kJ/kg by regeneration heat source temperature of 80℃.

Previous study by El-Shrkawy et al. (2015) [34] presented a new treated activated carbon as adsorbent with ethanol as refrigerant. The researcher alleged that the adsorption uptake of ethanol onto the presented spherical phenol resin based adsorbents are remarkably larger than the adsorption capability of ethanol onto any other developed adsorbent.

Recent study by Miyazaki et al. (2017) [35] found the optimum pores size of activated carbon by means of a grand-canonical monte carlo (GCMC) simulation, which was 1.6 nm. Moreover, they introduced original new breakthrough activated carbon, namely spherical activated carbon (SAC) which has a total surface area of 3000 m^2/g and average pore width of 1.6 nm. According to their theoretical study, a thermodynamic cycle analysis described that the effective adsorption was largely improved by the new activated carbon compared with that of a commercialized ACP.

2.4 Component analysis and cycle performance work

The second step is the final validation of the adsorbent-refrigerant performance such as component analysis and cycle performance test. At this stage, selected working pair is applied to the system that consists of the adsorber/desorber, evaporator, condenser and heat source such as exhaust gas, solar energy and waste heat from industry. The cycle conditions test can be investigated by both experiment and simulation. Over several years, many researchers have tried to study the component analysis or cyclic performance of adsorption system by means of experimental or simulation. Some works will be introduced and compared in the following section.

2.4.1 Lump model

This dissertation works includes the validation of lumped parameter model and modification of previous model for the activated carbon – ethanol pair. The lumped parameter model to simulate the performance will be explained in Chapter 5 and improved model will be discussed in Chapter 6. The performance of adsorption refrigeration is defined by heat and mass transfer in the adsorber. Yong and Sumathy [36] discussed the available simulation model which are classified into three groups as: (a) thermodynamic model, (b) lumped parameter model, (c) heat and mass transfer model. According to their study, there was no incontrovertible proof that which model was superior. For this thesis works, the lumped parameter model is employed due to its

simplicity resulted in short calculation time with good accuracy. Several recent researches on using lumped model as a simulation tool are summarized in Table 2-2.

2.4.2 Distributed model

Recent some studies of the activated carbon-alcohol pair adsorption cooling system based on distributed model are listed in Table 2-3. Ramji et al. (2014) [41] investigated the effect of wall thickness of adsorber on regeneration temperature and cooling effect by means of CFD as the simulation technique. The author employed the fluid flow modeling reported in [44] to solve the Navier-Stokes equations. They described that CFD simulation results showed the reasonable agreements with the experimental data. The cooling power of 0.52 kW and COP of 0.27 were achieved at the regeneration temperature of 120℃ with the wall thickness of 20mm.

Table 2-2 Lumped model studies for cycle performance simulation

Adsorbent-refrigerant pair	Description	System parameter	System performance
Silica gel-water [37]	Input parameter is from experimental studies by Wang [38]	Hot water inlet temperature/Chilled water inlet temperature/Mass of adsorbent:75.6℃/30℃/75.6kg	COP:0.45 SCP:120.8 W/kg
Zeolite 13x-water [39]	Input parameter was taken by themselves	Hot water inlet temperature/Coo water inlet temperature/Mass of adsorbent:80℃/10℃/45kg	COP:0.41 SCP:45 W/kg
Silica gel–water, CaCl2-in-silica gel–water, AQSOA-Z01–water, SOAZ02–water [40]	CaCl2 in silica gel–water gives the highest performance	Hot water inlet temperature/Mass of adsorbent : 80 °C/8 kg	COP:0.39 SCP:3775 W/kg

Table 2-3 Distributed model works on component analysis and cycle performance test of activated carbon-alcohol pairs

Adsorbent-refrigerant pair	System parameter	System performance	Remarks
Solidified activated carbon-methanol [41]	Desorption temperature /Mass of adsorbent: 110°C/60 kg	COP: 0.125 SCP: 16.3 W/kg	Cycle experiment
Granular palm activated carbon-methanol [42]	Desorption temperature /Adsorption temperature/Mass of adsorbent: 90°C/40°C/800 g	COP: 0.27 SCP: 324.78 W/kg	CFD simulation
Granular palm activated carbon-methanol [43]	Desorption temperature /Adsorption temperature/Mass of adsorbent: 120 °C/40°C/800 g	COP: 0.19 SCP: 396.6 W/kg	Cycle experiment

2.4.3 Cyclic experimental study on activated carbon-alcohol pair

Influence of heat and mass transfer on the performance of activate carbon-methanol pair adsorption system were presented by Wang et al. (2003) [41]. They investigated the three types of adsorber categorized based on size and shape. They found that the highest COP and specific cooling power achieved were 0.125 and 16 W/kg respectively with solidified adsorbent bed and optimum refrigerant channel design.

The system performance of activated carbon fiber-ethanol pair was studied experimentally by Saha et al. (2006) [45]. The adsorption system they fabricated has a plate fin tube heat exchanger adsorber, an evaporator and a condenser. They came to a conclusion that the plate-fin reactor for ACF-ethanol pair appeared to be advisable for adsorption cooling system. They also reported that it would be desirable to have a lightweight adsorbent bed to reduce the sensible heat transfer losses.

Adsorption air-conditioning driven by exhaust heat from auto mobile was proposed by

Lim and Abdullah (2010) [43]. They selected the palm-derived activated carbon as adsorbent and methanol as refrigerant. From their achievements, the COP and SCP were achieved about 0.19 and 396.6 W/kg respectively. However, they pointed out that further enhancement of efficiency and the associated control system for auto mobile application was required.

2.4 Conclusions

This chapter has explained an overview on the development of an adsorption cooling system based on activated carbon-alcohol pair. From the preliminary studies, many methods and techniques can be applied to improve the properties of activated carbon. As for the current conditions, lumped model simulation have showed greatly favorable outcomes. As for the distributed simulation and experimental studies, it was ensured that the activated carbon was the right adsorbent material and adsorption cooling power was highly competitive. The reason for low performance were due to the periodic heating and cooling which caused the unnecessary energy losses, and low heat transfer rate of the activated carbon during adsorption/desorption process. Thus, it is required to conduct a comprehensive analysis based on experimental conditions, i.e. heat transfer fluid temperature and cycle time.

Chapter 3: Experimental investigation with one bed adsorber

Our laboratory project has been trying to develop a compact adsorption cooling system using activated carbon-ethanol pair [46]. Operating conditions such as regeneration (desorption) temperature, the flow rate of heat transfer fluid and chilled water temperature play am essential role in order to achieve the superlative performance for a compact adsorption cooling system. Since one of our targeted applications is to install the adsorption cooling system into a vehicle using the exhaust waste heat, the performance such as COP/SCP and how much of adsorption heat or cooling capacity the adsorption cooling system utilizing activated carbon-ethanol pair can generate should be investigated. In this works the performance of the adsorption cooling system employing activated carbon and ethanol pair has been experimentally examined by varying the regeneration temperatures ranging from 60℃ to 80℃. According to the theoretical studies, it was revealed that the adsorption heat value increase with increasing the regeneration temperature. This chapter deals with an actual adsorption cooling system whose performance was studied. Note here that, the experiments were not conducted in cyclic condition since this works focus on finding out the transient response and the amount of heat rejection and cooling capacity during the adsorption process.

3.1 Experimental apparatus

The schematic diagram and pictorial view of the compact adsorption cooling system are shown in Fig. 3-1 and Fig. 3-2. The system consists of a adsorber (1) which has single adsorbent bed (5) and evaporator/condenser (2) which has a heat exchanger operating as condenser or evaporator (6) with thermostats (3) for the proper manage of the cooling and heating source. (4) represents the flow meters. The adsorber bed is packed with activated carbon (MaxsorbIII) the amount of which is 115g with some binder which helps adsorbent attach to the heat exchanger easily. Ethanol is used as the liquid refrigerant and the temperature of the components are maintained to be constant by thermostat. The heat transfer medium flow going through the heat exchanger is controlled by valves and measured by flow meters. The parameters are gathered by data loggers from the measuring sensors and the measuring points of temperature, pressure and flow rate are detailed in Fig. 3-1 as well.

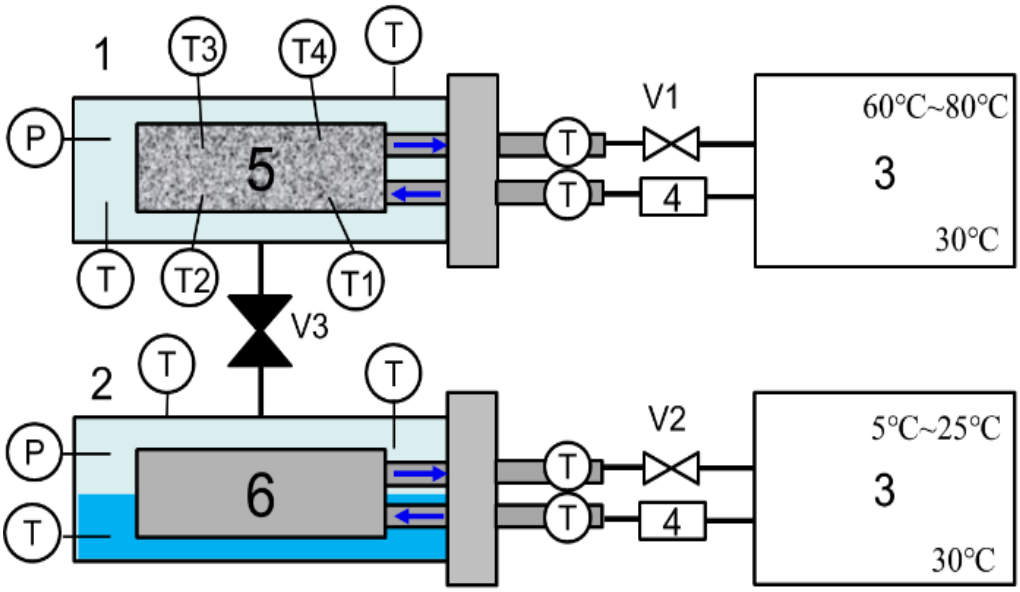

Fig. 3-1 The schematic diagram of experimental setup

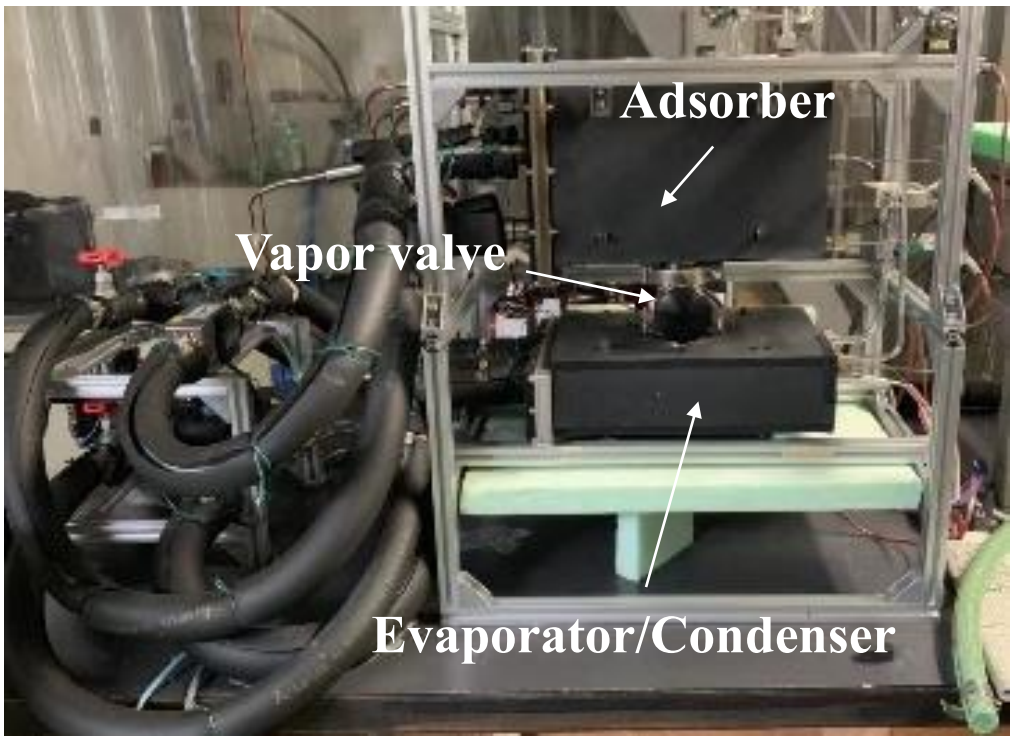

Fig 3-2 The pictorial view of experimental apparatus

3.1.1 Adsorber

There are many types of heat exchanger which have been used as adsorber as depicted in Fig. 3-3. Four different types of adsorbent bed were generally used in many experimental researches of adsorption cooling system. The requirement of heat exchangers for adsorber bed is to advance the thermal transfer surface area between the heat transfer medium and particles of adsorbent.

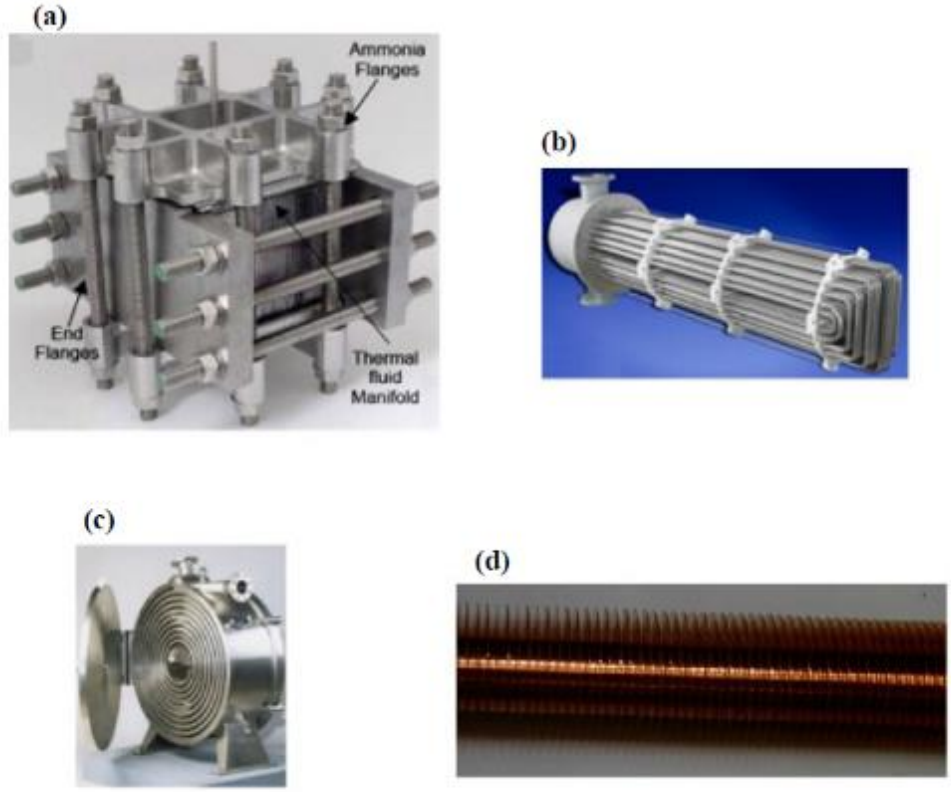

Fig. 3-3 A series of heat exchanger types utilized as adsorbent bed. (a) Plate heat exchanger [47], (b) Hairpin [48], (c) Spiral plate [49] and (d) Fin tube [50]

The heat exchanger employed in the adsorber for this works is a corrugated fins and tube heat exchanger which is constructed from aluminum and composed of thin fins and 24 possess of channel tubes. The specifications such as physical features and parameters of the corrugated fins and tube heat exchanger are listed in Table 3-1. The schematic views of the heat exchanger and pictorial view of heat exchanger are shown in Fig. 3-4 and Fig. 3-5 respectively.

Table 3-1 Specifications of heat exchanger for adsorber

Description	Value
Channel tube thickness [mm], δ	1.5
Channel tube height [mm], h_c	29
Channel tube length [mm], l_c	203
Fin height [mm], h_f	5.28
Fin pitch [mm], p_f	0.95
Fin thickness [mm] , t_f	0.07
Number of pitch of fins [-], N_f	214
Number of fin columns [-], N_{fc}	25

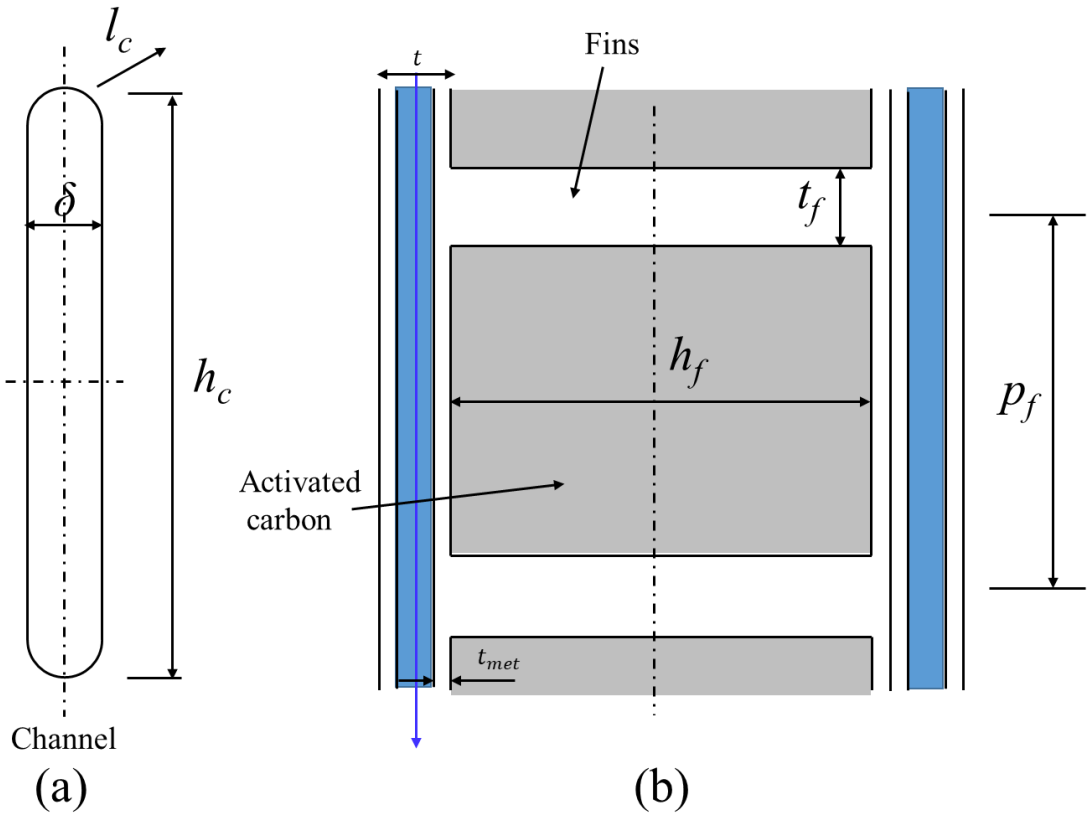

Fig. 3-4 (a) Cross-section of tube, (b) detailed view of fins

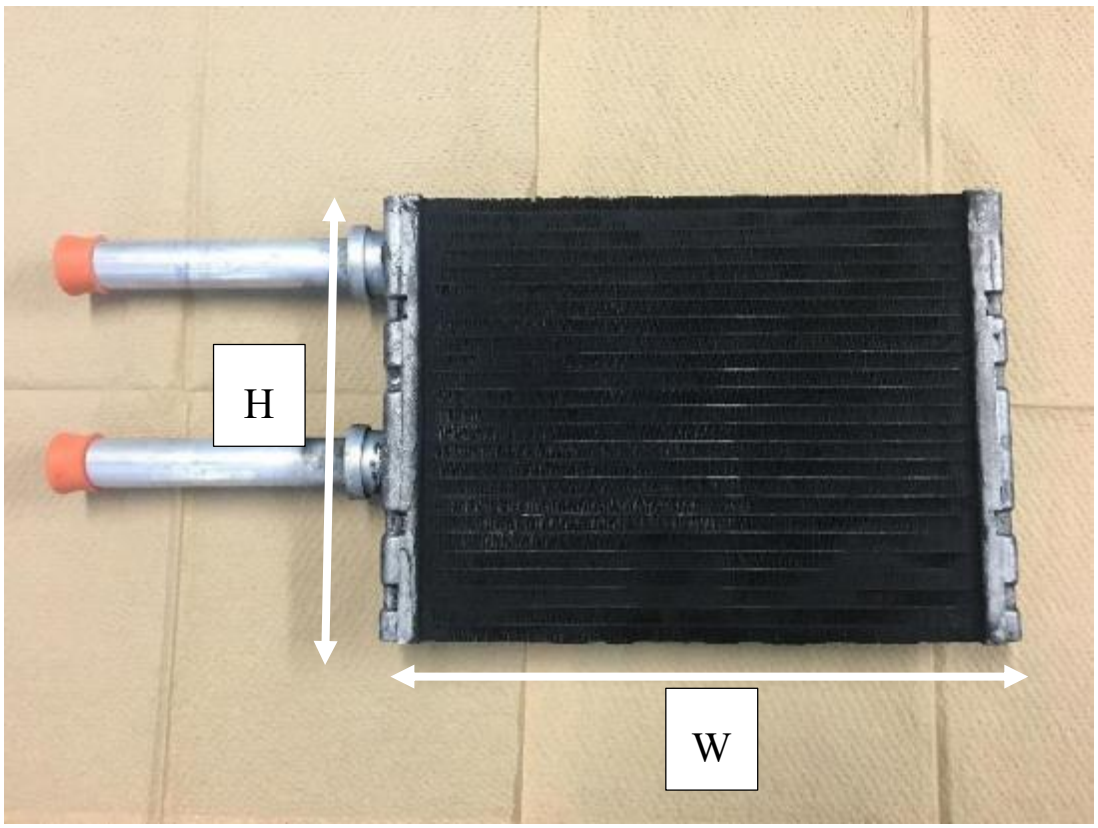

Fig. 3-5 Pictorial view of adsorber heat exchanger packed with activated carbon

Long life coolant fluid is selected as the heat transfer fluid used in the heat exchanger for both the adsorber and evaporator/condenser. The heat exchanger material is an aluminum alloy. Aluminum material is quite attractive in the HVACR (heating, ventilation, air-conditioning and refrigeration) heat exchanger production in terms of flexibility of shape, the cost efficiency, reduction on weight in comparison to copper or stainless steel. In order to achieve the small scale applications such as residential and automobile cooling system, the material having above-mentioned pros is desirable.

In order to attach the adsorbent (activated carbon) easily to the heat exchanger, some binder which is made from kinds of urethane resin is mixed with activated carbon to make it sturdy and last the life-time longer.

The size and volume of heat exchanger is shown in Table 3-2. The amount of activated carbon and binder packed for this research are also listed in Table 3-2.

Table 3-2 Information of base heat exchanger for adsorber

Description	Value
Core size W×D×H [mm]	203×166×29
Volume [cm^3]	1166
Packed adsorbent volume [cm^3]	701
Heat capacity [J/K]	493.7
Amount of activated carbon [g]	113.3
Amount of binder [g]	17.0

3.1.2 Adsorbent

The activated carbon namely Maxsorb III used in this research is manufactured by Kansai Thermochemical Co. The properties of activated carbon are listed in Table 3-2.

Table 3-3 Physical properties of activated carbon

Parameter	Value
Surface area [m^2/g]	3045
Thermal conductivity [W/mK]	150
Average particle diameter [μm]	70
Microspore volume [cm^3/g]	1.7
Average pore width [nm]	1.12

3.1.3 Refrigerant

The refrigerant used as adsorbate in this study is an ethanol (C_2H_5OH) with 99.5% purity which is created by Kishida Chemical Co., Ltd. The amount of ethanol is about 0.75L.

3.1.4 Heat transfer medium

The heat transfer medium applied in this research was antifreeze fluid which is usually used inside the vehicle system. The antifreeze fluid called LLC (Long Life Coolant) manufactured by Nissan Motor Co., Ltd. is used as heat transfer medium in this research. Due to its possessing the long term freeze prevention properties, it is usually used in the

vehicle system. The characteristics of LLC are shown in Table 3-4.

Table 3-4 Characteristics of LLC

Type	Pre-diluted type of non-amine
Based glycol	Ethylene glycol
Freezing temperature	-36℃
Density [kg/m^3]	$-2\times10^{-6}T^2\times-4\times10^{-4}T+1.0848$
Specific heat capacity [kJ/kg K]	$\{0.00489T+3.373\}\times10^3$

The specific heat capacity of LLC was measured experimentally of which detailed procedure can be seen in Appendix A. T in the above table is in Celsius scale.

3.1.5 Evaporator and Condenser

As mentioned before, there are two heat exchanger used in this research. One plays a role in adsorbent bed, the other one works as evaporator or condenser depending on operation mode. Specifically, it works as the evaporator with connecting to the adsorber during adsorption process while it performs as the condenser with connecting to the adsorber during desorption process (Fig. 3-6).

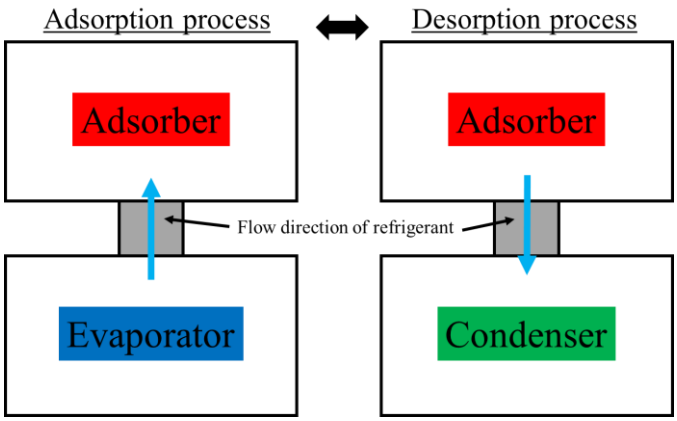

Fig. 3-6 Explanation of switching the evaporator/condenser

The specifications such as physical dimensions and parameters of the heat exchanger used as the evaporator/condenser are listed in Table 3-5. The size and volume of heat exchanger is also shown in Table 3-6.

Table 3-5 Specifications of heat exchanger for evaporator/condenser

Description	Value
Channel tube thickness [mm], δ	1.5
Channel tube height [mm], h_c	29
Channel tube length [mm], l_c	203
Fin height [mm], h_f	5.28
Fin pitch [mm], p_f	0.95
Fin thickness [mm] , t_f	0.07
Number of pitch of fins [-], N_f	214
Number of fin columns [-], N_{fc}	25

Table 3-6 Information of base heat exchanger for evaporator/condenser

Description	Value
Core size W×D×H [mm]	203×166×29
Volume [cm^3]	1164
Packed adsorbent volume [cm^3]	701
Heat capacity [J/K]	493.7

3.2 Measurement method

3.2.1 Measurement item

Some thermocouples are installed to measure the temperature, pressure gauges are used for mearing the pressure inside adsorber and evaporator/condenser and electromagnetic flow meter are used for measuring the flow rate of heat transfer medium (LLC). The data logger is used for collecting all data from each measurement apparatus.

3.2.2 Temperature measurement

T-type thermocouples manufactured by Toyo Netsu Kagaku Co., Ltd. were installed to measure the fluid temperature flowing through both heat exchangers, the adsorbent bed

temperature and the adsorber tank and the evaporator/condenser tank. K type thermocouple manufactured by Yamari Industries is used for the ambient temperature measurement. The details of thermocouple calibration are presented in Appendix B. The temperature inside the heat exchanger are collected using T type thermocouples at the center part of the fluid source inlet and outlet from adsorbent heat exchanger and evaporator/condenser heat exchanger. 4 points temperatures of adsorbent bed are measured by T type thermocouples and temperatures of each tank are also measured. Temperature of internal gas inside adsorber are measured at bottom, middle and top part of adsorber and temperature of refrigerant vapor and liquid inside evaporator/condenser are also collected as well. The location of each thermocouple are illustrated in Fig. 3.7

3.2.3 Pressure measurement

The inner pressure of the adsorber and evaporator/condenser were measured by high precision small pressure gauge manufactured by Yokogawa Electric Corp. type FP201A. The measurement range is 0 ~ 50 kPa and measurement accuracy is ± 0.25% of full scale. The detailed pressure gauge is shown in Table 3-7.

3.2.4 Flow measurement

The flow rate of adsorber and evaporator/condenser were measured by the volume flow rate manufactured by KEYENCE Co. electromagnetic digital flow sensor type FD-MA1A. The measurement range is 0 ~ 10 L/min and the measurement error is ± 0.5%.

3.2.5 Temperature control

Temperature of heat transfer medium for adsorber is controlled by the thermostat manufactured by ADVANTEC type TBF320DA while the thermostat for evaporator/condenser is type LV-600 manufactured by ADVANTEC.

3.2.6 Data collection

Voltage output from each measurement devices are gathered into data logger manufactured by Yokogawa Electric Corp. type MX100. Data such as temperature, pressure and flow rate are calculated by software called MXLOGGER.

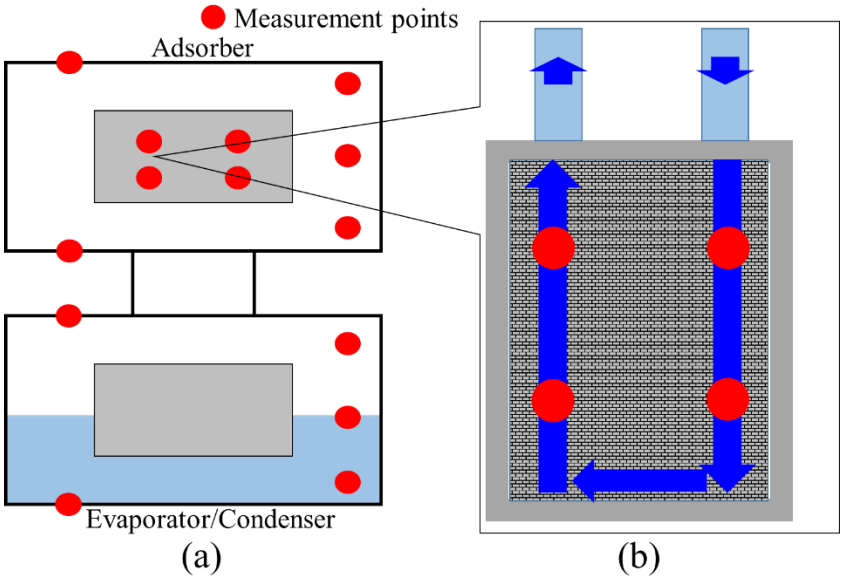

Fig 3-7 Temperature measuring position

Table 3-7 Details of measuring devices

Properties	Measurement points	Sensor type	Accuracy
Temperature	Adsorbent bed	T type sheathed thermocouple (Sheath diameter 1.6 mm)	± 0.03 K
	Adsorbent tank		
	Adsorber inlet heat transfer medium		
	Adsorber outlet heat transfer medium		
	Adsorber internal gas		
	Evaporator/Condenser inlet heat transfer medium		± 0.05 K
	Evaporator/Condenser outlet heat transfer medium		
	Vapor refrigerant		
	Liquid refrigerant		
	Evaporator/Condenser tank		
	Ambient	K type sheathed thermocouple (Sheath diameter 1 mm)	± 0.04 K

Pressure	Adsorber	Diaphragm type pressure transmitter	± 0.25% F.S.
	Evaporator/Condenser		
Flow rate	Adsorber	Volumetric flow meter	± 0.5% R.D.
	Evaporator/Condenser		

3.3 Experimental procedure

The experimental conditions used in the series of experiments can be seen in Table 3-8. Regeneration thermal source ranging from 60℃ to 80℃ were applied in this study as this range found to be good for activated carbon-ethanol pair to obtain requiring relative pressure for operating as cooling cycle system. Experimental procedure can be described as follows;

(1) Turn on all devices and adjust the air conditioner as necessary to keep the room temperature above the evaporator temperature.
(2) Set the temperature of adsorber to be regenerate temperature and of condenser to be condensate temperature. Open the duct valve to connect the adsorber and evaporator/condenser.
(3) After each temperature reach to the set temperature above mentioned, keep this status for one hour to desorb the adsorbed refrigerant from adsorbent bed.
(4) When the inside of system reach to a desorption equilibrium state, the valve is closed to shut off the adsorber and evaporator for next step. Then, the temperature of adsorber is set to be an adsorption temperature whilst the temperature of evaporator is set to be an evaporation temperature.
(5) After each temperature reach to the set temperature mentioned in procedure (4), the flow rate of heat transfer medium flowing through heat exchanger are adjusted to be 1~3 L/min.
(6) When the flow rate and temperature of heat transfer medium are stable, record is started.
(7) Wait for the first 10 minutes from the start of recording without any operation. (Measure the temperature of the circulating heat transfer medium without adsorption phenomenon progressing. This is the process for measuring the heat loss of the equipment)
(8) After that, connected gate between adsorber and evaporator opens to let ethanol gas move towards adsorbent bed. This process is continuously measured for one hour until get to the equilibrium state along with the set relative pressure.
(9) Valve between adsorber and evaporator/condenser is shut and evaporator will be

heated up to be ready for the next experiments

(10) Process from (2) to (9) are repeated for each experimental conditions.

Table 3-8 Experimental conditions

Desorption temperature [℃]	Condensation temperature [℃]	Adsorption temperature [℃]	Evaporation temperature [℃]	Flow rate of heat medium [L/min]
60,70,80	30	30	5,15,25	1,2,3

3.4 Experimental data reduction

3.4.1 Heat loss

In this research, the mean heat exchange rate per second in the heat loss collection process is considered to be the heat loss per unit time for each experiment. The heat loss Q_{loss} is given as;

$$Q_{loss} = \frac{1}{600}\int_{1}^{600} m_w c_w (T_{out} - T_{in})dt \tag{3.1}$$

The average heat loss calculated by this equation will be considered and added in the process of calculating the Q_{ad} and Q_{eva} later.

m_w [kg/s] denotes mass flow rate of heat transfer medium, c_w[kJ/kg/K] represents specific heat capacity of LLC and T_{in} is the temperature of inflow to the heat exchanger and T_{out} is the temperature of outflow from the heat exchanger. m_w [kg/s] is given as;

$$m_w = \rho V/60 \tag{3.2}$$

ρ [kg/L] denotes density of heat transfer medium and V [L/min] is the flow rate. ρ[kg/L] of LLC can be expressed by

$$\rho = -0.00002\frac{T_{in} + T_{out}}{2}^2 - 0.0004\frac{T_{in} + T_{out}}{2} + 1.0848 \tag{3.3}$$

c_f[kJ/kg/K] is given as;

$$c = 0.0048927\frac{T_{in} + T_{out}}{2} + 3.3730 \tag{3.4}$$

Specific heat capacity was measured experimentally which can be seen in Appendix A.

3.4.2 Adsorption heat and cooling effect

Heat output Q[W] during adsorption process can be calculated by Eq. (3.5)

$$Q = m_w c_w (T_{out} - T_{in}) - Q_{loss} \tag{3.5}$$

Accumulated adsorption rejection and cooling effect can be expressed by Eq. (3.6)

$$Q_{total} = \int_o^t Q dt \tag{3.6}$$

The average adsorption heat and cooling effect output at an arbitrary elapsed time from the start of adsorption process can be obtained as follows:

$$Q_{ave} = \frac{1}{t}\int_0^t Q dt \tag{3.7}$$

Equation (3.5) ~ (3.7) are calculated for both adsorber side and evaporator side.

3.4.3 Theoretical adsorption uptake

The equilibrium adsorption uptake depends on the adsorbent temperature and vapor pressure. In this study, Dubinin-Astakhov (D-A) quation [51] is used to estimate the theoretical adsorption uptake. The equilibrium adsorption uptake W_{th}[kg/kg] can be obtained as follows:

$$W_{th} = W_0 \exp - \left\{ \frac{R(T_S + 273.15)}{E} \ln \frac{P_{sat}}{P} \right\}^n \tag{3.8}$$

where W_0 is the maximum adsorption uptake, E denotes the adsorption characteristic energy [kJ/kg] and n defines the best fitting parameter. Numerical values of those were found to be 1.2[kg/kg], 139.5[kJ/kg] and 1.8 respectively.

3.4.4 Desorption heat

Since this research focus on adsorption process, desorption heat was not measured experimentally. However, desorption heat is needed in order to calculate COP as input heat. It can be said that the desorption heat can be deemed the adsorption heat [52]. Thus, the desorption heat can be estimated using Clausius-Clapeyron equation. Isosteric adsorption heat Q_{st}[kJ/kg] can be calculated by Eq. (3.9)

$$Q_{st} = -R \frac{d \ln P}{d(1/T)} \tag{3.9}$$

while latent heat of refrigerant Q_{LH}[kJ/kg] can also be given as;

$$Q_{LH} = -R \frac{d \ln P_{sat}}{d(1/T)} \tag{3.10}$$

Following equation can be obtained from Eq. (3.8),

$$\ln P = \ln P_0 - \frac{E}{RT} \ln \left(\frac{W_0}{W} \right)^{1/n} \tag{3.11}$$

Isosteric adsorption heat Q_{st}[kJ/kg] can be obtained by differentiating both sides of Eq. (3.11) and substituting (3.9) and (3.10) for (3.11),

$$Q_{st} = Q_{LH} - E \ln \left(\frac{W_0}{W} \right)^{1/n} \tag{3.12}$$

3.4.5 COP

Coefficient of performance (COP) is one of the evaluation index of refrigeration system. COP is the ratio of refrigeration capacity to input heat defined as Eq. (3.13).

$$COP = \frac{\int_0^t Q_{eva} dt}{Q_{de} + \left(M_s c_s + M_s c_v \left(W_{ad} + W_{de}\right)/2 + M_{hex} c_{hex}\right)\left(T_{de} - T_{ad}\right)} \tag{3.13}$$

where Q_{de} is the desorption heat, M_s is the amount of packed adsorbent, c_s represents the specific heat capacity of adsorbent, c_v defines the heat capacity of refrigerant. W_{ad} is the equilibrium uptake at adsorption state whilst W_{de} defines the equilibrium uptake at desorption state. M_{hex} and c_{hex} are the mass and specific heat capacity of heat exchanger respectively. Accumulating cooling capacity at 600s were employed as cooling capacity used in calculating COP since the adsorption reach an equilibrium state at around 600s. Strictly speaking, a subtle amount of adsorption is still occurred after 600s. However, it can be considered that the adsorption equilibrium state has been reached when the heat output asymptotically approaches zero. For the input heat, the calculated value assuming that the experimental conditions are ideal was employed. Input heat consist of the desorption heat requiring for desorbing the refrigerant and sensible heat. Heat capacity of the heat exchanger, activated carbon, adsorbed refrigerant is considered as sensible heat while the heat capacity of the binder is neglected because it is estimated to be less than 1% of the total. Latent heat of vaporization and specific heat capacity of ethanol used as refrigerant is taken from REFPROP [52].

3.5 Experimental results and discussion

In this section, experimental data of the compact adsorption cooling system using activated carbon powder with ethanol on various operating conditions will be presented and evaluated. Influence of regeneration temperature, evaporation temperature and flow rate will be revealed in next sections.

3.5.1 Influence of regeneration temperature

The heat rejection on adsorbent heat exchanger and cooling effect on evaporator under

various regeneration temperatures are compared in Fig. 3-8. The activated carbon heat exchanger is heated applying the regeneration temperature of 60, 70 and 80℃ and the coolant inlet temperature to the evaporator is kept at 15℃. The flow rates of heat transfer medium are set at 3L/min. It can be observed that the higher the regeneration temperature, the higher the peak value of adsorption heat and the longer it takes to reach adsorption equilibrium state. Accordingly, the higher peak value of cooling effect was obtained as the regeneration temperature increased. Since the refrigeration capacity is generated along with the adsorption phenomenon, the results on adsorber side will be focused here to discuss the reasons. When the higher regeneration temperature is applied with other parameters remained the same, the relative pressure of the refrigerant at desorption equilibrium state will decrease which cause the larger effective adsorption uptake. This can be also confirmed from Fig. 3-9 that the higher regeneration temperature resulted in the higher accumulated heat rejection and cooling effect. It is said that one of the factors influencing on the adsorption rate is the disparity between the instantaneous adsorption uptake and the equilibrium adsorption uptake at an arbitrary point which means the larger the effective adsorption uptake, the greater the difference between the instantaneous adsorption uptake and the equilibrium adsorption uptake. Thus, the higher regeneration temperature resulted in the faster adsorption rate which led to the high peak value of adsorption heat. Since the total heat output was larger and the time to adsorption equilibrium was longer in descending order of desorption temperature, the higher average refrigeration capacity was attained with increasing regeneration temperature regardless of the adsorption time as shown in Fig. 3-10. Note here that it can be said that the adsorption occurrence almost reached equilibrium state at around 600s. However, the mass conveyance effect on the evaporator side can be recognized from a little bit late peak in cooling effect. This is because that the heat transfer commission for adsorber is particularly larger than that for the evaporator even though both manages the same quantity of refrigerant mass removal.

3.5.2 Influence of evaporation temperature

The heat rejection and cooling effect obtained under various evaporation temperature are compared in Fig. 3-11. Fig. 3-12 and Fig. 3-13 indicate the amount of heat rejection to the coolant heat transfer fluid and the amount of cooling effect during the adsorption process. It can be detected in Fig. 3-11 that the higher peak value of refrigeration effect increases with increasing evaporation temperature while duration of refrigeration effect

increases with decreasing the evaporation temperature. Since the refrigeration capacity is generated along with the adsorption phenomenon, the results on adsorber side will be focused here to discussed the reasons. Theoretical adsorption uptake of activated carbon-ethanol pair on this experimental conditions are estimated by D-A equation (3.8) as shown in Table 3-9. It is observed from Table 3-9 that the effective adsorption uptake for evaporation temperature of 5℃ is notably smaller than other two conditions. As mentioned in previous section, the difference between instantaneous adsorption uptake and equilibrium adsorption uptake is a driving force of adsorption. Therefore, the low peak value of adsorption heat for the conditions of evaporation temperature 5℃ can be attributed to the small amount of effective adsorption uptake. In addition to that, higher evaporation temperatures lead to higher adsorption pressure, accordingly, higher amount of uptake. Therefore, the higher adsorption heat can be obtained for higher evaporating temperature yield by the raised heat transfer responsibility with limited heat transfer area.

3.5.3 Influence of flow rate of heat transfer medium

The rejected heat and cooling effect gained using 3 sets of flow rate (1,2 and 3L/min) are compared in Fig. 3-14. Note here that other temperature parameters remained the same which means that theoretical adsorption uptake for all conditions is equivalent. Thus, accumulated heat rejection and cooling effect for all conditions should be equal after the equilibrium state is reached. It is confirmed in Fig. 3-15 that the total output gradually approaches to be more or less equal as adsorption progresses except for the condition of flow rate 2L/min which might be experimental error. For this reason, the results except for flow rate 2L/min will be discussed and compared to find out the influence of flow rate of the heat transfer medium. Again, the adsorber side will be focused to discuss here. It is observed from Fig. 3-14 that peak value of adsorption heat rises with incrementing the flow rate of LLC while the duration of adsorption grows with reducing the flow rate. Adsorption phenomena generate the heat which warms up the adsorbent itself. This temperature rise of adsorbent causes a decrease in the relative pressure of the vapor refrigerant resulted in delaying the adsorption progress. In this study, the adsorption heat is collected by the heat transfer medium flowing through heat exchanger and assessed as heat output. The higher the flow rate, the more adsorption heat can be gathered more quickly. This might be due to the fact that the heat transfer coefficient inside the channel increases with increasing the flow rate. In summary, heat output per unit time increases and the time to the equilibrium state becomes shorter as

the flow rate of the antifreeze increases. Note here that cooling effect on the evaporator side can be recognized from a little bit late peak of the cooling effect in comparison to adsorption heat. This can be explained by the following reasons. As mentioned before, evaporation is driven by adsorption occurred on the adsorbent. The adsorption heat is easily transferred to the heat transfer medium as it generates on heat exchanger packed with the adsorbent. However, the evaporation effect is not transferred to the heat transfer medium as smoothly as adsorption heat because some amount of cooling effect generated by the latent heat of vaporization might be used for the sensible heat of the inner wall of the evaporator and liquid ethanol. Assuming the heat is not released to the ambient, all produced cooling effect will be collected by the heat transfer medium eventually. Based on this, the cooling effect is transferred to the heat transfer medium and used for the sensible heat at the beginning of adsorption process. Cooling energy stored in inner wall and liquid ethanol is gradually transferred to the heat transfer medium as adsorption time increases.

Fig. 3-15 illustrates the accumulated rejection heat from adsorbent and cooling effect from evaporator. It is observed that some difference between conditions of 1LPM and 3LPM can be seen even at around 600s, however, it should be equal since the effective adsorption uptake is the same. This could be attributed to the fact that the adsorption doesn’t reach the equilibrium state yet on the flow rate of 1LPM.

3.5.4 System performance

Coefficient of performance (COP) along with desorption heat and the sensible heat of adsorbent heat exchanger for all experimental data is summarized in Table 3-10 ~ 3-12. Note here that cooling performance used as output in calculating COP is an accumulated cooling effect at adsorption time 600s. Moreover, desorption heat is estimated as isosteric adsorption heat as it isn’t measured experimentally. The sensible heat of adsorbent heat exchanger is determined depending on the regeneration temperature as it can be seen from the denominator of Eq. (3.13). Since the accumulated heat output should be equal regardless of the flow rate, COP is supposed to be equivalent regardless of the flow rate if adsorption reach the equilibrium state at 600s. Huge variation of COP can be found in Table 3-10 for evaporation temperature of 5℃. This can be due to the great amount of heat loss to the ambient against a produced cooling effect. Therefore, system performance at this condition of this research cannot be evaluated appropriately. Maximum COP of 0.59 and cooling amount of 80.6 kJ at adsorption time 600s were achieved where the regeneration temperature of 80℃ and evaporation temperature of

25℃ while the adsorption and condensation temperature are maintained at 30℃. Some abnormalities in COP are detected which might be due to the failure in heat loss estimation. However, on the whole, COP increases as the regeneration and evaporation temperature increases.

Since the pre-cooling and pre-heating process is not taken into account in this study, it can be difficult to compare in terms of SCP. Instead of that, the cooling capacity per adsorbent mass and per adsorber volume are compared with some other similar works using other working pairs that have been published. Vasta et al [54] investigated the adsorption cooling system employing the zeolite (FAM-Z02) – water pair which achieved the cooling capacity per adsorbent mass of 1.1 W/g and the cooling capacity per adsorber volume of 500 W/L respectively. Lim and Abdullah [43] presented that they achieved the cooling capacity per adsorbent mass of 0.40 W/g and the cooling capacity per adsorber volume of 79 W/L respectively by the compact adsorption cooling system using activated carbon-methanol pair. Kubota et al [55] studied the compact adsorption cooling system using silica gel-water pair and they obtained the cooling capacity per mass of 0.54 W/g and the cooling capacity per adsorber volume of 173W/L respectively. Present work of the cooling capacity per adsorbent mass and adsorbent volume calculated by the average cooling effect at the time of 180s under the best condition are 3.52 W/g and 343 W/L respectively. The present study achieved the highest cooling effect per adsorbent mass as compared to other works above literatures while the cooling effect per adsorber volume inferior to the one obtained by Vasta et al [54], however, prior to others.

Table 3-9 Theoretical adsorption uptake of ACP

Temperature [℃]				Uptake at adsorption equilibrium state	Uptake at desorption equilibrium state	Effective adsorption uptake
T_{de}	T_{con}	T_{ad}	T_{eva}	W_{ad}	W_{de}	W_{eff}
80	30	30	5	0.770	0.211	0.560
80	30	30	15	1.063	0.211	0.852
80	30	30	25	1.186	0.211	0.975

Table 3-10 Experimental performances for regeneration temperature of 60℃ where the adsorption and condensation temperature is maintained at of 30℃

Evaporation temperature	Flow rate	Cooling performance	Sensible heat	Desorption heat	COP
T_{eva} [℃]	V [L/min]	Q_{eva} [kJ]	Q_{sh} [kJ]	Q_{de} [kJ]	[-]
5	1	4.9	18.63	6.23	0.20
	2	2.3			0.10
	3	9.8			0.40
15	1	30.0		37.48	0.53
	2	30.2			0.54
	3	29.1			0.52
25	1	36.7		50.62	0.53
	2	39.0			0.56
	3	37.6			0.54

Table 3-11 Experimental performances for regeneration temperature of 70℃ where the adsorption and condensation temperature is maintained at of 30℃

Evaporation temperature	Flow rate	Cooling performance	Sensible heat	Desorption heat	COP
T_{eva} [℃]	V [L/min]	Q_{eva} [kJ]	Q_{sh} [kJ]	Q_{de} [kJ]	[-]
5	1	23.9	24.88	36.52	0.39
	2	23.2			0.38
	3	34.8			0.56
15	1	48.7		68.36	0.52
	2	52.1			0.56
	3	50.0			0.54
25	1	53.8		81.66	0.50
	2	58.4			0.55
	3	57.3			0.54

Table 3-12 Experimental performances for regeneration temperature of 80℃ where the adsorption and condensation temperature is maintained at of 30℃

Evaporation temperature	Flow rate	Cooling performance	Sensible heat	Desorption heat	COP
T_{eva} [℃]	V [L/min]	Q_{eva} [kJ]	Q_{sh} [kJ]	Q_{de} [kJ]	[-]
5	1	37.3	31.15	60.34	0.41
	2	38.0			0.42
	3	39.0			0.42
15	1	66.6		92.44	0.54
	2	53.0			0.43
	3	65.6			0.53
25	1	68.0		105.82	0.50
	2	79.4			0.58
	3	80.6			0.59

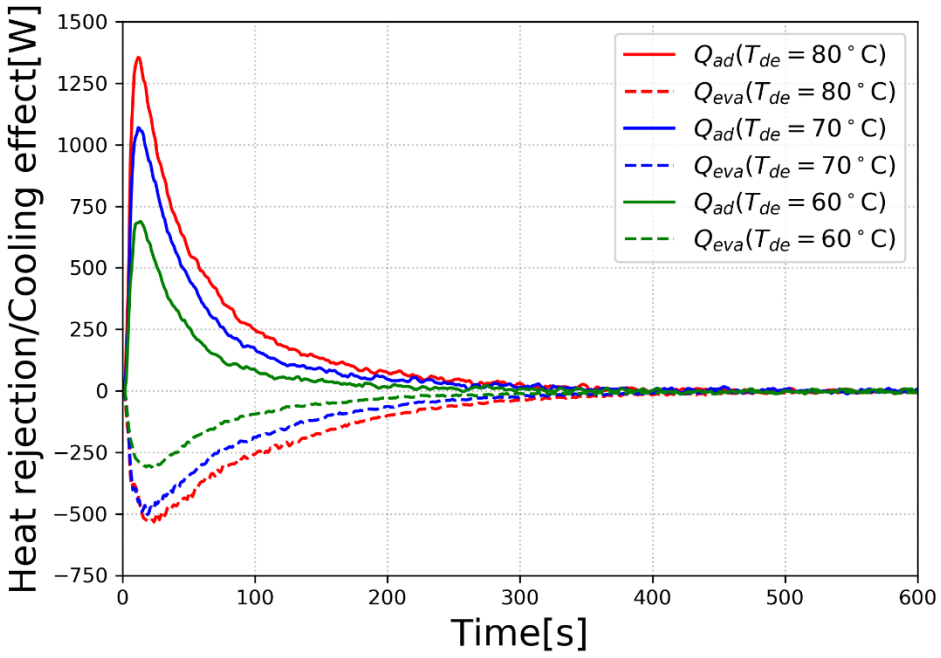

Fig. 3-8 Heat output profiles for various regeneration temperature where the adsorption and condensation temperature are set at 30℃, evaporation temperature is 15℃ and flow rate of the heat transfer medium is set at 3LPM.

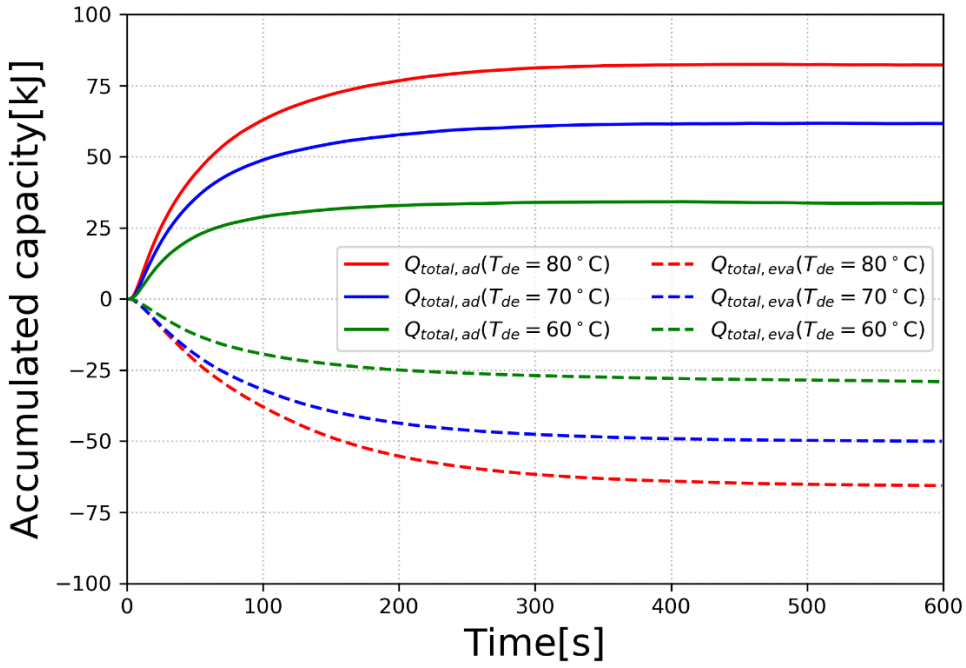

Fig. 3-9 Accumulated heat output profiles for various regeneration temperature where the adsorption and condensation temperature are set at 30℃, evaporation temperature is 15℃ and flow rate of the heat transfer medium is set at 3LPM.

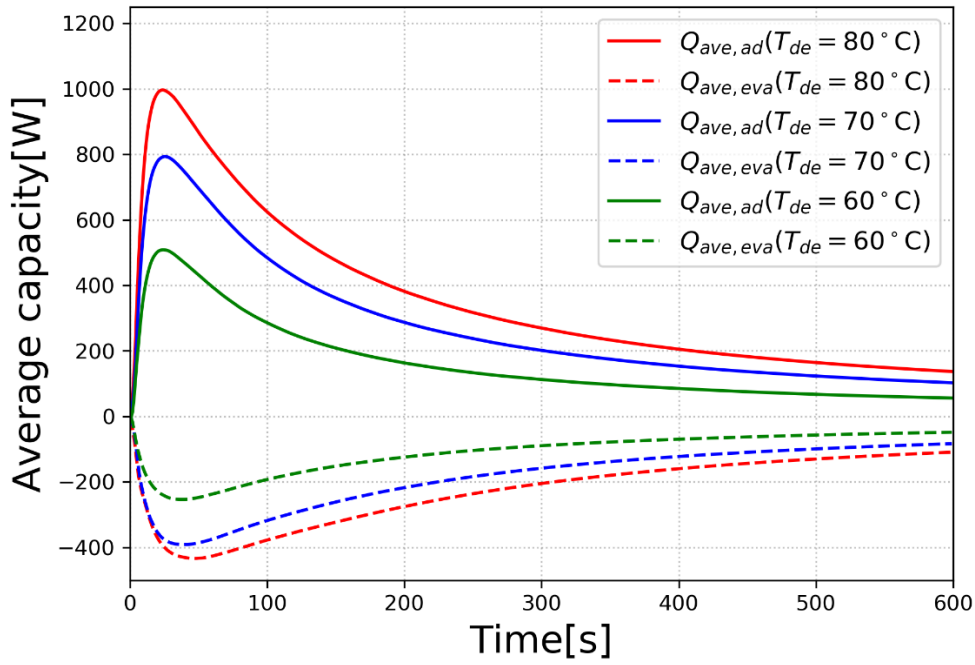

Fig. 3-10 Average heat output profiles for various regeneration temperature where the adsorption and condensation temperature are set at 30℃, evaporation temperature is 15℃ and flow rate of the heat transfer medium is set at 3LPM.

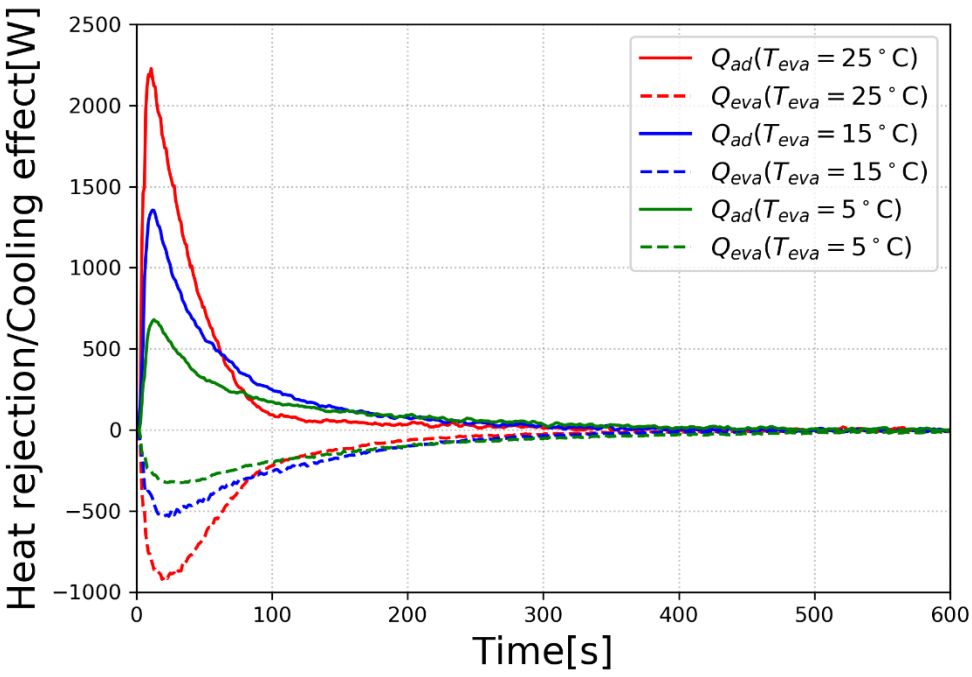

Fig. 3-11 Heat output profiles for various evaporation temperature where the adsorption and condensation temperature are set at 30℃, desorption temperature is 80℃ and flow rate of the heat transfer medium is set at 3LPM.

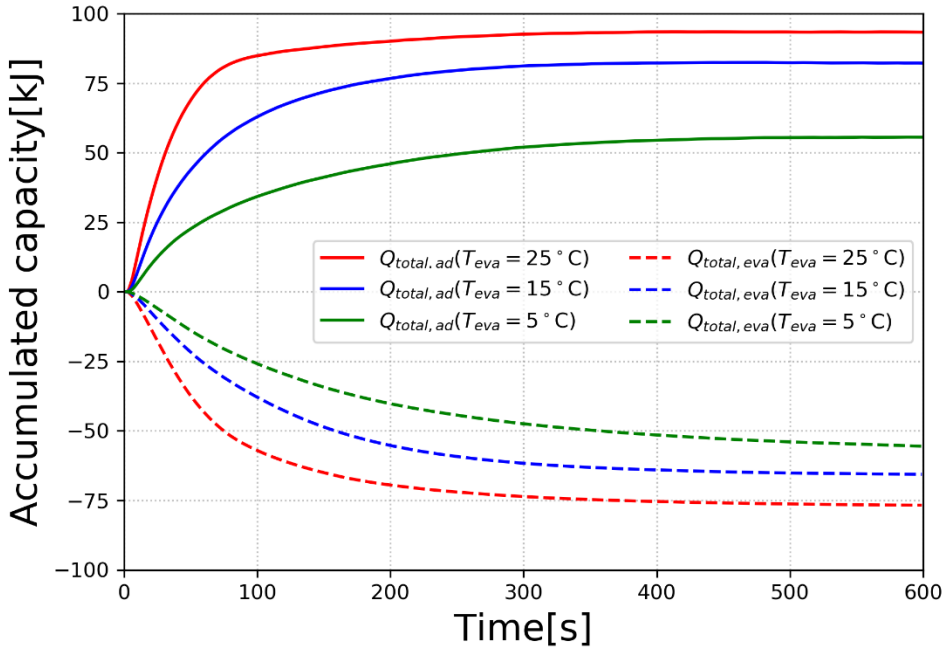

Fig. 3-12 Accumulated Heat output profiles for various evaporation temperature where the adsorption and condensation temperature are set at 30℃, desorption temperature is 80℃ and flow rate of the heat transfer medium is set at 3LPM.

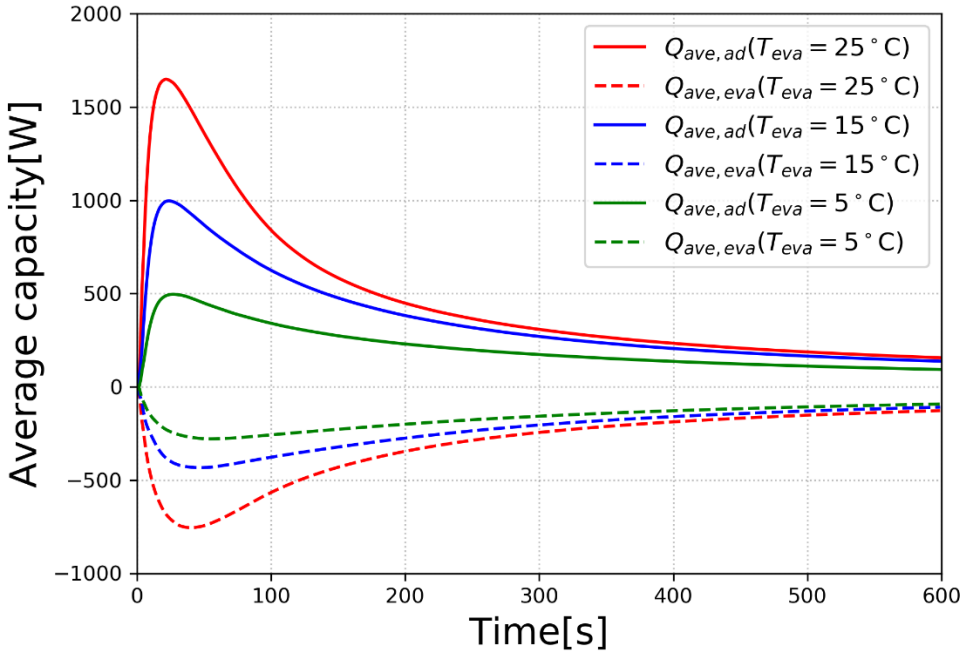

Fig. 3-13 Average heat output profiles for various evaporation temperature where the adsorption and condensation temperature are set at 30℃, desorption temperature is 80℃ and flow rate of the heat transfer medium is set at 3LPM.

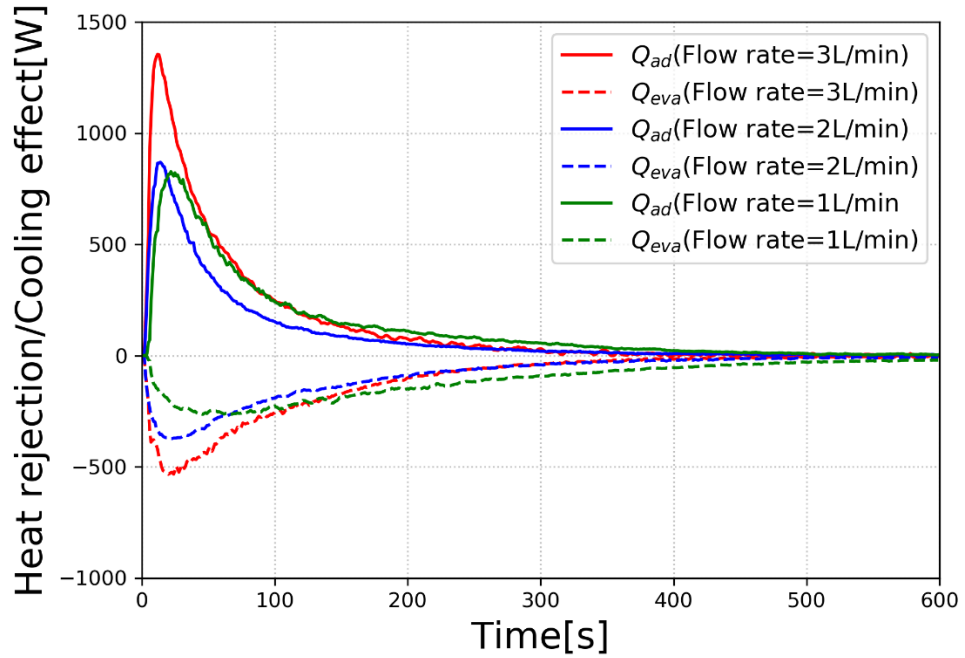

Fig. 3-14 Heat output profiles for various flow rate where the adsorption and condensation temperature are set at 30℃, desorption and evaporation temperature are set at 80℃ and 15℃ respectively.

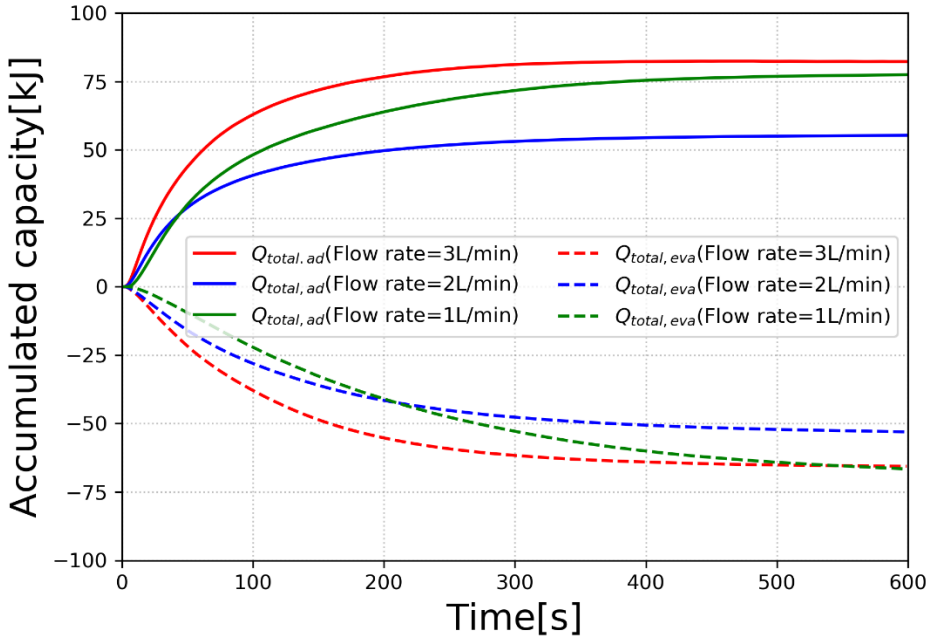

Fig. 3-15 Accumulated heat output profiles for various flow rate where the adsorption and condensation temperature are set at 30℃, desorption and evaporation temperature are set at 80℃ and 15℃ respectively.

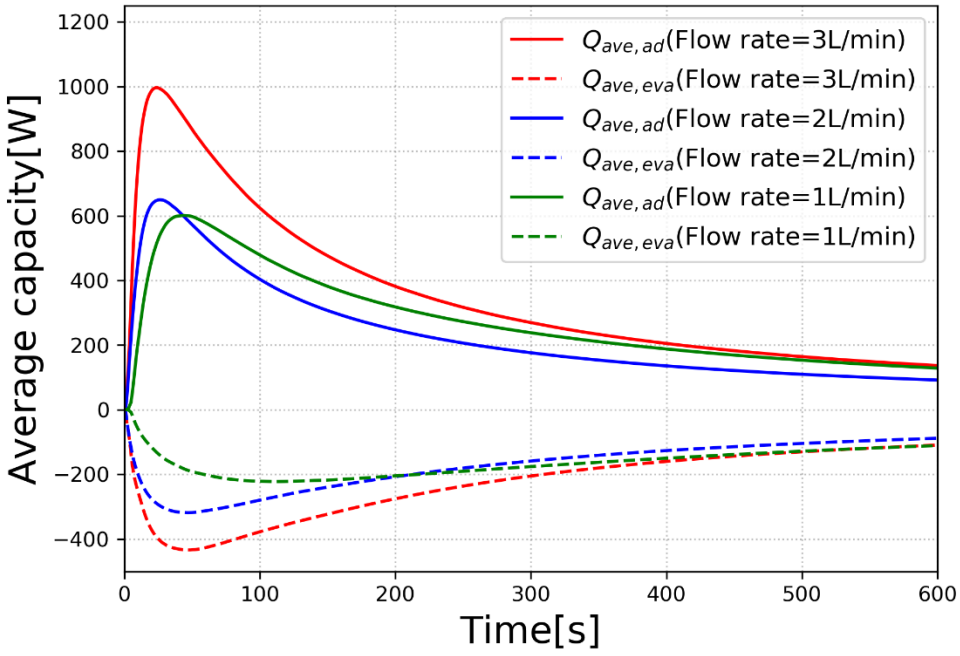

Fig. 3-16 Average heat output profiles for various flow rate where the adsorption and condensation temperature are set at 30℃, desorption and evaporation temperature are set at 80℃ and 15℃ respectively.

3.6 Conclusions

In this chapter, the experimental results based on heat rejection and cooling effect and COP have been discussed to find out the optimum operating condition. This study has shown:

- The increment of the regeneration temperature enhances the heat rejection and cooling effect.
- The heat rejection and cooling performance increase with increasing the evaporation temperature. The maximum peak value of the cooling effect reaches about 900W on evaporation temperature of 25℃ with the desorption temperature of 80℃, the adsorption and condensation temperature of 30℃. However, if this adsorption cooling system is used as residential air conditioner in summer, the evaporation temperature of 15℃ would be suitable.
- It is revealed that the higher the flow rate, the more adsorption heat can be gathered more quickly.
- The maximum COP of 0.59 was achieved by the compact adsorption cooling system under the best operating condition.

Chapter 4: Calculation of prediction model for overall thermal conductance

This study deals with the development of prediction model for overall thermal conductance. It is important to know the overall heat transfer coefficient as it refers to how well heat is conducted through several resistant mediums. The overall heat transfer coefficient is greatly influenced by the thermal conductivity of the mediums and thickness. The bigger the coefficient, the easier heat is conveyed from its source to the substances being heated. In previous simulation studies, UA value calculated from experimental data or assumption value have been applied to predict the dynamic behavior of the adsorption system. However, it could be greatly useful to be able to estimate the overall thermal conductance not only for using as one of the value in the simulation but also for optimizing the design of the heat exchanger. Here, UA value prediction model will be introduced and evaluated in comparison to experimental data.

4.1 Overall thermal conductance model

4.1.1 Prediction of the effective thermal conductivity

It is reported that the effective thermal conductivity of a packed bed is changed depending on the refrigerant pressure [56]. Since the system pressure of the compact adsorption cooling system used in this study is varying from 0 to 40kPa, prediction of the effective thermal conductivity is estimated by Eq. (4-1) [57] which considers the influence of the refrigerant pressure. Heat transfer model for this equation can be seen in Fig. 4-1. The mechanism of heat transfer for a packed bed can be broke down into following three parts, (1) Conductive and radiative heat transfer in the gas phase. (2) Conductive and radiative heat transfer in the solid and gas phase. (3) Conductive transfer through the touching surface. Since the temperature of the adsorbent used in this study is less than 100℃, radiative terms in the equation can be ignored and the effective thermal conductivity can be estimated by,

$$\lambda_{eff} = \frac{1}{2}(3\varepsilon - 1)\lambda_{vl} + \frac{3\beta'(1-\varepsilon)(1-\delta^*)}{2\{(\phi^* + 2\beta l_m / d_S)/\lambda_v + (1-\phi^*)/\lambda_S\}} + \frac{3}{2}(1-\varepsilon)\delta^*\lambda_S \qquad (4\text{-}1)$$

where ε denotes the void fraction, λ_{vl} and λ_v defines the thermal conductivity of fluid in void space and thermal conductivity of fluid. d_s represents the average particle diameter and λ_S is the thermal conductivity of adsorbent. The thermal conductivity of fluid in void space λ_{vl} is given by Eq. (4-2).

$$\lambda_{vl} = \frac{\lambda_v}{1 + 2\beta l_m / d_e} \tag{4-2}$$

where the l_m represents the mean free path of fluid molecule and the d_e defines the equivalent diameter for void space. These are expressed as Eq. (4-3) and (4-4).

$$l_m = \frac{kT_{bed}}{\sqrt{2}\pi P d_m^2} \tag{4-3}$$

$$d_e = d_S \sqrt{\frac{3\varepsilon - 1}{3(1-\varepsilon)}} \tag{4-4}$$

where k [j/K], T_{bed} [K], P [Pa] and d_m [m] denotes the Boltzmann's constant (1.386×10^{-23} J/K), the temperature of adsorbent bed, the refrigerant pressure and the molecular diameter of gas (ethanol: 6.4×10^{-10}).

The factor β' in Eq. (4-1) is correlated to an angle of the actual heat flow direction and the center line between particle and the factor β' and δ* defined in Eq. (4-1) can be determined from Eq. (4-5) and (4-6) respectively.

$$\beta' = 0.9 + \frac{(\varepsilon - 0.260)(1 - 0.9)}{0.476 - 0.260} \tag{4-5}$$

$$\delta^* = \frac{2\lambda_{eff\,0}}{3(1-\varepsilon)\lambda_S} \tag{4-6}$$

$$\beta = \frac{(2 - \alpha^*)(9\gamma - 5)}{2\alpha^*(\gamma + 1)} \tag{4-7}$$

where λ_{eff0} defines the thermal conductivity at sufficiently low pressure. The numerical value of φ^* in Eq. (4-1) is a measure of the effective thickness of the gas film adjacent the contact spot between particles and it can be defined as following equations.

$$\phi^* = \phi_1^* \qquad (\varepsilon \geq 0.476) \qquad (4\text{-}8)$$

$$\phi^* = \phi_2^* + \frac{(\varepsilon - 0.260)(\phi_1^* - \phi_2^*)}{0.476 - 0.260} \qquad (0.476 \geq \varepsilon \geq 0.260) \qquad (4\text{-}9)$$

$$\phi^* = \phi_2^* \qquad (\varepsilon \geq 0.260) \qquad (4\text{-}10)$$

where φ_1^* and φ_2^* represents the φ^* for loose packing and close packing which can be estimated as Eq. (4-11)

$$\phi_{1,2}^* = \left(\frac{K^*}{K^* - 1}\right)\left[\frac{0.5\left\{(K^* - 1)\sin\theta_{1,2}/K^*\right\}^2}{\ln\left\{K^* - (K^* - 1)\cos\theta_{1,2}\right\} - (K^* - 1)(1 - \cos\theta_{1,2})/K^*} - \frac{1}{K^*}\right] \qquad (4\text{-}11)$$

k

where K^* [-] denotes the ratio of the thermal conductivity of solid and that of fluid near solid-solid contract spot. θ_1 [rad] and θ_2 [rad] are the angle corresponding to boundary of heat flow area for a contact point to loose packing and clos packing. These are represented as following equations.

$$K^* = \frac{\lambda_s}{\lambda_{vl}} \qquad (4\text{-}12)$$

$$\theta_1 = 1/(\sin 1)^2 \qquad (4\text{-}13)$$

$$\theta_2 = \frac{1}{\left[\sin\left\{1/\left(4\sqrt{3}\right)\right\}\right]^2} \qquad (4\text{-}14)$$

The a^* in Eq. (3-7) is taken from [1] which is 0.315 and λ_{eff0} is assumed to be 0.02325 as it cannot be measured [2].

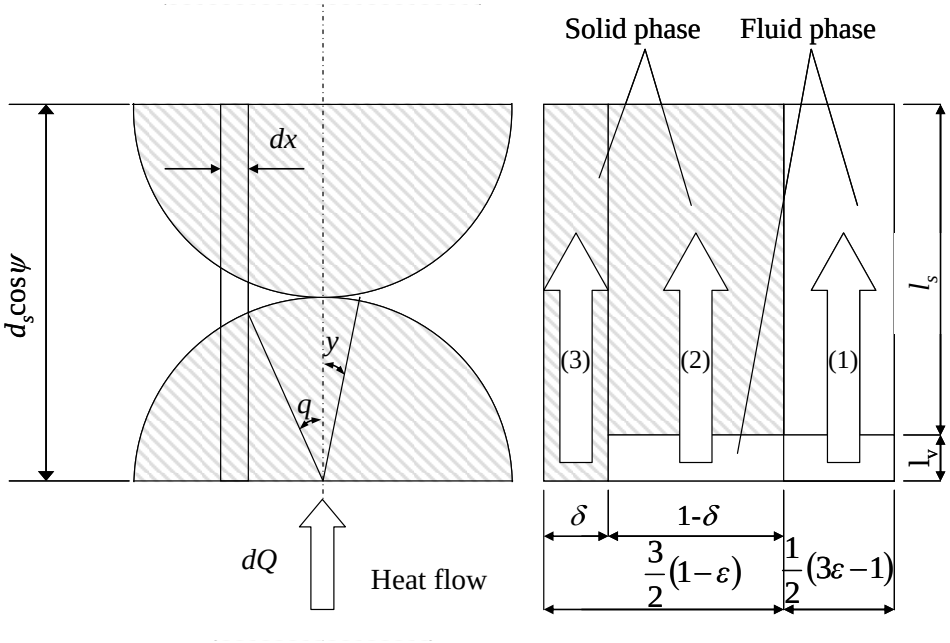

Fig. 4-1 Model for heat transfer at contact point

4.1.2 Prediction of UA value

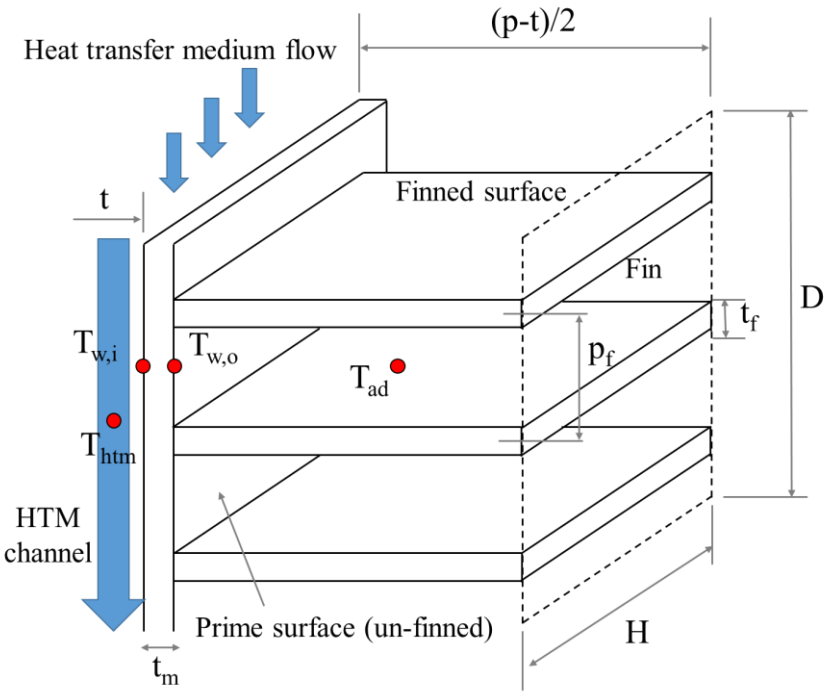

Fig. 4-2 Modelled adsorbent heat exchanger

The heat exchanger used in this study is assembled by flat channel tubes with flat fins. The estimation of UA value is modeled for this heat exchanger. Fig. 4-2 shows the schematic of modelled flat-tube fin heat exchanger. The detailed geometrical parameters of heat exchanger such as the number of channels and fins are extracted from Table 3-1 in previous chapter. The heat is conducted from the ethanol to the adsorbent firstly and from the heat transfer medium to the inner wall surface at $T_{w,i}$ by convection. Then, heat is transferred across the channel plate by conduction. Finally, the heat is moved to the adsorbent from the outer wall surface by conduction. The overall thermal conductance estimation model is established based on the following assumptions which helped to simplify the mathematical program.

- The overall heat transfer coefficient is uniform on the heat exchanger
- The equivalent convection heat transfer is not changed over the surface.
- The thermal conductivity of the aluminum is not changed depending on the temperature.
- The heat is transferred via the fins under only in longitudinal direction
- The temperature of the base of the fins is the same as the surface

Fig. 4-3(a) and (b) illustrates the control volume and the equivalent heat transfer thermal resistance of adsorbent bed.

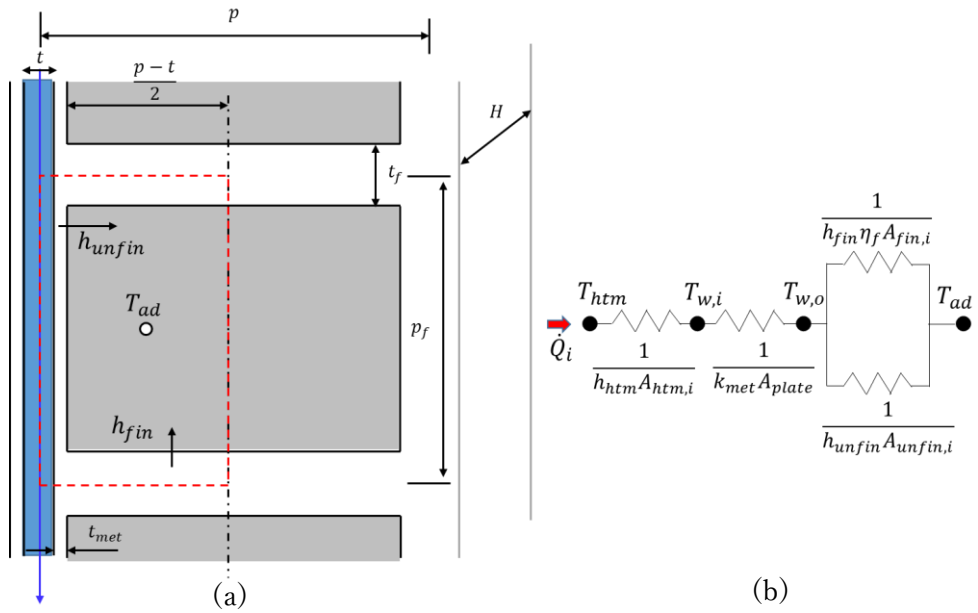

Fig. 4-3 Schematic diagram of the (a) control volume and (b) equivalent heat transfer thermal resistance of adsorbent bed.

The total thermal resistance from the heat transfer medium to the adsorbent in one control volume is given by Eq. (4-15).

$$R_{total} = \frac{1}{h_{htm} A_{htm,i}} + \frac{t_{met}}{k_{met} A_{plate,i}} + \frac{1}{h_{unfin} A_{unfin,i} + h_{fin} \eta_f A_{fin,i}} \tag{4-15}$$

where the first term ont the right hand side is the convection thermal resistance from the heat transfer medium to the inner wall of tube. The second term on the right side of Eq. (4-15) is the conduction resistance through the plate wall. Final term is the convection resistance for the prime surface as well as along the fins. Here, the heat transfer area A for heat transfer side, finned and un-finned surfaces is determined by $A_{htm}=A_{plate,i}=p_f D$, $A_{fin,i}=2(p-t)D/2$ and $A_{unfin,i}=(p_f-t_f)D$ respectively. The fin efficiency is expressed as:

$$\eta_f = \frac{\tanh\left(mL_f\right)}{mL_f} \tag{4-16}$$

where

$$m = \sqrt{\frac{p_f h_{fin}}{A_{c,f} \lambda_{met}}} = \sqrt{\frac{2Dh_{fin}}{t_f D \lambda_{met}}} = \sqrt{\frac{4\lambda_{ads}}{\lambda_{met} t_f \left(p_f - t_f\right)}} \tag{4-17}$$

$$L_f = \frac{\left(p-t\right)}{2} \tag{4-18}$$

Therefore, the Eq. (4-19) can be obtained.

$$mL_f = \frac{1}{2}\sqrt{\frac{4\lambda_{ads}}{\lambda_{met}}} \sqrt{\frac{1}{\frac{p_f}{p}\left(\frac{t_f}{p}\right)^{-1} - 1}} \left(\frac{t_f}{p}\right)^{-1} \left(1 - \frac{t}{p}\right) \tag{4-19}$$

The equivalent convection heat transfer coefficients of finned and prime surfaces can be gained as:

$$h_{unfin} = \frac{\lambda_{ads}}{\left(\frac{p-t}{4}\right)} = \frac{4\lambda_{ads}}{(p-t)} \tag{4-20}$$

$$h_{fin} = \frac{\lambda_{ads}}{\left(\frac{p_f - t_f}{4}\right)} = \frac{2\lambda_{ads}}{(p_f - t_f)} \tag{4-21}$$

The convective heat transfer coefficient on the heat transfer side can be obtained as a function of the Nusselt number:

$$h_{htm} = \lambda_{htm} \frac{Nu}{D_h}$$

where the hydraulic diameter of the channel is assumed to be $D_h=2(t-2t_{met})$. Therefore, the overall thermal resistance UA_{total} of the adsorbent bed can be estimated as

$$UA_{total} = \frac{1}{\frac{1}{\lambda_{htm}\frac{Nu}{2p\left(\frac{t}{p}-2\frac{t_{met}}{p}\right)}} + \frac{t_{met}}{\lambda_{met}} + \frac{p\left(1-\frac{t}{p}\right)}{4\lambda_{ads}\left(1-\frac{t_f}{p_f}+\frac{\eta_f}{2}\left[\frac{p^2\left(1-\frac{t}{p}\right)^2}{p_f^2\left(1-\frac{t_f}{p_f}\right)}\right]\right)}} A_{htm,i} \tag{4-23}$$

Where the Nu value is given as a function of flow rate which is expressed by Eq. (4-24).

$$Nu = 3.66 + \frac{0.0499}{L^*} \tag{4-24}$$

where

$$L^* = \frac{L/D}{\mathrm{Re}\,\mathrm{Pr}} \tag{4-25}$$

where *Re* is calculated accordingly the flow rate of heat transfer medium and *Pr* is given as 17 in this study.

4.1.3 Experimental data reduction

The experimental results of overall thermal resistance are evaluated based on the heat exchange that determined based on the log mean temperature difference (LMTD). Log mean temperature difference in this study is a precise temperature difference between the adsorbent bed temperature and the heat transfer medium. LMTD, ΔT_m and UA_{bed} in this study can be obtained by Eq. (4-26) and (4-27).

$$\Delta T_m = \frac{T_{f,i} - T_{bed} - \left(T_{f,o} - T_{bed}\right)}{\ln \frac{T_{f,i} - T_{bed}}{T_{f,o} - T_{bed}}} \tag{4-26}$$

$$UA_{bed} = \frac{Q_{ad}}{\Delta T_m} \tag{4-27}$$

4.1.4 Comparison conditions

The operating conditions used in this study to validate the prediction model can be seen in Table 4-1.

Table 4-1 Conditions for validating the prediction of overall thermal conductance

case	T_{ads} [℃]	T_{eva} [℃]	m_f [L/min]
1	30	5	3
2	30	15	3
3	30	25	3

4.2 Results and discussion

Fig. 4-4(a)~(c) show the comparison of overall thermal conductance between experiment and calculation. The estimation model is evaluated by varying the evaporation temperature and flow rate of heat transfer medium in comparison to

experimental results.

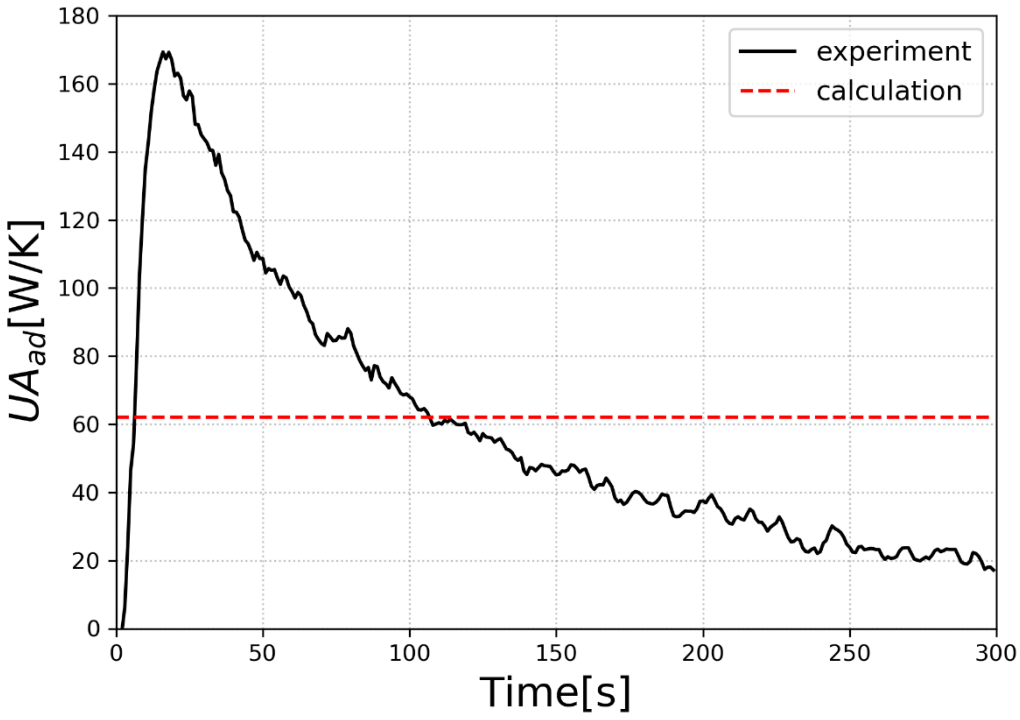

(a)

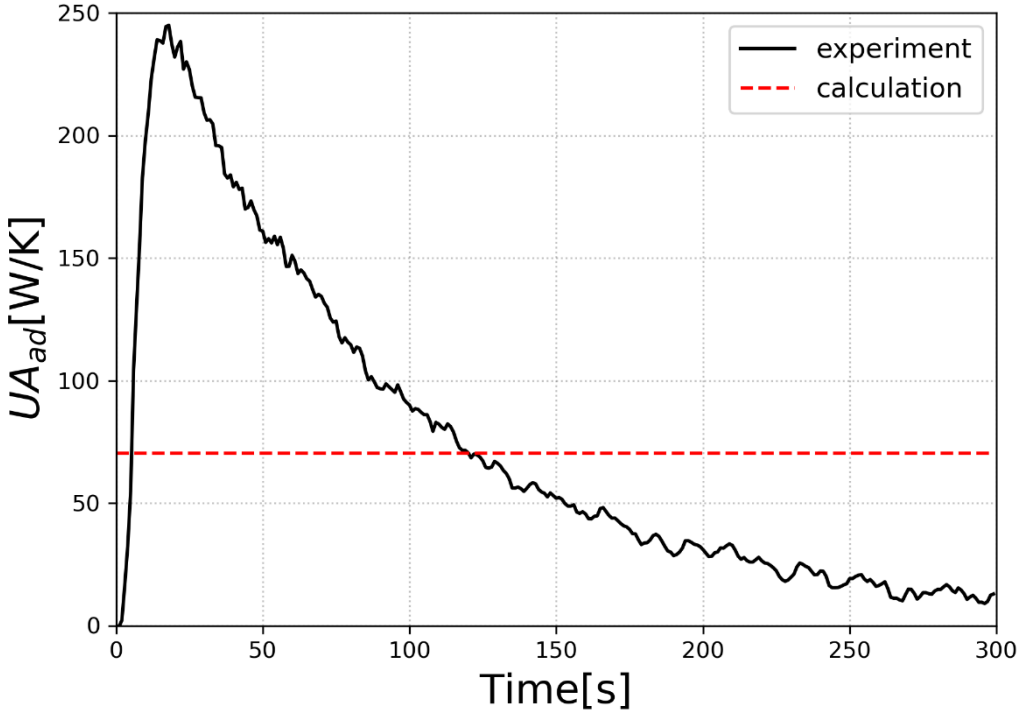

(b)

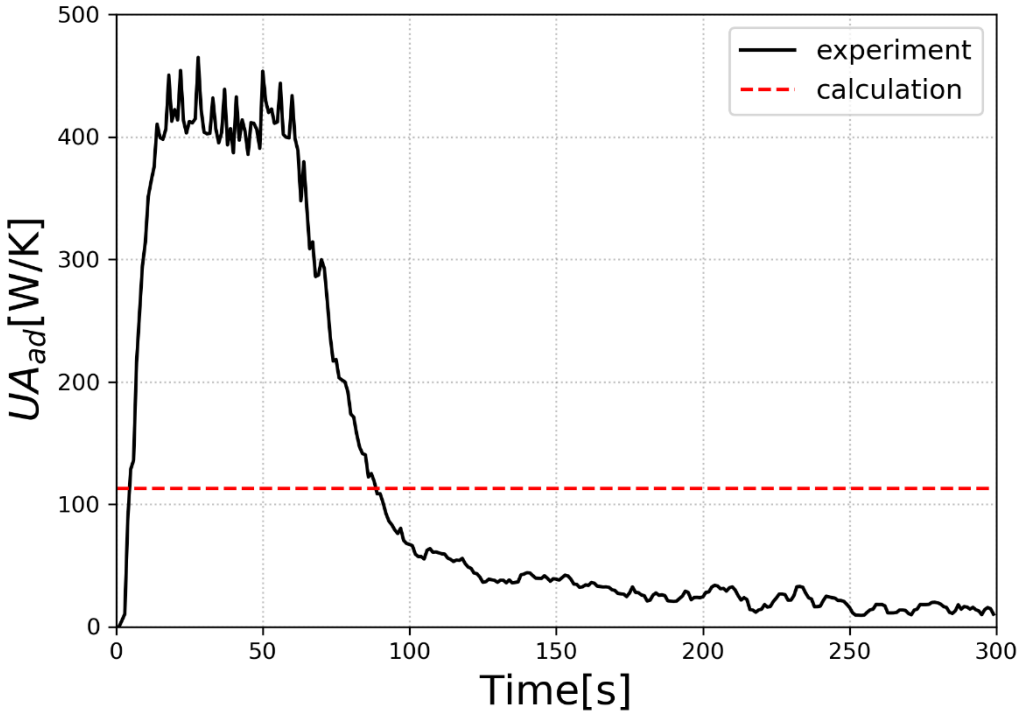

(c)

Fig. 4-4 Comparison of overall thermal conductance (UA) value of adsorbent heat exchanger, (a) case1, (b) case2, (c) case 3

Table 4-2 Comparison of overall thermal conductance between experiment and calculation

Case	UA [W/K]		Difference between estimation and average of experiment data up to 300s [%]
	Experimental average up to 300s	Estimation	
1	59.1	62.1	5.1
2	74.9	70.3	-6.1
3	117.5	112.6	4.2

It can be observed that the UA value increases rapidly at the initial stage and reaches the maximum value at around 20s for all cases, then decreases as time goes. This is due to the fact that adsorption is actively performed in the initial stage, and the adsorbent approaches an equilibrium state and adsorption becomes inactive as time passes. In this manner, the UA value obtained from experimental results changes with time while the

UA value estimated by model shows a constant value regardless of the time, so it is difficult to compare. Therefore, the average of the experimental UA values up to 300s were calculated and compared with estimation values. The reason that the adsorption time up to 300 seconds is chosen is that the estimation model assumes a state where the temperature difference between the inlet and outlet of the heat transfer fluid is large, that is the initial state. It can be seen from Table 4-2 that the estimated UA values are within ±6.1% of the UA values extracted from experiments.

4.3 Conclusions

In this chapter, the prediction model of overall thermal conductance was built to estimate the UA value. The estimation model showed the good agreement with the UA values extracted from experimental results. It was obtained that when the evaporation temperature 5℃, 15℃, 25℃ then, 5.1%, -6.1%, 4.2% of accuracy were presented. It comes to conclude that the estimation model can predict the overall thermal conductance (UA value) with reasonable agreement, so this model can be applied in the performance simulation of the adsorption cooling system.

Chapter 5: Comparison of prediction using two types of adsorption kinetics parameters

In this chapter, the validation of two kinds of kinetics parameters will be conducted by comparing with experimental results. Kinetics is one of crucial factor of adsorption as it defines the adsorption rate. Here, comparison of outlet temperature responses and accumulated adsorption heat and cooling effect obtained from simulation works and experimental research has been presented and compared. The main aim in this chapter is to clarify an influence of isothermal assumption in the kinetics model for activated carbon-ethanol pair.

5.1 Physical and mathematical modeling

5.1.1 Adsorption isotherms

The Dubinin-Radushkevich (D-R) [58] and Dubinin-Astakhov (D-A) [51] equations are widely recognized for an adsorption equilibrium of gases and vapors onto microporous adsorbents. The Dubinin-Astakhov (D-A) equation is generally adopted to estimate the equilibrium uptake of ACP-ethanol pairs while the D-R equation is used to assume that of ACP-methanol pair. D-R and D-A equations are can be expressed as (5.1) and (5.2) respectively.

$$W = W_0 \exp\left[-\left(\frac{A^*}{E}\right)^2\right] \tag{5.1}$$

$$W = W_0 \exp\left[-\left(\frac{A^*}{E}\right)^n\right] \tag{5.2}$$

where A^* represents the adsorption potential, described as the molar energy calls for the isentropic compression of the adsorbed species to the saturation pressure. A can be calculated by Eq. (5.3):

$$A^* = R_g T \ln\left(\frac{P_S}{P}\right) \tag{5.3}$$

W_0 denotes the maximum adsorption capacity [kg/kg] and E denotes the adsorption characteristic energy [kJ/kg]. The exponential parameter n provides the best fitting of $ln(W)$ versus A^n. T is the adsorption temperature [K], R_g is the gas constant, Ps describes the saturated refrigerant pressure at adsorbent temperature whereas P denotes the saturated vapor pressure at the evaporator internal refrigerant temperature. The numerical values of W_0, n and E for activated carbon-ethanol pair were extracted experimentally by El-Sharkawy et al. [59] as shown in Table 5-1.

Table 5-1 Isotherm parameters of ACP-ethanol pair

W_0 [kg/kg]	n [-]	E [kJ/kg]
1.2	1.8	139.5

5.1.2 Adsorption kinetics

The adsorption rate is essential factor for proper performance prediction of adsorption cooling systems. The adsorption kinetics models for activated carbon ethanol pair were investigated experimentally and theoretically. The adsorption rate is usually estimated using the well-known linear driving force (LDF) equation which is expressed as following Eq. (5.4):

$$\frac{dw}{dt} = k_m(W - w) \tag{5.4}$$

where k_m refers the overall mass transfer coefficient for activated carbon-ethanol pair which is given as,

$$k_m = \frac{15 D_S}{R_p^2} \tag{5.5}$$

where R_p is the radius of activated carbon and D_s defines the surface diffusivity which is determined by Arrhenius equations as,

$$D_S = D_{S0} \exp\left(-\frac{E_a}{RT}\right) \tag{5.6}$$

Combining equations (5.5) and (5.6) in Eq. (5.3):

$$\frac{dw}{dt} = \alpha \exp\left(-\frac{E_a}{RT}\right)(W - w) \tag{5.7}$$

5.1.2.1 Isothermal condition kinetics model

Adsorption kinetics of activated carbon-ethanol pair have been measured using magnetic suspension adsorption measurement unit by El-Sharkwy [59]. The Fickian diffusion model was used to estimate the adsorption kinetics in this study. Numerical values of α and E_a were obtained experimentaly as shown in Table 5-2.

5.1.2.2 Non-isotheral condition kinetics model

Numerical values of adsorption kinetics obtained by El-Sharkwy explained in previous section have been used in the simulation to predict the performance of the adsorption system. Skander Jribi et al. (2016) [60] reported that the isothermal supposition used in calculating the diffusion time constant of Fickian diffusion and LDM models caused divergence and underestimation of adsorption uptake as the adsorption heat during adsorption occur is not considered. They investigated the adsorption kinetics of activated carbon-ethanol pair with a help of CFD simulation considering the non-isothermal condition. They found corrected adsorption rate by simulating the change in adsorbent temperature. Numerical values of modified non-isothermal adsorption kinetics equation of activated carbon-ethanol pair are presented in Table 5-2 with previous isothermal assumption one.

Table 5-2 Numerical values of kinetics parameters

Authors	α [s^{-1}]	E_a [kJ mol^{-1}]
El-Sharkwy et al. [59]	0.24	10.37
Skander Jribi et al [60]	132.89	22.97

5.1.3 Mass balance

The total mass of refrigerant inside the compact adsorption system always keeps constant. The amount of refrigerant liquid inside the evaporator and the condenser can be calculated by addressing the amount of adsorbed refrigerant during the adsorption process or desorbed refrigerant during the desorption process, it is given by:

$$\frac{dM_{x,l}}{dt} = -M_S \frac{dw}{dt} \tag{5.8}$$

5.1.4 Energy balance for adsorber

Applying the lumped parameter model for the adsorption bed, which contains the activated carbon powder, the heat exchanger, the energy balance equation, is given by:

$$\left[M_S c_S + M_b c_b + M_S w_b c_l\right]\frac{dT_a}{dt} = \dot{m}_w c_w \left(T_{ca,i} - T_{ca,o}\right) + M_S Q_S \frac{dw_a}{dt} \tag{5.9}$$

where *a* indicates adsorption. The left hand side of the adsorber energy balance equation (Eq. (5.9)) is the thermal capacity of the adsorption bed heat exchanger (metal + adsorbent (activated carbon) + refrigerant (ethanol)) during adsorption and desorption. The first term on the right side of Eq. (5.9) denotes the total amount of heat released to the cooling heat transfer medium upon adsorption. The second term on the right of Eq. (5.9) represents the release of adsorption heat in the process of adsorption. The outlet temperature is proper to be calculated by the log mean temperature difference method which is expressed as:

$$T_{ca,o} = T_a + \left(T_{ca,i} - T_b\right)\exp\left(-NTU_a\right) \tag{5.10}$$

The number of transfer units (*NTU*) is a dimensionless number which describes the relative size of heat exchanger expressed as,

$$NTU_a = \frac{(UA)_a}{m_w c_w} \tag{5.11}$$

5.1.5 Energy balance for desorber

The energy balance for desorption bed is given by:

$$\left[M_S c_S + M_b c_b + M_S w_d c_l\right]\frac{dT_d}{dt} = \dot{m}_w c_w\left(T_{h,i} - T_{h,o}\right) + M_S Q_S \frac{dw_d}{dt} \tag{5.12}$$

where *d* indicates desorption. The left hand side of the adsorber energy balance equation (Eq. (5.12)) is the thermal capacity of the adsorption bed heat exchanger (metal + adsorbent (activated carbon) + refrigerant (ethanol)) during adsorption and desorption. The first indication on the right of Eq. (5.12) denotes the sum of heat taken into the heat transfer medium upon given by the high temperature medium for desorption. The second expression on the right of Eq. (5.12) gives the input of desorption heat in the process of desorption. The outlet temperature and NTU for the desorber are given by:

$$T_{h,o} = T_d + \left(T_{h,i} - T_b\right)\exp\left(-NTU_d\right) \tag{5.13}$$

$$NTU_d = \frac{(UA)_d}{m_w c_w} \tag{5.14}$$

5.1.6 Energy balance for evaporator/condenser

Generally, the adsorption system has the evaporator connecting with adsorber and the condenser connecting with desorber. However, our adsorption system has the heat exchanger acting as the evaporator and the condenser depending on the operation mode. During the desorption process, it works as the condenser to condense the desorbed refrigerant from adsorber. On the other hand, it works as the evaporator during the adsorption process to produce the cooling effect by evaporating the refrigerant. Thus the energy balance equation for the condenser/evaporator can be expressed as:

$$\left[M_x c_x + M_{x,l} c_l\right]\frac{dT_x}{dt} = \dot{m}_w c_w\left(T_{x,i} - T_{x,o}\right) - L_{eth} M_S \frac{dw}{dt} \tag{5.15}$$

where the subscript x = e denotes the evaporator and x = c indicates the condenser. The term on the left hand side of Eq. (5.15) indicates the energy variation required by the

metallic parts of heat exchanger tubes and cooling heat transfer medium in the evaporator/condenser. The first expression on the right of Eq. (5.15) represents the total amount of heat taken into the cooling heat transfer medium or the cooling production on the evaporator depending on the operation mode. The final expression on the right shows the latent heat of evaporation because of the sum of adsorbed refrigerant and desorbed from the adsorber bed during the condensation mode. Appling the log mean temperature difference (LMTD) technique, the outlet temperature of the evaporator/condenser is given by:

$$T_{x,o} = T_x + \left(T_{x,i} - T_x\right)\exp\left(NTU_x\right) \tag{5.16}$$

where the subscript x = e indicates the evaporator and x = c refers to the condenser. NTU can be described as,

$$NTU_x = \frac{(UA)_x}{m_w c_w} \tag{5.17}$$

5.1.7 System performance

The accumulated cooling effect Q_{ch} and the adsorption heat Q_{ad} during a cycle can be calculated by following Eq. (5.18), (5.19) and (5.20).

$$Q_{ch} = \int_0^{t_{ad}} m_w c_w \left(T_{e,i} - T_{e,o}\right) dt \tag{5.18}$$

$$Q_{ad} = \int_0^{t_{ad}} m_w c_w \left(T_{ca,i} - T_{ca,o}\right) dt \tag{5.19}$$

5.2 Validation of the model with experimental results

5.2.1 Experimental set-up

An experimental setup of the compact adsorption cooling system for comparing to evaluate the kinetics model is depicted in Fig. 3-1. Experimental facilities and procedures are also explained in Chapter 3. To investigate an influence of kinetics

parameters, dynamic behaviors of outlet temperature responses are mainly used to compare the results and validate the kinetics models.

5.2.2 Performance evaluation

The experimental operating conditions are listed in Table 5-3.

Table 5-3 Experimental operating conditions

Parameter	Symbol	Value
Flow rate of LLC	m_w	3 L/min
Adsorbent bed		
Hot inlet temperature	$T_{h,i}$	80 ℃
Cooling inlet temperature	$T_{ca,i}$	30 ℃
Evaporator		
Chilled inlet temperature	$T_{e,i}$	25 ℃
Condenser		
Cooling inlet temperature	$T_{c,i}$	30 ℃

Thermal properties of working pairs adopted in the simulation are listed in Table 5-4.

Table 5-4 Thermal properties of working pairs in simulation

Parameter	Symbol	Value
Specific heat capacity of adsorbent	c_S	890 J/kg·K
Specific heat capacity of refrigerant (liquid)	c_l	2597 J/kg·K
Specific heat capacity of refrigerant (vapor)	c_v	1612 J/kg·K
Specific heat capacity of LLC	c_w	3.37+0.0049(T) J/kg·K
Latent heat of refrigerant	*Leth*	919.7×10^3 J/kg
Adsorption heat	Q_S	1026×10^3 J/kg

Actual heat exchanger design is detailed in Table 5-5. Heat transfer conductance was calculated by using the log mean temperature method which is expressed as,

Table 5-5 Actual heat exchanger design

Parameter	Symbol	Value
Adsorber		
Mass of activated carbon	M_s	0.113 kg
Heat capacity ratio	α_b	4.82
Number of heat transfer unit	NTU_a	
Adsorber heat transfer conductance	UA_a	203
Evaporator/Condenser		
Number of heat transfer unit	NTU_x	
Heat transfer conductance	UA_x	300

5.3 Results and discussion

In this section, the two types of kinetics parameters will be evaluated when they are applied in the lumped parameter model in comparison to experimental results. Kinetics parameters define the adsorption rate, in other words, how fast adsorbent can adsorb the refrigerant. Given that, the outlet temperature responses are mainly discussed to assess the kinetics models. Here, the affection of the assumption of isothermal condition will be clear. In order to distinguish the kinetics models easily, the kinetics parameters which was evaluated by El-Sharkwy et al. [57] was named “ModelA”, and the one validated by Skander Jribi et al. [58] was named “ModelB”. These names are used in this section.

Fig. 5-1 shows a comparison between simulated and experimental results for the outlet temperature profiles of the adsorber and evaporator during the adsorption process at the operating condition where the regeneration temperature of 80℃, the adsorption temperature of 30℃, the evaporation temperature of 25℃, the condensation temperature of 25℃, and flow rate of 3LPM. It can be seen from Fig. 5-1, ModelA was not able to calculate the response of outlet temperature both of adsorber and evaporator obviously. This can be due to the fact that the kinetics parameters are not perfectly evaluated which means the adsorption rate might be wrong. Moreover, it is observed that the adsorption occurrence is obviously settled at 600s in the experiments while the outlet temperature of ModelA explains that adsorption process is still continued after

600s. That means that the adsorption rate should be faster in order to capture the response of the outlet temperature of the adsorption system. On the other hand, the outlet temperature profile obtained by ModelB improved significantly in describing the experimental data. It can be said that the simulation model using ModelB can predict the outlet temperature profile well especially on the evaporator side, however, some difference can be seen at around the peak temperature on the adsorber side. This is because the outlet temperature is calculated using mean adsorber bed temperature since the geometry of the adsorbent bed is not considered in the lumped parameter model. This may cause incorrect prediction since the adsorber bed actually has temperature distribution depending on the points. For the better prediction of outlet temperature, the heat and mass transfer model would be able to estimate the outlet temperature more accurately in comparison to experimental data since this model is expressed in nonlinear ordinary and partial differential equations, however, it takes more time and computation cost as compared with the lumped model.

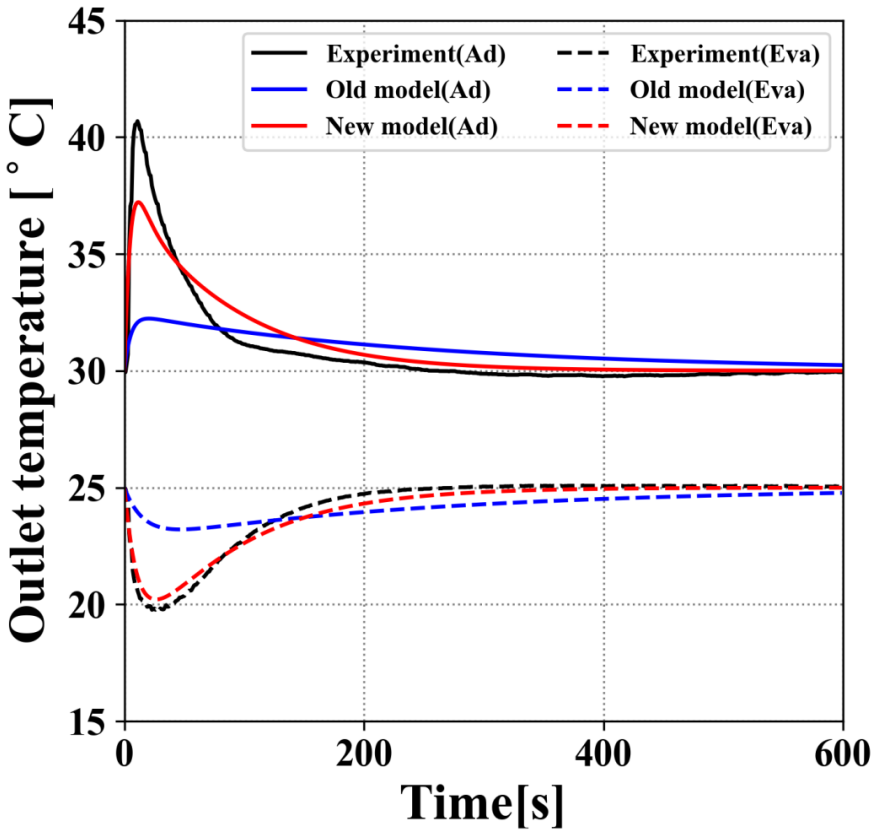

Fig. 5-1 Outlet temperature profiles of heat transfer medium for ACP – ethanol adsorption cooling system using the different kind of kinetics parameters

The total amount of heat rejection to the heat transfer medium by the adsorber and cooling capacity of the cooling energy from the chilled fluid at adsorption time of 600s are shown in Fig. 5-2. It can be observed that both of the simulation model overestimated the heat rejection and cooling capacity in comparison with experimental dada. This is because that the existing simulation models don't consider the pressure change inside the adsorber whilst the pressure in the adsorber is changing by heating up or cooling down especially in the process of the pre-heating and pre-cooling. The pressure can be assumed as saturated vapor pressure during evaporation-adsorption process and desorption-condensation process but cannot be assumed during the pressurization and depressurization. The over-estimation of total amount of capacity will lead to the over-estimation of the system performance.

The comparison between ModelA and ModleB for total output tells that blue bars are a bit smaller than the red bars. This small difference can be explained by the previous discussion that the adsorption process is not completed at the adsorption time of 600s in the simulation using ModelA. If the adsorption time was set at more than 600s (until equilibrium), the total capacity would be the same.

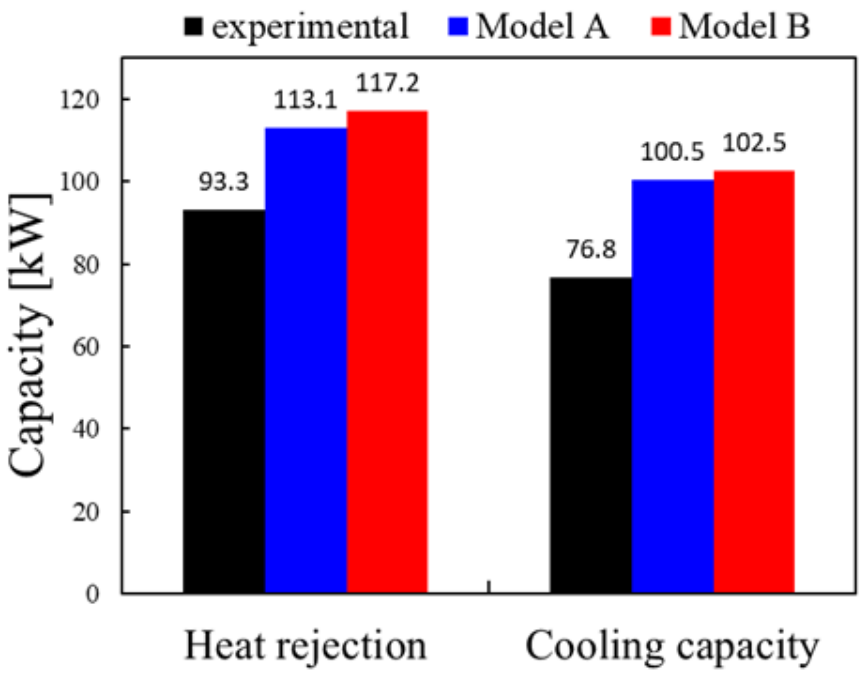

Fig. 5-2 Accumulated heat rejection and cooling capacity at the adsorption time of 600s.

5.4 Conclusions

This chapter evaluated the kinetics model which was modeled in a different way by predicting the outlet temperature and total amount of capacity of the compact adsorption cooling system in comparison with experimental observation. We found that the accuracy of the prediction especially for the response of outlet temperature can be enhanced by utilizing the non-isothermal adsorption kinetics equation. Estimation of outlet temperature is surely important for prediction of transient cooling capacity and heat rejection, and finding the peak output to determine the best switching time.

From the above perspective, we need to apply the kinetics model (ModelB) which consider the change of adsorption temperature in fitting the LDF model for the estimation of the dynamic response of the adsorption cooling system using activated carbon (MaxsorbIII) – ethanol pair.

Chapter 6: Development of the detailed simulation model for a compact adsorption cooling system

In this chapter, a detailed simulation model of thermal compression process for a compact adsorption cooling system will be introduced and influence of the adsorber design will be investigated. Many researches have focused on an advanced cycles and new adsorbent-refrigerant pairs, and of which the performances have been investigated with lumped parameter model which was also carried out in chapter 5. Validity of the lumped parameter model was ascertained by comparing with experiment and it was found to be well predicted in terms of such as coefficient of performance (COP) and cooling capacity in some studies. In most cases, pressure of vapor refrigerant inside adsorber is not estimated [61]. The pressure during adsorption/evaporation process or desorption/condensation process is presumed as vapor pressure at liquid refrigerant temperature in evaporator or condenser since the adsorber and evaporator and condenser are connected and the pressure in the system will be roughly homogeneous. According to the recent research results of our laboratory, it is reported that the adsorption uptake change during pre-cooling/pre-heating process might be happened due to the pressurization and depressurization, which might cause a decrease in performance. It is said that the adsorption uptake change become bigger if the adsorber design is not optimized which means adsorber has a relatively huge vacant volume. On the basis of above consideration, development of simulation model that can predict the behavior during pre-cooling/pre-heating process is necessary. In the present circumstances, the lumped parameter model cannot predict the changes in adsorption uptake during pressurization and depressurization, which are estimated as isosteric process. The prediction of COP is not affected that much by assuming the isosteric change as these performance indices are based on the accumulation of cooling effect during evaporation process. In spite of that, the isosteric approximation affect the optimum volume of adsorber and optimum cycle time for pre-cooling and pre-heating duration. From the above perspective, the present lumped parameter model was modified to be able to predict the not only pressure change but also changes in adsorption uptake during pre-cooling and pre-heating processes. Here, one bed adsorption cooling system as illustrated in Fig. 6-1 was modelled mathematically.

6.1 New physical and mathematical modeling

6.1.1 Adsorption isotherms

The equilibrium uptake of ACP-ethanol pairs can be estimated by the Dubinin-Astakhov (D-A) equation [51]. D-A equations can be expressed as Eq. (6.1)

$$W = W_0 \exp\left[-\left(\frac{R_g}{E} T \ln\left(\frac{P_S}{P}\right)\right)^n\right] \tag{6.1}$$

where W_0 refers the maximum adsorption capacity [kg/kg] and E denotes the adsorption characteristic energy [kJ/kg]. The exponential parameter n provides the best fitting of $ln(W)$ versus A^n. T is the adsorption temperature [K], R_g is the gas constant, Ps describes the saturated refrigerant pressure at adsorbent temperature whilst P denotes the saturated vapor pressure at the evaporator internal refrigerant temperature. The numerical values of W_0, n and E for the activated carbon as adsorbent with ethanol as refrigerant were extracted experimentally by El-Sharkawy et al. [59] as shown in Table 6-1 in previous chapter.

6.1.2 Adsorption kinetics

Again, the adsorption rate is estimated by the well-known linear driving force (LDF) equation which is expressed as following Eq. (6.2):

$$\frac{dw}{dt} = \alpha \exp\left(-\frac{E_a}{RT}\right)(W - w) \tag{6.2}$$

The numerical value of α and E_a were introduced in chapter 5 which are 132.89 [1/s] and 22.97 [kJ/mol] [60]. Results from chapter 5 works, non-isothermal kinetics parameters are employed in this study.

6.1.3 Mass balance

Assuming here that the vapor flow inside the connecting duct between adsorber and evaporator/condenser is laminar flow. Thus, the vapor mass flow rate inside the

connecting duct can be gained by Eq. (6.3).

$$\dot{m}_{p,x} = \frac{\pi d^4 \rho}{128\mu} \frac{\Delta P_x}{l} \tag{6.3}$$

where ρ and μ define the density and the viscosity of the refrigerant. d is the diameter of the connecting duct. the subscript $x = e$ indicates the evaporator and $x = c$ refers to the condenser. $\Delta P_e = P_e - P_b$ during the adsorption-evaporation process and $\Delta P_c = P_c - P_b$ during the desorption-condensation process.

The density of refrigerant inside adsorber can be obtained by using vapor mass flow rate as:

$$V_b \frac{d\rho_b}{dt} = \delta\left[\gamma \dot{m}_{p,e} - (1-\gamma)\dot{m}_{p,c}\right] - M_S \frac{dw}{dt} - \dot{m}_{bl} \tag{6.4}$$

where δ represents the status of the connecting valve (δ=1: when the valve is open, δ=0: when the valve is closed). Thus, δ will be 1 during adsorption and desorption and δ will be 0 during pressurization and depressurization. γ denotes the status of adsorption, in other words, γ will be 1 only during adsorption process while γ will be 0 for the other process. The condensation rate m_{bl} will be introduced later. The density of refrigerant is assumed as ideal gas which is valid as the pressure inside the adsorber is almost less than 10 kPa in case that refrigerant is ethanol. The density of ideal gas is given as Eq. (6.5)

$$\rho = \frac{P}{RT} \tag{6.5}$$

where the R is the gas constant. Pressure of refrigerant inside evaporator/condenser can be estimated as saturated vapor pressure which can be provided by Antoine equation expressed as Eq. (6.6).

$$\log\left(\frac{P}{1000}\right) = 7.3382 - \frac{1652.05}{231.48 + (T - 273.15)} \qquad (270.65 \leq \text{T[K]} \leq 369.65) \tag{6.6}$$

The total mass of refrigerant inside the compact adsorption system always keeps

constant. The amount of refrigerant liquid inside the evaporator and the condenser can be calculated by considering the amount of adsorbed refrigerant during the adsorption period or desorbed refrigerant for the time of the desorption process, it is given by:

$$\frac{dM_{x,l}}{dt} = -\dot{m}_{p,x} \tag{6.7}$$

It is reported that the condensation of refrigerant occurs on the inner surface wall of the adsorber tank in actual system which have not been considered in the simulation model. In order to take it into account, condensation (or evaporation) rate inside adsorber can be estimated by the pressure difference between the vapor refrigerant pressure and the saturated vapor pressure at the temperature of inner surface of adsorber tank expressed by Eq. (6.8)

$$\dot{m}_{bl} = h_t A_t \left(P_b - P_{t,sat} \right) \tag{6.8}$$

where A_t is the inner surface of adsorber tank and h_t denotes the coefficient of condensation rate which is given as 1×10^{-8} kg/(m^2 s Pa) in this study. The driving force of condensation is the pressure difference between the vapor refrigerant pressure, P_b, and the saturated vapor pressure at the temperature of inner surface of adsorber tank, $P_{t,sat}$.

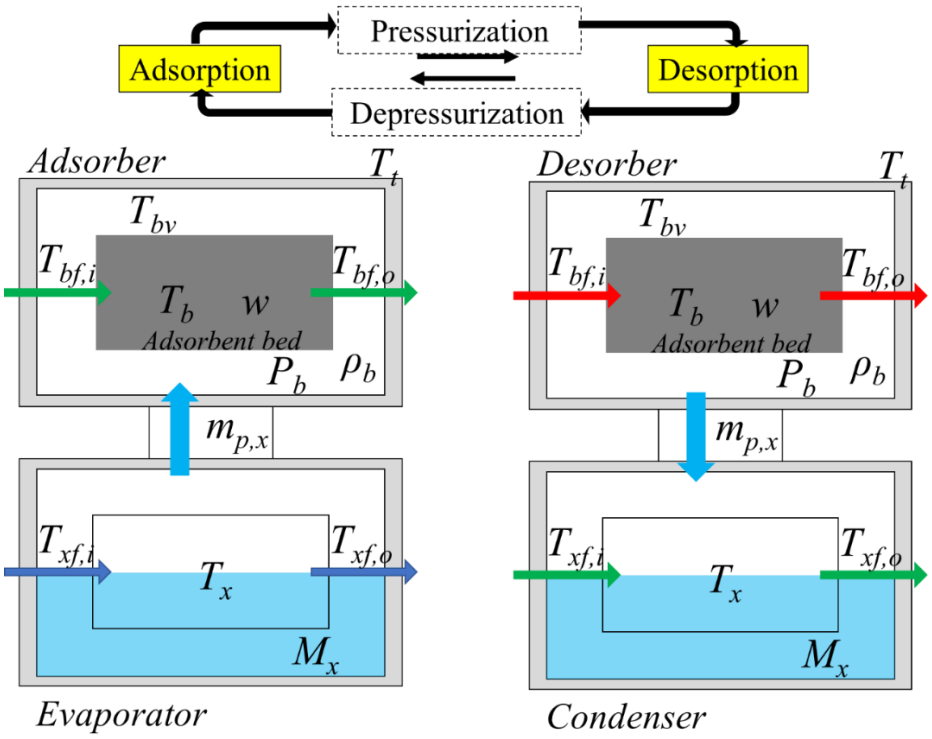

Fig. 6-1 Schematic diagram of one-bed adsorption cooling system

6.1.4 Energy balance for adsorber

Applying the lumped parameter model for the adsorption bed, which contains the activated carbon powder, the heat exchanger, the energy balance equation, is given by:

$$\left[M_S c_S(1+\alpha_b)+M_S w c_l\right]\frac{dT_b}{dt}=\dot{m}_w c_w \varepsilon_b\left(T_{bf,i}-T_b\right)+M_S Q_S\frac{dw}{dt}+h_b A_b\left(T_{bv}-T_b\right) \qquad (6.9)$$

where ε_b indicates heat exchanger effectiveness, h_b and A_b denote the heat transfer coefficient between adsorbent bed and vapor refrigerant and the heat exchange area. T_b is the temperature of adsorbent bed and T_{bv} is the temperature of refrigerant vapor inside adsorber. α_b expresses the ratio of heat capacity of me metallic par of heat exchanger to that of adsorbent. M_s and c_s are the mass and specific heat of adsorbent. The left hand side of the adsorber energy balance equation (Eq. (6.9)) is the thermal capacity of the adsorption bed heat exchanger (metal + adsorbent (activated carbon) + refrigerant (ethanol)) during adsorption and desorption. m_w and c_w are the mass flow rate and specific heat of the heat transfer medium, and $T_{f,i}$ denotes the temperature of heat transfer medium at inlet. The first term on the right side of Eq. (6.9) denotes the total

amount of heat taken into the cooling heat transfer medium upon adsorption or given by the high temperature medium for desorption. The second expression on the right of Eq. (6.9) denotes the release of adsorption heat for the time of adsorption or the given desorption heat in the process of desorption. The last indication on the right of Eq. (6.9) indicates the heat exchange between adsorbent bed and vapor refrigerant. The heat transfer coefficient hb is estimated by Eq. (6.10).

$$h_b = Nu_L \frac{k}{D} \tag{6.10}$$

where the Nusselt number Nu can be obtained assuming that the flow inside adsorber is laminar free convection heat transfer condition expressed as

$$Nu_L = 0.68 + \frac{0.670 Ra_L^{1/4}}{\left[1 + \left(0.492/\mathrm{Pr}\right)^{9/16}\right]^{4/9}} \tag{6.11}$$

where the Rayleigh number Ra_L can be estimated by Eq. (6-12).

$$Ra_L = \frac{g\beta(T_b - T_{bv})L^3}{\nu^2} \tag{6.12}$$

Here, Pr is given as 0.83. β is the volumetric thermal expansion coefficient calculated by the fluid temperature. g is the gravity force given as 9.8 m/s^2 and v is the viscosity given as 0.5×10^{-4} m^2/s.

6.1.5 Energy balance for refrigerant vapor

The energy balance of vapor refrigerant which have not been considered in the present lumped parameter model is given by Eq. (6.13).

$$\rho_b c_v V_b \frac{dT_{bv}}{dt} = h_b A_b (T_b - T_{bv}) + h_t A_t (T_t - T_{bv}) + \delta\gamma \dot{m}_{p,e} c_v (T_e - T_{bv}) - (1-\gamma) M_S \frac{dw}{dt} c_v (T_b - T_{bv}) \tag{6.13}$$

where ρ_b, c_v and V_b define the density of refrigerant calculated by Eq. (6.4), the heat capacity of vapor refrigerant and vacant volume inside adsorber tank. T_t represents the

temperature of adsorber tank which has a certain capacity resulted in the temperature change inside the adsorber. h_t and A_t are the heat transfer coefficient on the inner surface and heat exchange area of the adsorber tank. Note again that δ represents the status of the connecting valve and γ denotes the status of adsorption. The first term on the right side of Eq. (6.13) denotes the heat exchange between adsorbent bed and vapor refrigerant. The second term on the right of Eq. (6.13) represents the heat exchange between vapor refrigerant and the adsorber tank. The third term on the right of Eq. (6.13) shows the sensible heat of transferred refrigerant that refers the sensible heat needed to warm up the vapor refrigerant temperature until the evaporator temperature. The last description on the right of Eq. (6.13) represents the sensible heat of adsorbed refrigerant which refers the sensible heat demanded to warm up the vapor refrigerant temperature until adsorbent bed temperature during desorption.

6.1.6 Energy balance for adsorber tank

The energy balance of adsorber tank is given by Eq. (6.14).

$$M_t c_t \frac{dT_t}{dt} = h_t A_t \left(T_{bv} - T_t\right) + \frac{k_i}{l_i} A_t (T_{amb} - T_t) + \dot{m}_{bl} L_{eth} \tag{6.14}$$

where k_i and l_i define the thermal conductivity and thickness of the insulation that is covered over the adsorber. T_{amb} denotes the ambient temperature and L_{eth} is the latent heat of ethanol. The first expression on the right of Eq. (6.14) indicates the heat exchange between vapor refrigerant and the adsorber tank. The second expression on the right of Eq. (6.14) represents the heat exchange between the ambient and the adsorber tank through thermal insulation. The final term on the right of Eq. (6.14) shows the latent heat of vaporization/condensation due to the amount of evaporated or condensed refrigerant inside the adsorber.

6.1.7 Energy balance for evaporator/condenser

The energy balance equation for the condenser and the evaporator can be expressed by Eq. (6-15).

$$\left[M_x c_x + M_{x,l} c_l\right] \frac{dT_x}{dt} = \dot{m}_w c_w \left(T_{x,i} - T_{x,o}\right) - L_{eth} \dot{m}_{p,x} \tag{6.15}$$

where the subscript $x = e$ denotes the evaporator and $x = c$ indicates the condenser. The term on the left hand side of Eq. (6.15) indicates the energy variation required by the metallic parts of heat exchanger tubes and cooling heat transfer medium in the evaporator/condenser. The initial description on the right of Eq. (6.15) represents the sum of heat rejection to the cooling heat transfer fluid or the cooling effect of the evaporator depending on the operation mode. The final description on the right shows the latent heat of evaporation owing to the sum of adsorbed refrigerant and desorbed from the adsorber bed during the condensation mode.

6.1.8 System performance

The accumulated cooling effect Q_{ch}, the desorption heat Q_{de} and the adsorption heat during a cycle can be calculated by following Eq. (6.16), (6.17) and (6.18).

$$Q_{ch} = \int_0^{t_{ad}} m_w c_w \left(T_{e,i} - T_{e,o}\right) dt \tag{6.16}$$

$$Q_{de} = \int_0^{t_{de}} m_w c_w \left(T_{h,i} - T_{h,o}\right) dt \tag{6.17}$$

$$Q_{ad} = \int_0^{t_{ad}} m_w c_w \left(T_{ca,i} - T_{ca,o}\right) dt \tag{6.18}$$

The performance indices, such as cooling capacity (CC), specific cooling power (SCP) and coefficient of performance (COP) are given as follows:

$$CC = \frac{Q_{ch}}{t_{ad}} \tag{6.19}$$

where t_{ad} denotes the cycle time during adsorption and pre-cooling time. The specific cooing power is defined based on the accumulation of the cooling effect to adsorbent mass ratio which can be calculated by Eq. (6.20)

$$SCP = \frac{CC}{M_S} \tag{6.20}$$

COP in this study can be obtained by Eq. (6-21).

$$COP = \frac{Q_{ch}}{Q_{de} + Q_{sh}} \tag{6.21}$$

6.2 Validation of the model with experimental results

6.2.1 Experimental set-up

An experimental setup of the compact adsorption cooling system for evaluating is depicted in Fig. 3-1. Experimental facilities and procedures are also explained in Chapter 3. To confirm the modified simulation model, dynamic behaviors such as bed temperature, outlet temperature and pressure change are compared to validate the new model.

6.2.2 Performance evaluation

The operating conditions are listed in Table 6-1. The regeneration temperature and the evaporation temperature are varying from 60℃ to 80℃ and from 5℃ to 25℃ respectively while the adsorption and condensation temperature are maintained at 30℃.

Table 6-1 Operating conditions

Parameter	Symbol	Value
Flow rate of LLC	m_w	3 L/min
Adsorbent bed		
Hot inlet temperature	$T_{h,i}$	60, 70, 80 ℃
Cooling inlet temperature	$T_{ca,i}$	30 ℃
Evaporator		
Chilled inlet temperature	$T_{e,i}$	5, 15, 25 ℃
Condenser		
Cooling inlet temperature	$T_{c,i}$	30 ℃

Constant some parameters are required throughout the simulation. These parameters are relevant to the physical properties of antifreeze fluid, adsorbent (activated carbon) and other components of the system and structure of the system. Thermal properties of working pairs adopted in the simulation are listed in Table 5-4 in chapter 5. System parameter used in this study can be seen in Table 6-2.

6.3 Results and discussion

In this section, the accuracy of the improved lumped parameter model in the prediction of bed temperature, outlet temperature, COP and SCP are investigated against the one predicted by previous model (old model) and the available data from the experimental works which were carried out in Chapter 3. Since the experimental works were performed to examine rather the adsorption performance of activated carbon powder with ethanol than the cycle work, the dynamic behavior response only during adsorption process can be compared to experimental results. However, some indices such as temperature, pressure only during adsorption period, COP and SCP are compared with experimental results.

Here, the previous lumped parameter model is called old model and the modified lumped parameter model is called new model in order to simplify the explanation. The operating conditions of the results used following discussion are the regeneration temperature of 80℃, the adsorption and condensation temperature of 30℃, the evaporation temperature of 15℃ and fluid flow rate of 3 L/min. Adsorption and desorption time for this simulation works are set to 600s since it is known that the outlet and inlet temperature of heat transfer fluid will be closely homogeneous after 600s from experiments and the past study. On the other hand, pre-cooling and pre-heating time for this simulation works are fixed to 300s randomly in order to observe the responses easily and clearly.

6.3.1 Validation of dynamic behavior

Fig. 6-2(a) shows the comparison of the pressure change of refrigerant during pre-cooling process between experiments and simulation results predicted by modified simulation model. It can be obviously noticed that pressure during pre-cooling was predicted well in comparison to experimental data. However, it can be observed that there is a difference at the commencement point of adsorption between experimental results and simulation at the commencement point of adsorption. The Pressure obtained

by experiments didn't reach the point where predicted pressure is at. This might be due to the fact that the density of refrigerant inside adsorber becomes small because of the adsorption simultaneously occurred when the connected valve is open. Therefore, experimental pressure didn't reach the predicted pressure. As far as pressure change during pre-heating process is concerned, it can be observed from Fig. 6-2(b) that the modified simulation model could estimate the pressure inside adsorber with a good agreement as compared to experimental result. Pressure firstly reached to the pressure at 47 kPa after switching to the pre-heating process and decreased gradually due to the condensation effect.

As mentioned before, the ordinal lumped parameter model usually doesn't calculate the pressure during thermal compression. However, pressure can be estimated from D-A equation with the condition of equilibrium uptake during pre-cooling/pre-heating process. Pressure during pre-cooling/pre-heating can be derived from Eq. (6.1) as:

$$P = \frac{P_S}{\exp\left\{\frac{E}{R_g T}\left[-\ln\left(\frac{W}{W_0}\right)\right]^{1/n}\right\}}$$

Note here that pressure change during pre-cooling/pre-heating can be assumed by above equation only under the condition where the adsorption uptake doesn't change during those period (equilibrium state).

Fig. 6-3(a) shows the comparison of the pressure change of refrigerant inside adsorber between the previous model and modified model. Fig. 6-3(b) depicts the comparison of pressure changes at around commencement of adsorption. Blue line in the graphs represent the pressure estimated by D-A equation and red line shows the pressure predicted by new simulation model. It is observed from Fig. 6-3(a) that there is pressure difference only during pre-heating process. This could be due to the fact that new simulation model takes into account the condensation effect which causes pressure difference in comparison to conventional lumped parameter model. Pressure with regard to pre-cooling process in Fig. 6-3(b), both old model and new model can predict the pressure well in comparison to experiment. It is hard to tell the difference between them. It can be said that pressure could be estimated with a good agreement by using D-A equation. However, it can be used only when the adsorption uptake remains constant. It requires the new simulation model to predict the pressure in case for non-equilibrium condition which is the matter in the actual system. Regarding to pressure during

pre-heating process, pressure calculated by D-A equation reached about 50 kPa while pressure by new model reached about 47 kPa and gradually declined because of the condensation effect. Old model can't consider the condensation effect while the modified model does. However, it can conclude that D-A equation provides a good pressure prediction if changes in adsorption uptake can be neglected during pre-cooling/pre-heating process.

Table 6-2 Actual heat exchanger design

Parameter	Symbol	Value
Adsorber		
Mass of activated carbon	M_s	0.113 kg
Heat capacity of heat exchanger	M_bc_b	493.7 J/K
Heat capacity ratio	α_b	4.82
Heat exchanger effectiveness	ε_b	0.66
Heat exchange area of adsorbent bed	A_b	0.115 m^2
Vacant volume	V_b	864×10^{-6} m^3
Heat capacity of tank	M_tc_t	2301 J/K
Heat exchange area of tank	A_t	0.3 m^2
Evaporator/Condenser		
Heat capacity of heat exchanger	M_xc_x	493.7 J/K
Heat exchanger effectiveness	ε_x	0.80

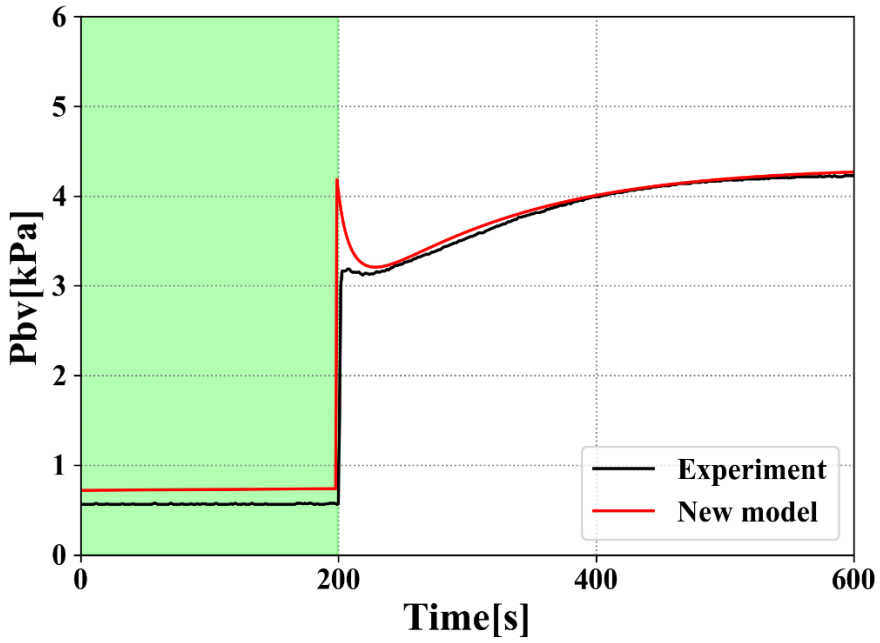

(a)

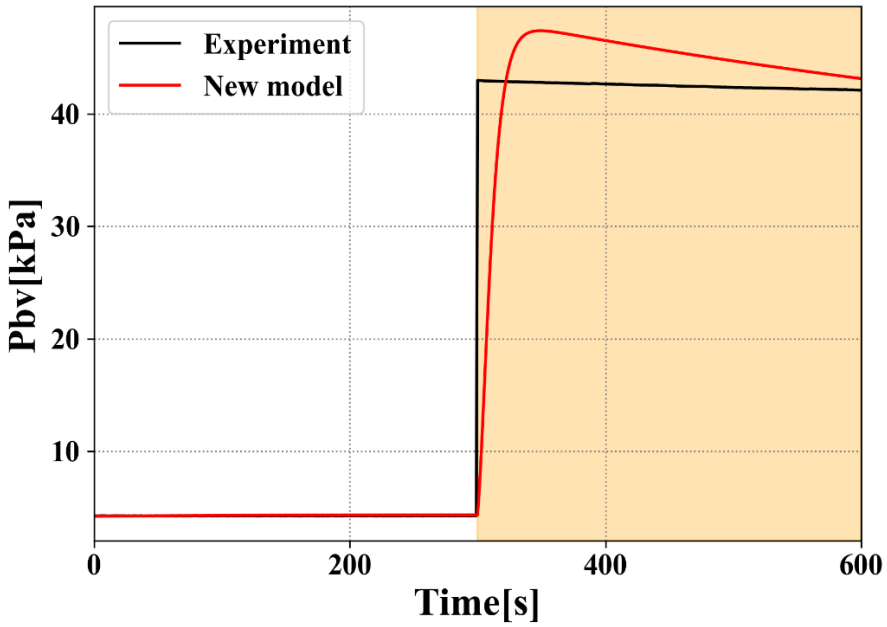

(b)

Fig. 6-2 Transient profiles for pressure change of vapor refrigerant, (a) Pressure change around pre-cooling, (b) Pressure profile around pre-heating process.

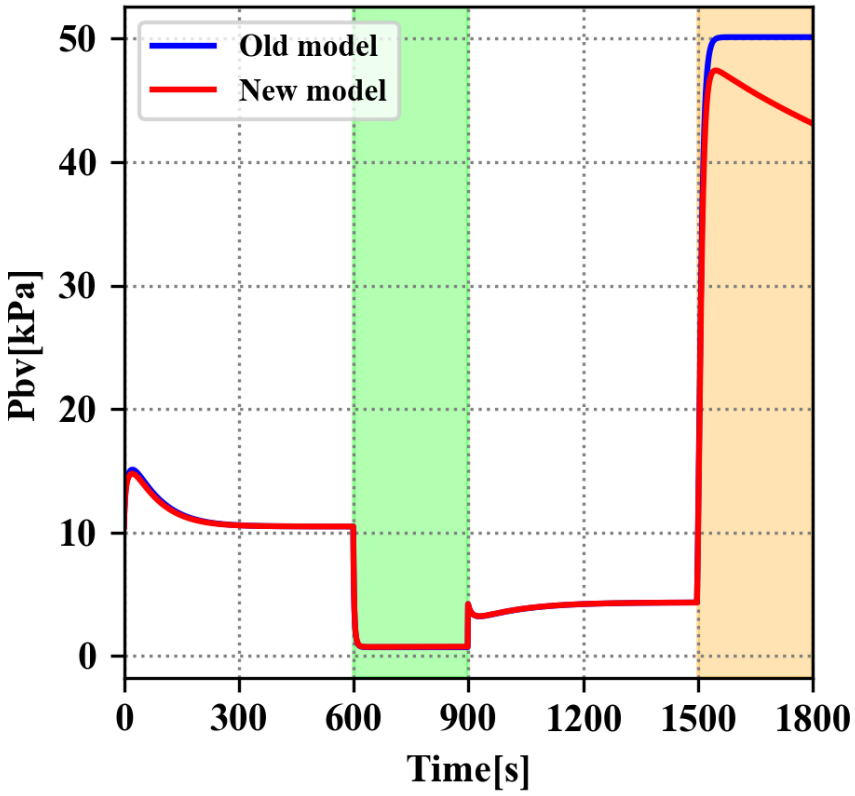
Old model
New model
Pbv[kPa]
Time[s]
0
10
20
30
40
50
0
300
600
900
1200
1500
1800

(a)

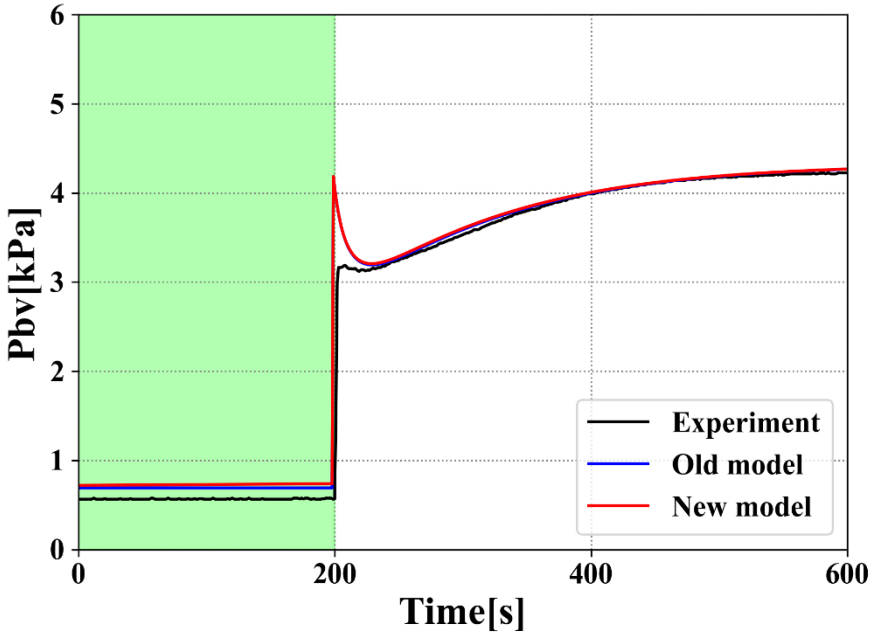
Experiment
Old model
New model
Pbv[kPa]
Time[s]
0
1
2
3
4
5
6
0
200
400
600

(b)

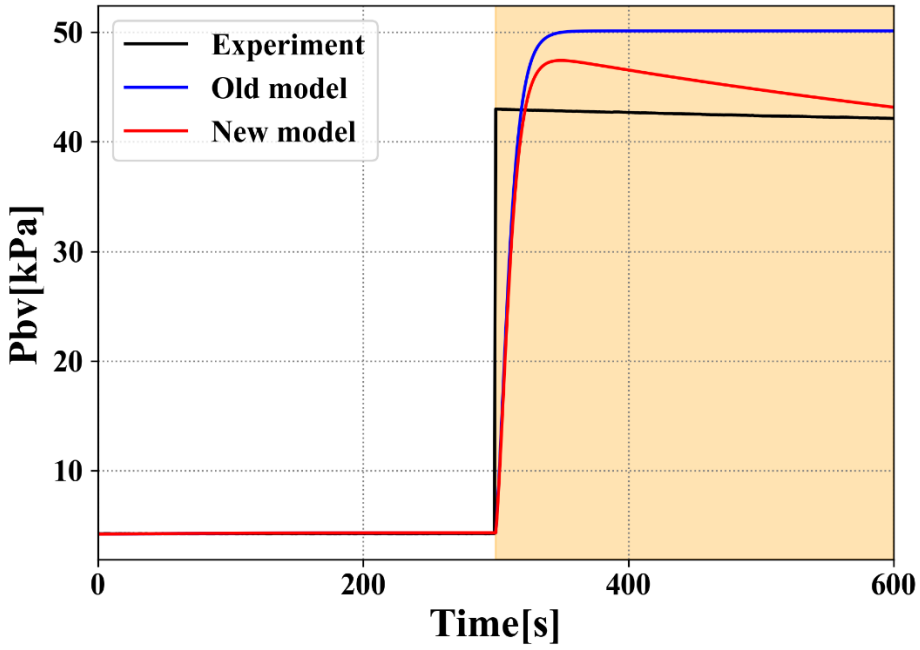

(c)

Fig. 6-3 Comparison results of transient profiles for pressure change of vapor refrigerant, (a) Whole process, (b) Pressure change around pre-cooling, (c) Pressure profile around pre-heating process.

This pressure drop tendency was also occurred in the experiment. However, the pressure taken from experiment rises vertically in contrast to the simulated one. Note here that the experiment was not done cyclically and our facility didn't possess the switching mechanism of thermal source. Therefore, the experimental data used in Fig. 6-3(c) is picked up and connected after the saturate pressure during adsorption process artificially.

For the changes in adsorption uptake, it can be observed in Fig. 6-4 that the small amount of adsorbed refrigerant is changing during the pressurization (blinded area by green) and depressurization (blinded area by orange). This means that for the pre-cooling process, the remained refrigerant inside adsorber as vapor after desorption will be adsorbed by cooling down the adsorbent bed, and for the pre-heating process, the adsorbed refrigerant on the adsorbent bed after adsorption will be desorbed to the inside adsorber as vapor by heating up the adsorbent bed. Note here that, since the adsorption cooling system used in this study was a compact scale adsorber which has the slight vacant volume inside adsorber tank against the volume of adsorbent bed, it

resulted in the small changes in adsorption uptake. The influence of vacant volume against the adsorbent bed volume will be discussed in more detail later in section 6.3.3.

Fig. 6-5(a) shows the comparison of simulation for the bed temperature responses for the whole process between old model and new model. Note here that, the simulation results for whole process cannot be compared since the experiments are not measured cyclically. It is observed that there is no distinct difference between the bed temperature prediction between them. Hence, it can be said that the modification of the mathematical model doesn't have a huge effect on the prediction of bed temperature. Fig. 6-5(b) depicts the comparison of simulation for the bed temperature responses during adsorption process with experimental results. Some variation can be seen especially on the evaporator side (dashed lines). This might be due to the fact that there is a heat loss to the ambient (ambient temperature: 26°C) in a real system, which resulted in the increment of evaporator temperature. However, as a whole, both model can predict the bed temperature.

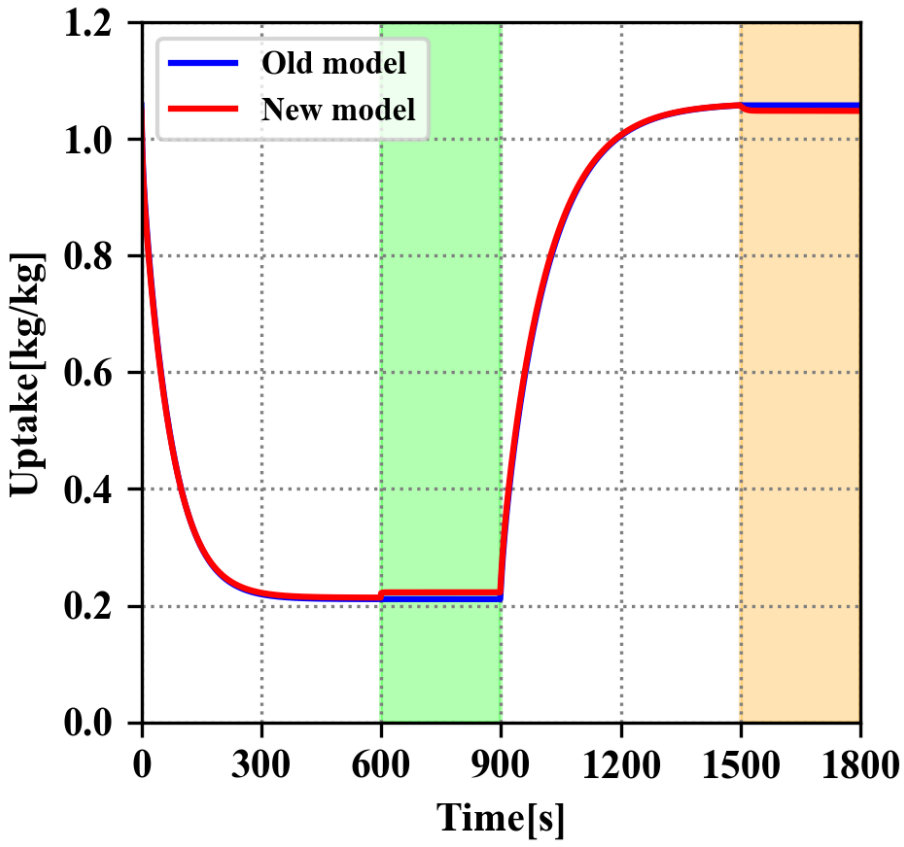

Fig. 6-4 Comparison of adsorption uptake profiles

The comparison of outlet temperature from adsorbent bed and evaporator/condenser heat exchanger can be seen in Fig. 6-6. Both old and new model can predict well the outlet temperature of heat transfer medium especially on evaporator side in comparison to experimental data. Some difference can be observed at the peak point of adsorption. This could be due to the fact that the kinetics parameters weren't taken into account well and there is a temperature distribution on the adsorbent bed in a real system which is not considered in the simulation model.

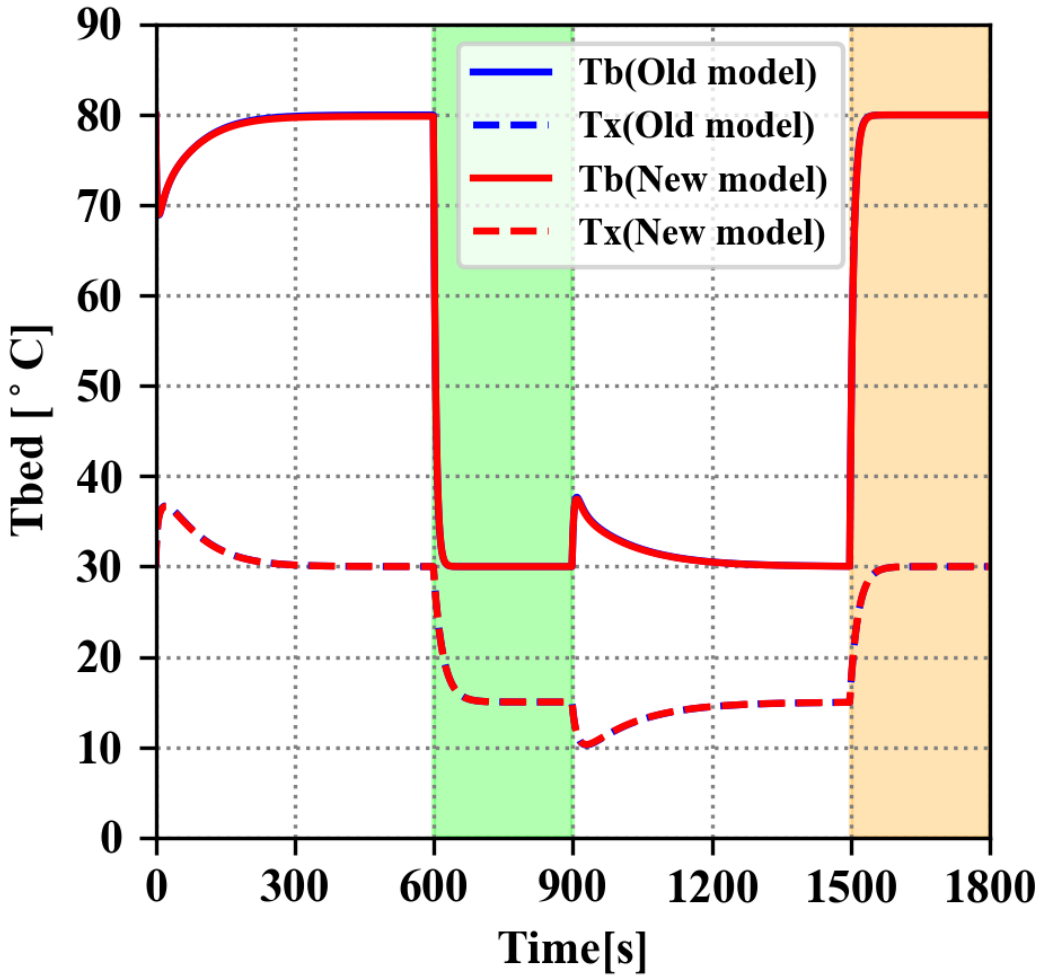

(a)

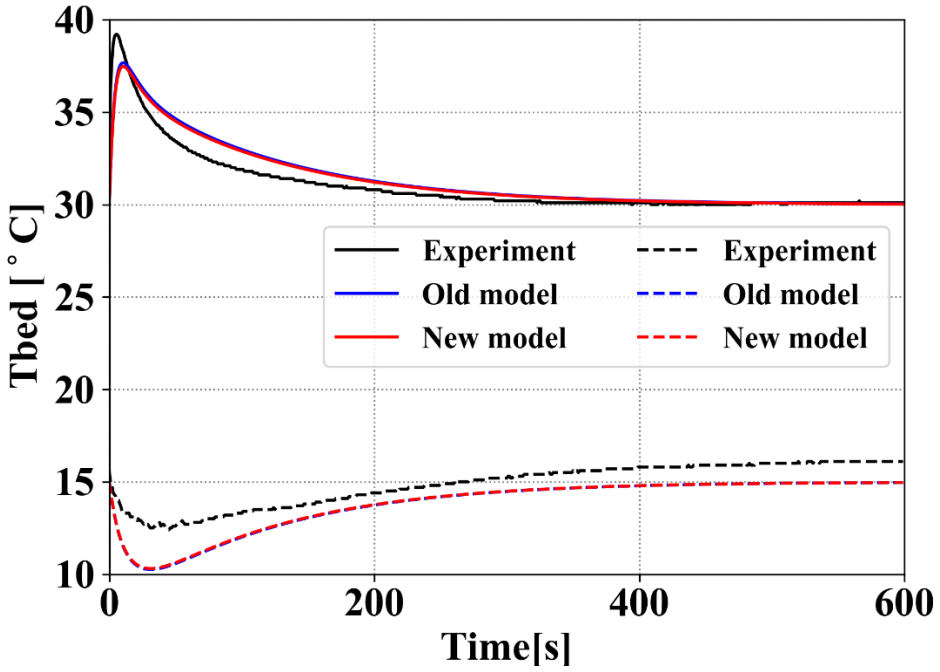

(b)

Fig. 6-5 Comparison of temperature profiles for adsorbent bed and evaporator/condenser heat exchanger, (a) Cycle, (b) During adsorption process

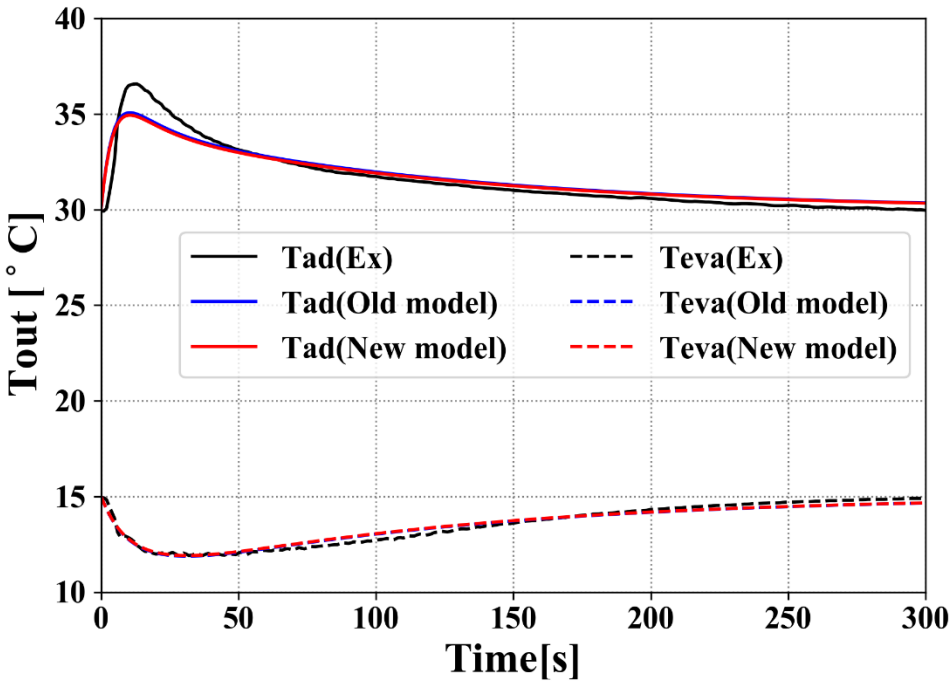

Fig. 6-6 Comparison of outlet temperature between experiment and simulation results during adsorption process.

6.3.2 Investigation of system performance

Here, some extra studies are presented to investigate the effect of pre-cooling/heating time and adsorption/desorption time. The influence of pre-cooling/heating time on the SCP and the COP are investigated and can be seen in Fig. 6-7. The SCP decreases notably after 100s with increasing the pre-cooling/pre-heating time while the COP increases with increasing the time up to 100s and remains the same closely regardless of the time after 100s. Therefore, it comes to conclusion that the optimum pre-cooling/heating time is around 100s. Fig. 6-8 illustrate the influence of adsorption/desorption time on the SCP and the COP. As it can be observed that the SCP reach the maximum point at the adsorption time of 200s and then decreases gradually with increasing the time. On the other hand, the COP increases with increasing the adsorption time. From both points of view, the crossing point of the two lines is optimum condition to reach the best performance. Therefore, the adsorption time of 400s is selected and used in the next study.

The simulation works on SCP and COP employing the optimum pre-cooling/heating and adsorption/desorption time are carried out to investigate the influence of regeneration and evaporation temperature and evaluate the simulation model. Fig. 6-9 shows the comparison results of the influence of regeneration on SCP and COP. The SCP and COP increases with increasing the regeneration temperature. Both the old and new model can predict the COP with approximately ±10% error. When it comes to the SCP prediction, the accuracy of the new model is better than that of the old model by around 10%. The same tendency can be observed in Fig. 6-10 which describes the comparison results of the influence of evaporation temperature. From both investigation studies, it can be concluded that the higher regeneration temperature and evaporation temperature among the selected temperature in this study, the higher system performance in terms of the SCP and COP can be obtained. Furthermore, the accuracy of prediction for cooling power advanced by taking into account the heat exchange through the adsorber tank to the ambient.

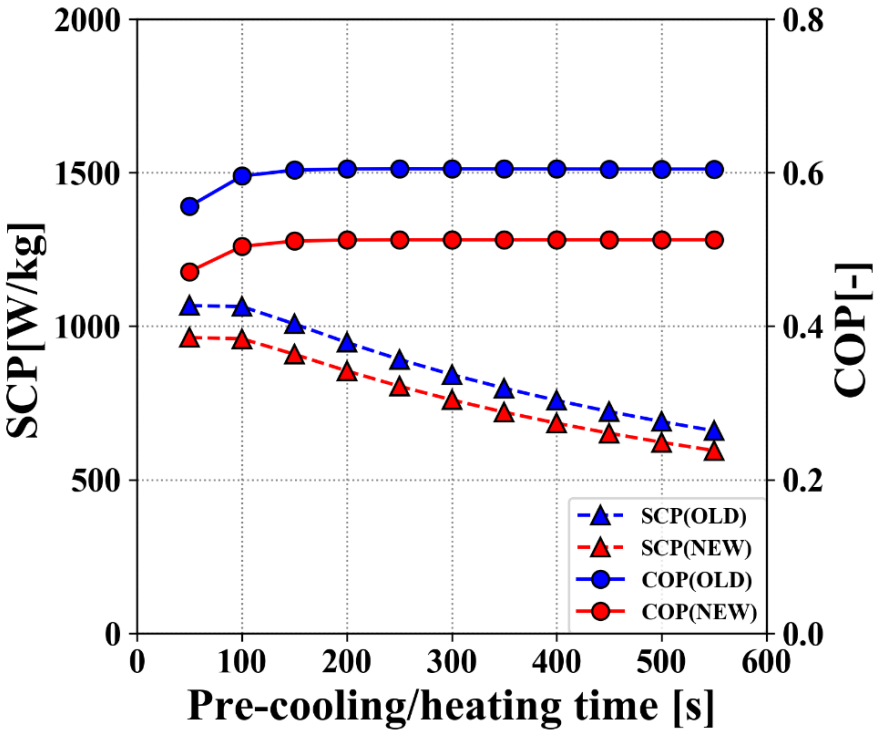

Fig. 6-7 Influence of pre-cooling/heating time on SCP and COP

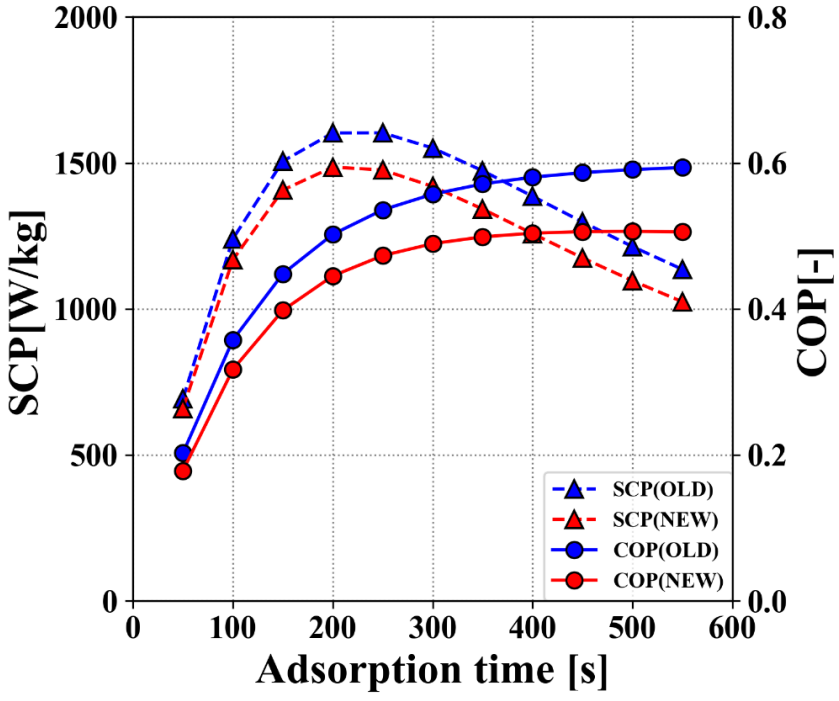

Fig. 6-8 Influence of adsorption time on SCP and COP

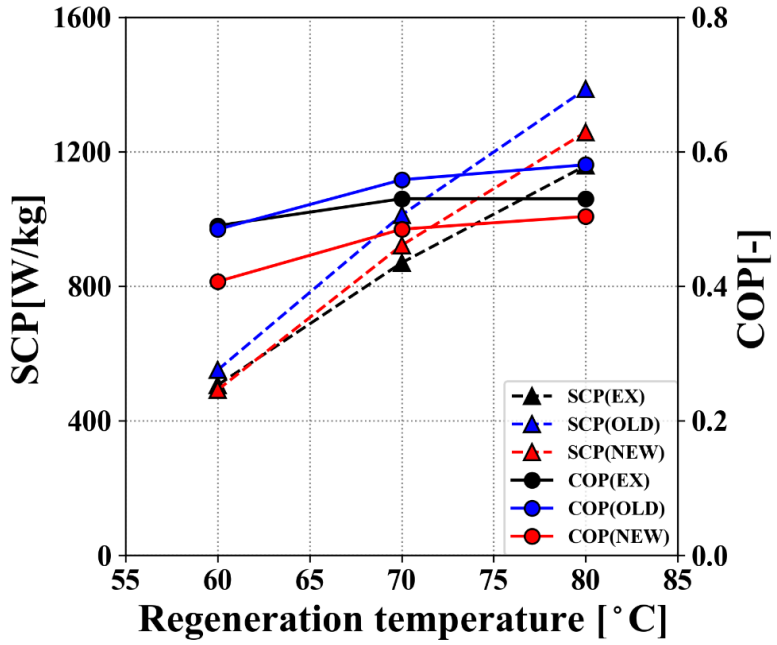

Fig. 6-9 Comparison results of the influence of regeneration temperature on SCP and COP

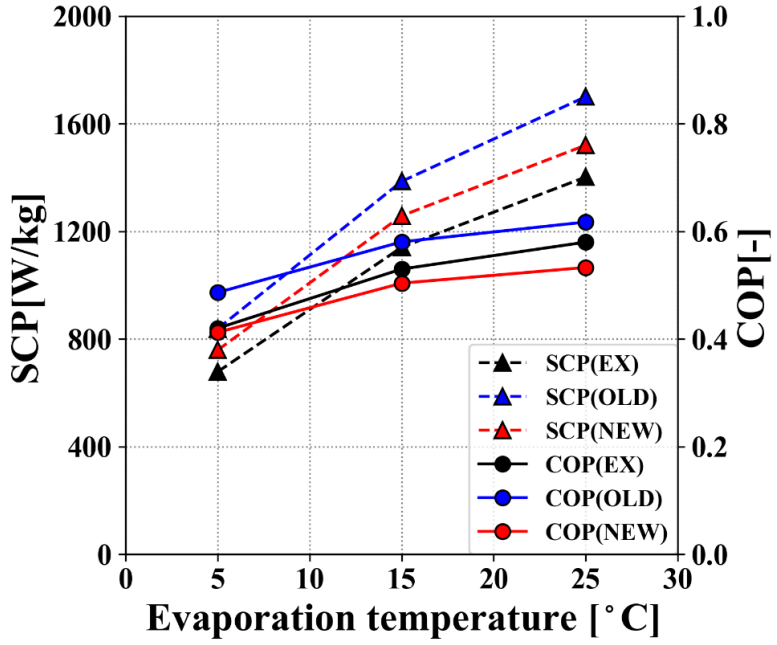

Fig. 6-10 Comparison results of the influence of evaporation temperature on SCP and COP

6.3.3 Investigation of influence of vacant volume

As mentioned in section 6.3.1, the small amount of uptake change was observed since the vacant volume value taken from experiment was almost optimized. What would the uptake change be like if the vacant volume against the volume of adsorbent bed become bigger? Thus, the influence of the ratio of vacant volume against volume of the adsorbent bed was investigated, and results of this study can be seen in Fig. 6-11. Y in Fig. 6-11 represents the ratio of vacant volume against volume of the adsorbent bed ($Y=V_b/V_s$). V_b is the vacant volume and V_S is the volume of adsorbent bed. The ratio Y of our system is about 2. It can be recognized that the changes in uptake during the thermal compression process increases with increasing the ratio Y. For the $Y=2$ case, and the amount of uptake during the thermal compression process changed by 1.4% against the effective adsorption uptake. The percentages of change in uptake against the effective adsorption uptake for $Y=5$ (green line) and $Y=10$ (orange line) cases are approximately 3.0% and 5.5% respectively. Therefore, if the adsorbent bed is not designed optimally, it does affect the amount of adsorption and the cooling effect as well as the system performance.

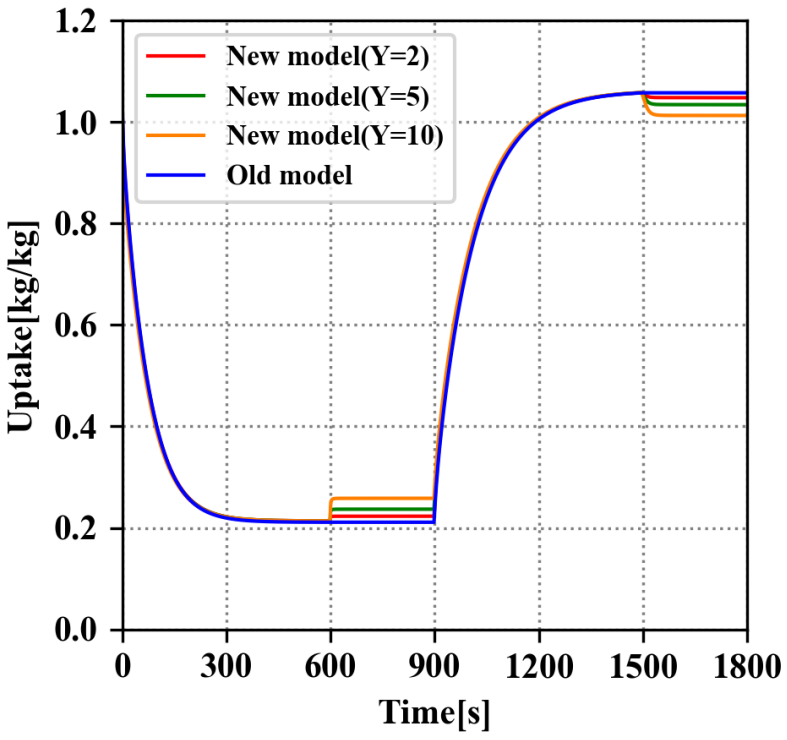

Fig. 6-11 Influence of vacant volume inside adsorber on adsorption uptake

The influence of the ration *Y* on COP and SCP can be found in Fig. 6-12 and Fig. 6-13 respectively. These studies were conducted under the condition where the adsorption/desorption time of 400s and pre-cooling/heating time of 100s which were found to be the best operating condition according to previous works. For the COP results, it can be seen that the COP decreased notably as the ratio *Y* increased. The average COP difference of 0.13 was obtained between *Y=2* (red line) and *Y=10* (orange line). If the adsorber is not designed properly, the COP of adsorption cooling system will be decreased. When it comes to the SCP, the similar tendency can be found in Fig. 6-13. It was found that the SCP decreased by about 300 W/kg when compared between Y=2 (red line) and Y=10 (orange line) at the regeneration temperature of 80℃. Based on the above considerations, it can be concluded that the optimal adsorber design is crucial to reach the potential performance and the modification of the mathematical model which has been done in this study can give us more detailed behavior of adsorption cooling system.

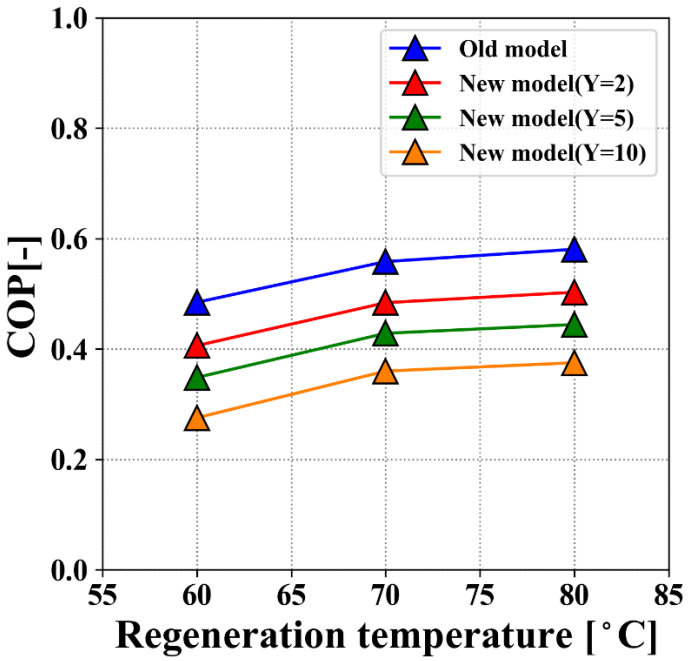

Fig. 6-12 Comparison of COP between various ratio Y (vacant volume against adsorbent bed volume)

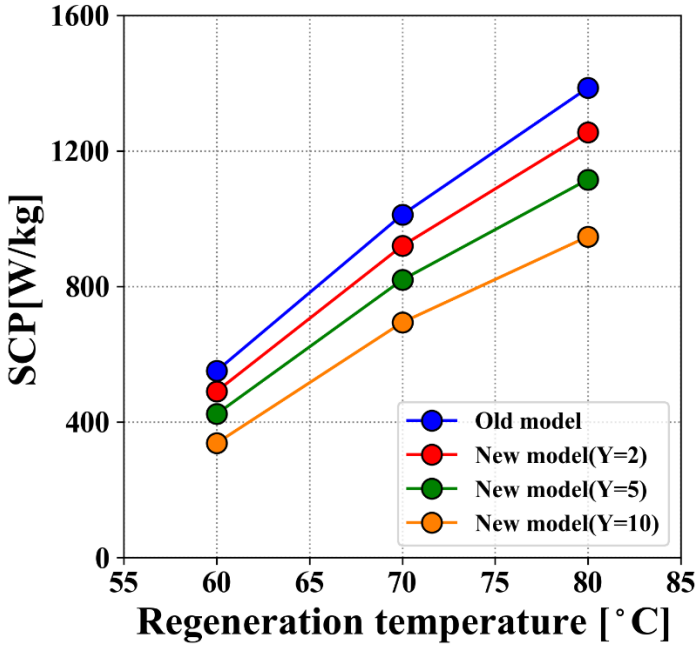

Fig. 6-13 Comparison of SCP between various ratio Y (vacant volume against adsorbent bed volume)

6.4 Conclusions

The modified simulation model for the one-bed compact adsorption cooling system was established and assessed with experimental results in this chapter.

- Pressure change during the thermal compression process was successfully obtained by modifying the existed lumped parameter model. The pressure during the pre-cooling process was compared with experimental data and it was predicted with reasonable agreement. As for the pressure change during pre-heating, the influence of condensation was taken into account.
- The influence of vacant volume inside adsorber was revealed by predicting using the detailed model. If the ratio design of adsorbent bed heat exchanger volume against vacant volume is not optimized, which means the vacant volume is relatively bigger than the adsorbent bed volume, the amount of adsorption uptake during pressurization or depressurization changes with increasing the vacant volume.
- Modification of mathematical model was not affected that much the prediction of

transient profiles for bed temperature and outlet temperature of heat transfer fluid. Both the previous and modified simulation model can predict the temperature profile well, however, some difference was observed especially on adsorber side. This could be due to the fact that the assumptions of lumped parameter model which are (1) the temperature is uniform in the adsorbent layer, (2) the refrigerant is adsorbed uniformly in the adsorber.

- The effect of pre-cooling/heating and adsorption/desorption time was also investigated to find out the best operating condition. According to the simulation results, the optimal pre-cooling/heating and adsorption/desorption time based on SCP and COP were 100s and 400s respectively.
- Both the previous and modified model were able to estimate the COP with approximately ±10% error. For the SCP prediction, it was found that the accuracy of the new model is better than that of the old model by around 10%.

Chapter 7: Overall conclusions

The main targets of this study are to investigate the performance of a compact adsorption cooling system using activated carbon-ethanol pair and to upgrade the existed simulation model to predict the dynamic responses of adsorption cooling system in more detail. According to the previous studies, activated carbon-ethanol could contribute to reducing the size of the heat exchanger which allow us to establish a compact adsorption cooling system. To achieve the target, the following studies were conducted.

1. A review of the past researches has been done to understand the efficiency and suitability of activated carbon with ethanol for cooling system application. According to the review study, it was found that the performance still has a room for improvement by reducing the unnecessary energy losses due to overheating and improving the heat transfer rate of the activated carbon during adsorption and desorption time.
2. To investigate the potential of the compact adsorption cooling system, the adsorption system consisted of one adsorber and heat exchanger working as evaporator or condenser depending on the operation has been set up to identify not only the adsorption reactions where the adsorbent is attached to the heat exchanger but also the optimum operating condition.
3. To estimate the overall thermal conductance which will be used in the lumped parameter simulation, the prediction model has been introduced and assessed by comparing with one extracted from experimental results.
4. To clarify the influence of assuming isothermal condition on kinetics parameter, lumped parameter simulation has been conducted by employing the two types of kinetics parameters that have been published in comparison to experimental data.
5. Modified lumped parameter model has been established to predict the more detail information of the thermal compression process. This model can estimate the changes in pressure and adsorption uptake during pressurization and depressurization which have not been considered in previous model.

The overall conclusions summarized from a lot of efforts for above mentioned studies are given as follows:

- From the experimental works, the adsorption heat rejection and cooling performance increase with increasing the regeneration and evaporation temperature. The maximum peak value of the cooling effect reaches about 900W with the COP of 0.59 under the condition of evaporation temperature of 25℃, the desorption temperature of 80℃, the adsorption and condensation temperature of 30℃. It is also found that the higher the flow rate, the more adsorption heat can be gathered more quickly. From the extensive experimental study, the activated carbon-ethanol pair adsorption cooling system are promising in order not only to reduce the mass volume of the adsorption system and also to increase the cooling effect per volume.
- The estimation model of overall thermal conductance presented the reasonable agreement with the UA values obtained from experimental results. For the conditions that the adsorption temperature of 30℃ with the evaporation temperature of 5℃, 15℃, 25℃, the estimation error of the model against the experimental data were 5.1%, -6.1%, 4.2% respectively.
- The simulation employing the non-isothermal kinetics parameter has shown a better agreement significantly with experimental results in terms of outlet temperature than the one using the isothermal kinetics parameter.
- Simple lumped parameter model was a useful technique to predict the adsorption cooling performance provided the input data was adopted from the actual experimental studies.
- The modified simulation model provided the more detail dynamic behavior of the compact adsorption cooling system as compared to the previous model. It was found that the changes in pressure and adsorption uptake could be obtained by improved simulation model. The prediction of COP was not affected that much by assuming the isosteric change as these performance indices are based on the accumulation of cooling effect during evaporation process. However, the changes in pressure and adsorption uptake could affect the optimum volume of adsorber and optimum cycle time for pre-cooling and pre-heating process.
- As a result of development of detailed simulation model, this approach allows us to find out the optimal design of adsorber and could be extended to other simulation works such as for heat pump system to predict the performance in more detail.

References

[1] Bakker, E. J. and de Boer, R., “TOPMACS Project – Development of a new 2.5 kW adsorption chiller for heat driven cooling” [N], IEA Heat Pump, Newsletter, 2010, 28(1): 39-42

[2] Critoph, R. E. and Metcalf, S. J. ‘Specific cooling power intensification limits in ammonia–carbon adsorption refrigeration systems’[J], Applied Thermal Engineering, 2004.

[3] American society of Heating, refrigerating and Air-Conditioning Engineers [Z]. 2009, ASHRAE handbook-fundamentals (I-P Edition).

[4] Wang, D.C. et al. ‘A review on adsorption refrigeration technology and adsorption deterioration in physical adsorption systems’ [J], Renewable and Sustainable Energy Reviews, Pergamon, 2010, 14(1): 344–353.

[5] Hassan, H. Z. and Mohamad, A. A. ‘A review on solar-powered closed physisorption cooling systems’ [J], Renewable and Sustainable Energy Reviews, Pergamon, 2012, 16(5): 2516–2538.

[6] Dabrowski, A., ‘Adsorption – from theory to practice’ [J], Adv. Colloid Interfac. Sci., 2001, 93: 135-224.

[7] Jung, D. et al. ‘Energy Storage in Zeolites and Application to Heating and Air Conditioning’ [J], Studies in Surface Science and Catalysis, Elsevier, 1985, 24: 555–562.

[8] Wang, D. C., Xia, Z. Z. and Wu, J. Y. ‘Design and performance prediction of a novel zeolite–water adsorption air conditioner’ [J], Energy Conversion and Management, Pergamon, 2006, 47(5): 590–610.

[9] Vasta, S. et al. ‘Development and lab-test of a mobile adsorption air-conditioner’ [J], International Journal of Refrigeration, 2012, 35(3), 701–708.

[10] Zhang, L. ‘Design and testing of an automobile waste heat adsorption cooling system’ [J], Applied Thermal Engineering, Pergamon, 2000, 20(1): 103–114.

[11] Li, A. et al. ‘Performance evaluation of a zeolite–water adsorption chiller with entropy analysis of thermodynamic insight’ [J], Applied Energy. Elsevier, 2014, 130: 702–711.

[12] Sakoda, A and Suzuki, M. ‘Fundamental study on solar powerd adsorption cooling system’ [J], Chemical Engineering of Japan, 1985, 17: 52－57.

[13] Suzuki, M. Sakoda, A. ‘Simultaneous Transport of Heat and Adsorbate in Closed Type Adsorption Cooling System Utilizing Solar Heat’ [J], Solar Energy

Engineering, 1986, 108: 239－245.

[14] Saha, B. B., Boelman, E.C., Kashiwagi, T., ‘Computer simulation of a silica gel-water adsorption refrigeration cycle - the influence of operating conditions on cooling output and COP’ [J], ASHRAE Trans, 1995, 101(2): 348-357

[15] Chua, H. T. et al. ‘Multi-bed regenerative adsorption chiller — improving the utilization of waste heat and reducing the chilled water outlet temperature fluctuation’ [J], International Journal of Refrigeration. Elsevier, 2001, 24(2): 124–136.

[16] Chen, C. J. et al. ‘Study on a compact silica gel–water adsorption chiller without vacuum valves: Design and experimental study’ [J], Applied Energy. Elsevier, 2010, 87(8): 2673–2681.

[17] Srivastava, N. C. and Eames, I. W. ‘A review of adsorbents and adsorbates in solid–vapour adsorption heat pump systems’ [J], Applied Thermal Engineering. Pergamon, 1998, 18(9–10): 707–714.

[18] Tamainot-Telto, Z. et al. ‘Carbon–ammonia pairs for adsorption refrigeration applications: ice making, air conditioning and heat pumping’ [J], International Journal of Refrigeration, 2009, 32(6): 1212–1229.

[19] Metcalf, S. J. and Tamainot-Telto, Z. ‘Optimal cycle selection in carbon-ammonia adsorption cycles’ [J], International Journal of Refrigeration, 2012, 35(3): 571–580.

[20] Yeo, T. H. C., Tan, I. A. W. and Abdullah, M. O., ‘Development of adsorption conditioning technology using modified activated carbon – A review’ [J], Renewable and Sustainable Energy Reviews, 2012, 16 (5): 3355-3363.

[21] Shen, C., Grande, C. A., Li, P., Yu, J., and Rodrigues, A. E., ‘Adsorption equilibria and kinetics of CO2 and N2 on activated carbon beds’ [J], Chemical Engineering Journal, 2010, 160 (2): 398-407.

[22] Tamainot-Telto, Z., Metcalf, S. J., Critoph, R. E., Zhong, Y., and Thorpe, R., “Carbon–ammonia pairs for adsorption refrigeration applications: ice making, air conditioning and heat pumping,” International Journal of Refrigeration, 2009, 32 (6): 1212–1229.

[23] Banker, N. D., Prasad, M., Dutta, P. and Srinivasan, K., ‘Development and transient performance results of a single stage activated carbon – HFC 134a closed cycle adsorption cooling system’ [J], Applied Thermal Engineering, 2010, 30 (10): 1126-1132.

[24] Henninger, S. K., Schicktanz, M., Hugenell, P. P. C., Sievers, H. and Henning, H. M., ‘Evaluation of methanol adsorption on activated carbons for thermally driven

chillers part I: Thermophysical characterisation' [J], International Journal of Refrigeration, 2012, 35 (3): 543-553.

[25] Uddin, K., El-Sharkawy, I. I., Miyazaki, T., Saha, B. B., Koyama, S., Kil, H.-S., Miyawaki, J. and Yoon, S.-H., 'Adsorption characteristics of ethanol onto functional activated carbons with controlled oxygen content' [J], Applied Thermal Engineering, 2014, 72 (2): 211–218.

[26] Miyazaki, T., El-Sharkawy, I. I., Saha, B. B. and Koyama, S., "Performance Simulation of Adsorption Refrigeration / Heat Pump with Silica Gel-Water and Activated Carbon-Ethanol Combinations' [C], 7th Asian Conference on Refrigeration and Air Conditioning, ACRA, 2014, Jeju, Korea: 1–2.

[27] Wang, L. W., Wang, R. Z. and Oliveira, R. G., 'A review on adsorption working pairs for refrigeration' [J], Renewable and Sustainable Energy Reviews, 2009, 13 (3): 518–534.

[28] Attan, D., Alghoul, M. A., Saha, B. B., Assadeq, J. and Sopian, K., 'The role of activated carbon fiber in adsorption cooling cycles' [J], Renewable and Sustainable Energy Reviews, 2011, 15(3): 1708–1721.

[29] Zheng, Q. R., Zhu, Z. W. and Wang, X. H., 'Experimental studies of storage by adsorption of domestically used natural gas on activated carbon' [J], Applied Thermal Engineering, 2015, 77: 134–141.

[30] Johannes. A., Daniel. R., Kai. T., Alexander. S., 'Combination of granular activated carbon adsorption and deep-bed filtration as a single advanced wastewater treatment step for organic micropollutant and phosphorus removal' [J], Water Research, 2016, 92: 131-139.

[31] Gong, J., Liu, J., Wan, D. Chen, X., Wen, X., Mijowska, E., Jiang, Z., Wang, Y. and Tang, T., 'Catalytic carbonization of polypropylene by the combined catalysis of activated carbon with Ni2O3 into carbon nanotubes and its mechanism' [J], Applied Catalysis A: General, 2012, 449: 112–120.

[32] Ruthven, D.M., 1984, 'Principles of adsorption and adsorption processes', John Wiley & Sons, Canada.

[33] El-Sharkawy, I.I., Saha, B. B., Koyama, S., He, J., Ng, K. C. and Yap, C., 'Experimental investigation on activated carbon–ethanol pair for solar powered adsorption cooling applications' [J], International Journal of Refrigeration, 2008, 31 (8): 1407-1413.

[34] El-Sharkawy, I.I., Uddin, K., Miyazaki, T, Saha, B. B., Koyama, S., Kil, H.-S., Yoon, S.-H. and Miyawaki, J., 'Adsorption of ethanol onto phenol resin based adsorbents for developing next generation cooling systems'[J], International

Journal of Heat and Mass Transfer, 2015, 81: 171–178.

[35] Miyazaki. T., Miyawaki. J., Ohba. T., Yoon. S. H., Saha. B. B., Koyama. S., 'Study toward high-performance thermally driven air-conditioning systems' [C], International Conference on Engineering, Science and Nanotechnology, 2016: 020002-1-020002-9.

[36] Yong, L. and Sumathy, K., 'Review of mathematical investigation on the closed adsorption heat pump and cooling systems' [J], Renewable and Sustainable Energy Reviews, 2002, 6: 305-337.

[37] Zhang, G., Wang, D. C., Zhang, J.P., Han, Y.P. and Sun, W. C., 'Simulation of operating characteristics of the silica gel water adsorption chiller powered by solar energy' [J], Solar Energy, 2011, 85: 1469-1478.

[38] Wang, D.C., Xia, Z.Z., Wu, J.Y., Wang, R.Z., Zhai, H. and Dou, W.D., 'Study of a novel silica-gel water adsorption chiller. part I. design and performance prediction' [J], International Journal of Refrigeration, 2005, 28: 1073–1083

[39] Zhang L. Z. and Wang L., 'Performance estimation of an adsorption cooling system for automobile waste heat recovery' [J], Applied Thermal Engineering, 1997, 17: 1127-1139.

[40] Ali, Syed M. and Chakraborty, A., 'Thermodynamic modelling and performance study of an engine waste heat driven adsorption cooling for automotive air-conditioning' [J], Applied Thermal Engineering, 2015, 90: 54-63.

[41] Wang, L., Wu, J., Wang, R., Xu, Y., Wang, S. and Li, X., 'Study of the performance of activated carbon–methanol adsorption systems concerning heat and mass transfer' [J], Applied Thermal Engineering, 2003, 23 (13): 1605–1617

[42] Ramji, H. R., Leo, S. L. and Abdullah, M. O., 'Parametric study and simulation of a heat-driven adsorber for air conditioning system employing activated carbon–methanol working pair' [J], Applied Energy, 2014, 113: 324–333.

[43] Lim, L. S. and Abdullah, M. O., 'Experimental Study of an Automobile Exhaust Heat-Driven Adsorption Air-Conditioning Laboratory Prototype by Using Palm Activated Carbon-Methanol' [J], HVAC&R Research, 2010, 16 (2): 221–231

[44] Rybak, I. V., Gray, W. G. and Miller, C. T., 'Modeling two-fluid-phase flow and species transport in porous media' [J], Journal of Hydrology, 2015, 521: 565–581.

[45] Saha, B. B., Koyama, S., El-Sharkawy, I. I., Kuwahara, K., Kariya, K. and Ng, K. C., "Experiments for Measuring Adsorption Characteristics of an Activated Carbon Fiber / Ethanol Pair Using a Plate-Fin Heat Exchanger," HVAC&R Research, 2006, 12 (2): 767 – 782.

[46] Kyaw, T., Nami, T., Takahiko, M., Saha. B. B., Shigeru, K., Tomohiro, M.,

Shinnosuke. M., Toru, K., ‘Experimental investigation on the performance of an adsorption system using Maxsorb III+Ethanol Pair’ [J], International Journal of Refrigeration, 2018, 0: 1-10

[47] Tamainot-Telto, Z., Metcalf, S. J. and Critoph, R. E, ‘Novel compact sorption generators for air conditioning’ [J], Materials Science and Engineering A280, 2009, 32: 727-733.

[48] Douss, N. and Meunier, F., ‘Experimental study of cascading adsorption cycles’ [J], Chemical Engineering Science, 44: 225-235.

[49] Wang, R. Z., Wu, J. Y., Xu, Y., X and Wang, W., ‘Performance researches and improvements on heat regenerative adsorption refrigerator and heat pump’ [J], Energy Convers Manage, 2001, 42: 233-249.

[50] Makimoto, N., Miyazaki, T. and Koyama, S., ‘The effect of heating temperature on the performance of an adsorption cooling system using a carbon powder-ethanol pair’ [C], Grand Proceeding of Cross Straits Symposium on Energy and Environmental Science and Technology (CSS-EEST 13), 2011, Jeju, Korea.

[51] Dubinin, M.M., Astakhov, V.A., ‘Development of the concepts of volume filling of micropores in the adsorption of gases and vapors by microporous adsorbents’ [J], Bulletin of the academy of sciences of the USSR, 1971, 20: 3-7.

[52] T. Miyazaki, ‘Thermodynamic Analysis of Adsorption Cooling Cycle based on Adsorption Characteristics of a Newly Developed Activated Carbon’ [N], Adsorption News, 2015, Vol. 29, 3:16-21.

[53] Lemmon E. W. Huber, M. L, McLinden, M. O., NIST standard reference database 23 [DB/OL], 2010, REFPROP version 9.1

[54] Vasta, S., Sapienza, A., Freni, A., Restuccia, G., ‘A new adsorbent bed for automotive applications: experimental test in a full scale laboratory chiller’ [C], International Sorption Heat Pump Conference, 2008, Seoul, Korea

[55] Kubota, M., Ueda, T., Fujisawa, R., Kobayashi, J., Watanabe, F., Kobayashi, N., ‘Cooling output performance of a prototype adsorption heat pump with fin-type silica gel tube module’ [J], Applied Thermal Engineering, 2008, 28: 87-93

[56] Makimoto, N., ‘Research on an adsorption system using activated carbon-ethanol’ [D], Fukuoka, Japan: Kyushu University, 2013

[57] Hayashi, S., Kubota, K., Masaki, H., Shibata, Y., Takahashi, K., ‘A theoretical model for the estimation of the effective thermal conductivity of a packed bed of fine paricles’ [J], The Chemical Engineering Journal, 1987, Vol. 35-1, pp. 51-66.

[58] Dubinin, M.M., ’Adsorption in microoires’ [J], Colloid Interface Sci., 1961, 23:

437.

[59] El-Sharkawy, I. I., Uddin, K, Miyazaki, T., Saha, B. B., Koyama, S., Miyawaki, J. and Yoon, S. H., ‘Adsorption of ethanol onto parent and surface treated activated carbon powders’ [J], International Journal of Heat and Mass transfer, 2014, 73: 445-455.

[60] Jribi, S., Miyazaki, T., Saha, B. B., Koyama, S., Maeda, S., Maruyama, T., ‘Corrected adsorption rate model of activated carbon-ethanol pair by means of CFD simulation’ [J], International Journal of Refrigeration, 2016, 71: 60-68.

[61] Saha, B.B., Boelman, E.C. and Kashiwagi, T., ‘Computer simulation of a silica gel-water adsorption refrigeration cycle – the influence of operating conditions on cooling ouput and COP’ [J], ASHRAE Transactions, 1995, 101: 348-357.

Acknowledgement

My deepest gratitude is to my supervisors, Professor Takahiko Miyazaki, Associate Professor Kyaw Thu of Energy and Environmental Engineering, IGSES at Kyushu University, for their invaluable and indispensable guidance and inspiration throughout not only my research work but also life as master student.

For double degree program, I really would like to thank Professor Jang Byung-koog, Associate Professor Wang Dong and Campus Asia stuff, Ms. Nahoko Ichimura and Ms. Kazuyo Nishiyama for their grateful support and encouraging me not only during double degree program but also throughout my entire study in master program.

I must express my profound gratitude to the fellows, Jun SAIKI, Tomomichi NOZAKI, Tomohiro MATSUNO, who joined this double degree program and support and encourage each other for everything.

I am also indebted to Ms. Nami Takeda and Mr. Yuta Aki for their valuable suggestion as well as helping me to do experiments smoothly. I also wish to express thanks to all my present and former lab members and Mr. Nobuo Takada, Ms, Yuri Yamato.

Special appreciation to Dr. Shinnosuke Maeda, Mr. Tomohiro Maruyama from MALELLI (Old name: Calsonic Kansei) Corporation for their assistance and giving advice during setting up the experimental apparatus.

I would also like to acknowledge that part of this research was supported by Thermal Management Material and Technology Research Association (TherMAT) under New Energy and Industrial Technology Development Organization (NEDO).

Last not but least, I would like to express my sincere gratitude to my parents, sister and both grandparents who agreed to go on to the master program and double degree program and encouraged me during my study.

Appendix A

Specific heat capacity of heat transfer medium

A1. Experimental apparatus

The pictorial view of the experimental apparatus can be seen in Fig. A-1. A heat flux type Differential Scanning Calorimeter of type DSC-60 by Shimadzu Corporation is employed to measure the specific heat capacity of long life coolant (LLC). The temperature program speed can be applied between 0.1℃/hour and 99.9℃/min.

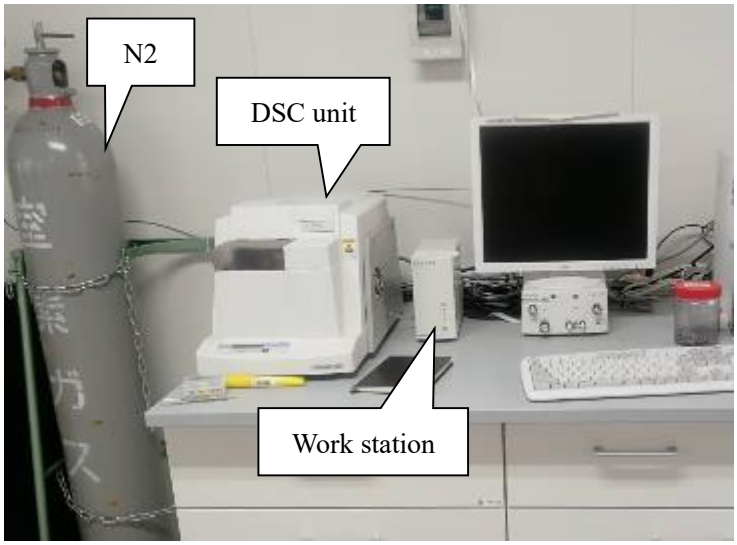

Fig. A-1 Pictorial view of the DSC experiment

A2. Experimental procedure

The samples of heat transfer medium, namely LLC here, empty crucible and standard sapphire (α-AlsO3) are required to measure the specific capacity. The weight of empty crucible was measured using a microbalance. LLC sample was placed in the crucible and took the weight of crucible and sample together from where the true sample weight was measured. For calibration, experiments were conducted with standard sapphire sample with known specific heat and weight. The schematic drawing of the differential scanning calorimeters can be seen in Fig. A-2.

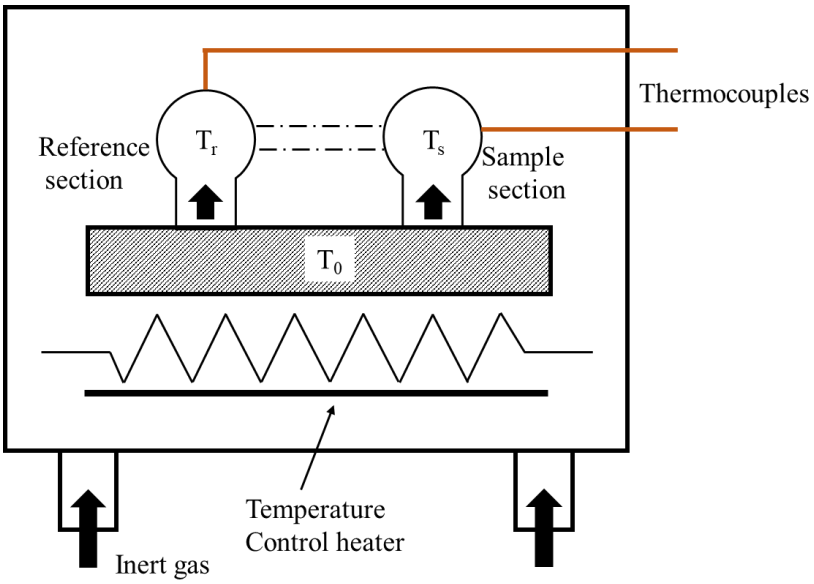

Fig. A-2 Schematic drawing of the DSC apparatus

The next three process of measures are conducted.

(1) Blank measurement is carried out placing an empty sample crucible and an empty reference crucible in designated position T_s and T_r as shown in Fig. A-2.

(2) Reference measure is conducted placing a fundamental material (α-AlsO3) with provided specific heat capacity and mass in the sample crucible as shown in Fig. A-2.

(3) Measurement of sample is carried out by changing fundamental material into sample material in the sample crucible with provided mass in the position of T_s as depicted in Fig. A-2.

The temperature range used in the measurement was between -10℃ and 95℃ considering the working range of adsorption cooling system for our research. So as to keep dry, inert atmosphere N_2 gas was pumped to the sample space while measurement is performed. The nitrogen helps to sweep away any off gasses which might be emitted when the sample is heated. The flow rate of nitrogen is about 50 mL/min.

A3. Experimental results

The result of measurements is shown in Fig. A-3. The measured value of specific heat

was approximated by the following equation using the least square method.

$$c_w = B_0 + B_1 T \tag{A.1}$$

where the coefficients of formula with confidence interval in Eq. (A.1) can be found in Table A-1.

Table A-1 Coefficients and 2σ approximation formula

B_0	B_1	2σ
3.37	0.0049	0.015

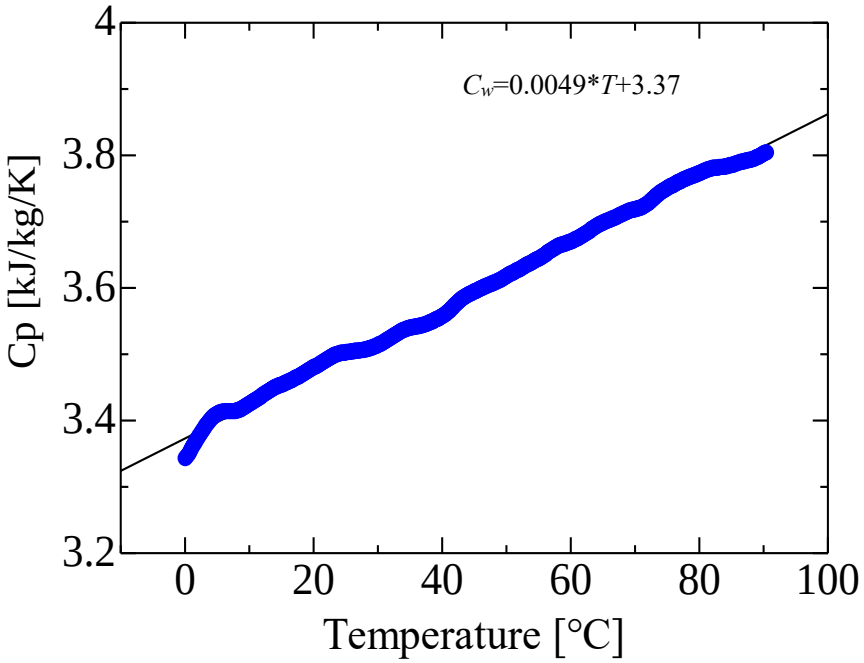

Fig. A-3 Specific heat of LLC

Appendix B

Thermocouple calibration

B1. Experimental apparatus

Fig. A-1 shows a schematic diagram of the experimental apparatus which is used to test the thermocouples. The platinum resistance thermometer is employed for measuring and T type sheathed thermocouple are the thermocouples to calibrate. A DC current is supplied to the current to the standard thermometer. A 1 mA current is supplied to the PT100 resistor and the voltage is obtained by the resistance (100Ω) according to Ohms law. A standard thermometer, the output voltage value for the T type sheath thermocouple and the standard resistor are measured and all the data is transferred to the data logger (MX100).

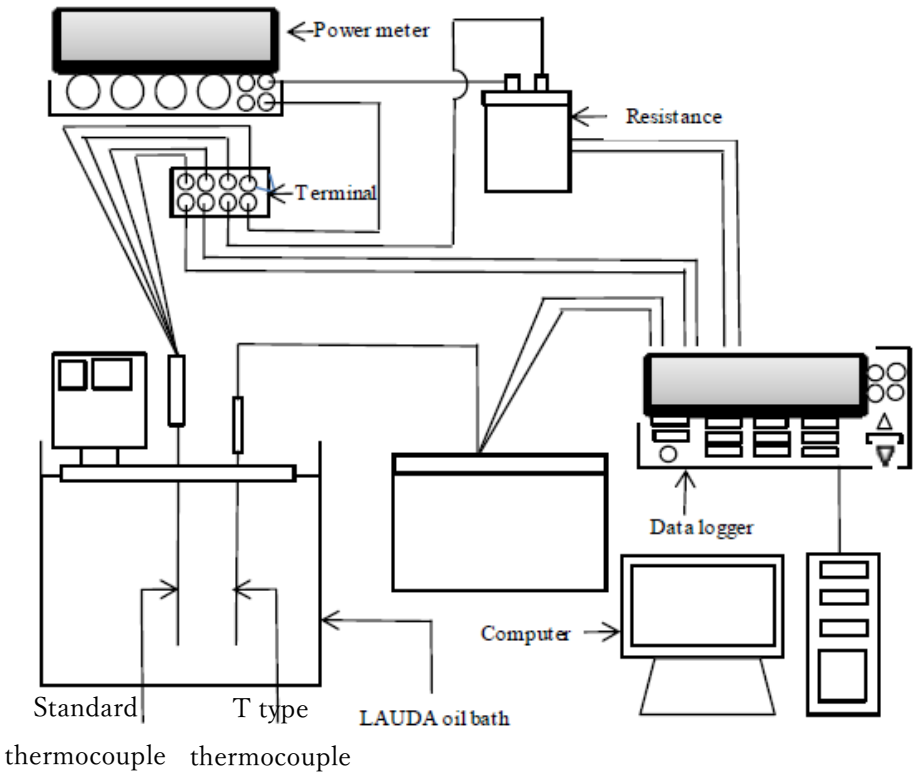

Fig. B-1 Schematic diagram of calibration

B2. Equations

B2.1 Standard thermometer temperature

The temperature of the standard thermometer is calculated from following equations:

$$R_{std,t} = A_0 + A_1 t + A_2 t^2 \tag{B.1}$$

$$t = \frac{-A_1 + \sqrt{A_1^2 - 4A_2\left(A_0 - R_{std,t}\right)}}{2A_2} \tag{B.2}$$

$$R_{std,t} = \frac{E_{std,t}}{I_{std,r}} \tag{B.3}$$

$$I_{std,r} = \frac{E_{std,t}}{R_{std,r}} \tag{B.4}$$

where $R_{std,t}$ [Ω], $E_{std,t}$ [V], $I_{std,t}$ [A], $E_{std,r}$ [V] and $R_{std,r}$ [Ω] are the resistance of the standard thermometer, the output voltage value of the standard thermometer, the current value flowing in the standard resistor, the output voltage value of the standard resistor and the resistance value of the standard resistor. A_0 [-], A_1 [-], and A_2 [-] respectively. The $R_{std,t}$ is 100Ω.

B2.2 Test equation for procedure

Temperature is defined by following equation.

$$t = a_0 + a_1 E_t + a_2 E_t^2 + a_3 E_t^3 + a_4 E_t^4 \tag{B.5}$$

where E_t [V] is the measured voltage value of each thermocouple, and a_0 [-], a_1 [-], a_2 [-], a_3 [-], a_4 [-] are constants. The procedure to test the calibration is as follows. Firstly,

the standard thermometer and T type thermocouples are inserted in the constant temperature circulating fluid tank (LAUDA Proline PR3530), and the output voltage is measured by the digital multimeter. After that, the temperature of the standard thermometer and the measured voltage value of each thermocouple are estimated by means of the fourth-order test equation by least square method. The test was carried out under the temperature range of 0~90℃ for each 2.5℃.

B2.3 Test results

The results of the test equation for each thermocouple obtained can be found in Table B-1.

Table B-1 Measurement accuracy of the thermocouple

Thermocouple	Confidence interval 2σ
Adsorber inlet	0.04
Adsorber outlet	0.03
Evaporator/condenser inlet	0.06
Evaporator/condenser outlet	0.05
Ambient	0.04